Comprehensive Analysis of the Cytoskeletal Protein Bactofilin in *Caulobacter crescentus*

Dissertation

zur Erlangung des Grades eines
Doktor der Naturwissenschaften
(Dr. rer.nat.)
des Fachbereichs Biologie der Philipps-Universität Marburg

Vorgelegt von
Ying Liu
Aus Ürümqi, P. R. China

Marburg (Lahn), September 2022

Vom Fachbereich Biologie der Philipps-Universität Marburg (HKZ: 1180)
als Dissertation angenommen am 20.10.2022

Erstgutachter: Prof. Dr. Martin Thanbichler
Zweitgutachter: Dr. Andreas Diepold

Tag der mündlichen Prüfung: 12.12.2022

Die Untersuchungen zur vorliegenden Arbeit wurden von September 2018 bis September 2022 an der Philipps-Universität Marburg und am Max-Planck-Institut für terrestrische Mikrobiologie unter der Leitung von Prof. Dr. Martin Thanbichler durchgeführt.

The investigations of the present work were carried out from September 2018 to September 2022 at the Philipps University of Marburg and the Max-Planck-Institute for Terrestrial Microbiology under the supervision of Prof. Dr. Martin Thanbichler.

Dedicated to who I love and respect

Abstract

Most bacteria contain protein filaments or filament systems collectively known as "bacterial cytoskeleton". Similar to their counterparts in eukaryotic cells, bacterial cytoskeletal proteins are essential in temporal and spatial organization of cellular machineries. They have been implicated in a wide range of fundamental processes, such as cell division, morphogenesis, DNA segregation, and polarity establishment. In the stalked model organism *Caulobacter crescentus* (*C. crescentus*), there are structural homologues of typical eukaryotic cytoskeletal proteins, such as the tubulin homologue FtsZ, the actin homologue MreB, and the intermediate filament-like protein crescentin. In addition, an increasing number of bacteria-specific cytoskeletal proteins have been discovered in recent years, among them the bactofilins. Previous studies have demonstrated that bactofilins adopt beta-helical structures and polymerize spontaneously into stable filaments that have a variety of roles in bacteria. However, so far, many aspects of their biology remain unclear.

In this work, we comprehensively investigated the properties of bactofilin using the homologue BacA from *C. crescentus* as a model. The aim is to elucidate its polymerization mechanism and its interaction with other proteins. The results showed that several conserved hydrophobic residues at the ends of the beta-helical bactofilin domain were crucial for the formation of protofilaments, which can further coalese into higher-order structures via lateral interactions, mediated by electrostatic forces. Moreover, studies of the membrane association of bactofilin not only indentified important amino acid residues for membrane-targeting but also revealed that polymerization and membrane binding are closely interdependent processes that promote each other. Additionally, the interaction between BacA and the penicillin-binding protein PbpC was analyzed in detail. Both interaction regions and the binding affinity were elucidated, which provides insights into the mode of interaction of bactofilins with client proteins. In an attempt to search for potential regulators of polymerization, various proteins were identified to interact with bactofilins in *C. crescentus in vivo*, indicating that bactofilins may play roles that go beyond their previously reported function in stalk biogenesis in this species. However, future studies are required to unravel the biological relevance of these interactions. Collectively, the findings made in this study for the first time shed light on the mode of action of bactofilins in *C. crescentus*, thus setting the basis for in-depth analyses of bactofilin function in other organisms.

Zusammenfassung

Die meisten Bakterien enthalten Proteinfilamente oder Filamentsysteme, die zusammen als „bakterielles Zytoskelett“ bezeichnet werden. Ähnlich wie ihre Gegenstücke in eukaryotischen Zellen sind bakterielle Zytoskelettproteine wesentlich an der zeitlichen und räumlichen Organisation zellulärer Maschinerien beteiligt. Sie sind in eine Vielzahl grundlegender Prozesse, wie z. B. Zellteilung, Morphogenese, DNA-Segregation und Polaritätsbildung, involviert. Im gestielten Modellorganismus *Caulobacter crescentus* (*C. crescentus*) existieren Homologe typischer eukaryotischer Zytoskelettproteine, wie das Tubulin-Homologe FtsZ, das Aktin-Homologe MreB und das Intermediärfilemtn-Protein Crescentin. Darüber hinaus wurden in den letzten Jahren zunehmend bakterienspezifische Proteine des Zytoskeletts entdeckt, darunter die Bactofiline. Vorausgehende Studien haben gezeigt, dass Bactofiline eine beta-helikale Struktur annehmen und spontan zu stabilen Filamenten polymerisieren, welche in Bakterien eine Vielzahl von Funktionen innehaben. Bislang sind jedoch viele Aspekte ihrer Biologie noch ungeklärt.

Diese Arbeit befasst sich mit der Untersuchung der Eigenschaften von Bactofilin am Beispiel des Homologs BacA aus *C. crescentus*, mit dem Ziel, seinen Polymerisationsmechanismus und seine Wechselwirkung mit anderen Proteinen aufzuklären. Die Untersuchungen in der vorliegenden Arbeit zeigten, dass mehrere konservierte hydrophobe Reste an den Enden der beta-helikalen Bactofilin-Domäne entscheidend für die Bildung von Protofilamenten sind, welche sich über laterale Wechselwirkungen, vermittelt durch elektrostatische Kräfte, weiter zu Strukturen höherer Ordnung zusammenlagern können. Darüber hinaus identifizierte eine Analyse der Membranassoziation von BacA nicht nur wichtige Aminosäurereste für das Membran-Targeting, sondern zeigte auch, dass Polymerisation und Membranbindung stark voneinander abhängige Prozesse sind, welche sich gegenseitig fördern. Zusätzlich wurde die Interaktion zwischen BacA und dem Penicillin bindenden Protein PbpC im Detail untersucht. Hierbei wurden sowohl die Interaktionsregionen als auch die Bindungsaffinität aufgeklärt, was Einblicke in den Interaktionsmechanismus zwischen Bactofilinen und ihren Klienten-Proteinen gewährte. Auf der Suche nach potenziellen Regulatoren der Polymerisation wurden verschiedene Proteine identifiziert, welche *in vivo* mit den Bactofilinen in *C. crescentus* interagieren. Dies deutet darauf hin, dass Bactofiline möglicherweise eine Rolle spielen, die über ihre zuvor beschriebene Funktion bei der Stielbiogenese in *C. crescentus* hinausgeht. Weitere Studien sind jedoch erforderlich, um die biologische Relevanz dieser Wechselwirkungen aufzuklären. Insgesamt beleuchten die in dieser Studie gewonnenen Erkenntnisse erstmals die Wirkungsweise von Bactofilinen in *C.*

crescentus und legen damit die Grundlage für tiefergehende Analysen der Bactofilin-Funktion in anderen Organismen.

Abbreviations

aa – amino acid
ABC – ATP-binding cassette
ATP – adenosine-5'-triphosphate
BLI – bio-layer interferometry
BSA – bovine serum albumin
CCRP – coiled-coil rich protein
Co-IP – co-immunoprecipitation
Cryo-EM – cryogenic electron microscopy
CV – column volume
DNA – deoxyribonucleic acid
GTase – glycosyltransferase
GTP – guanosine-5'-triphosphate
HDX-MS – hydrogen-deuterium exchange mass spectrometry
IF – intermediate filament
IPTG – isopropyl β–D-1-thiogalactopyranoside
kDa – kilodaltons
K_{off} – dissociation rate constant
LB – Luria-Bertani broth
LC-MS/MS – liquid chromatography-mass spectrometry/mass spectrometry
M2G – M2 minimal medium with glucose
MFP – membrane fusion protein
MSD – mean squared displacement
MALS – multi-angle light scattering
nt – nucleotide
PBP – penicillin-binding protein
PCR – polymerase chain reaction
PG – peptidoglycan
pI – isoelectric point
PMSF – phenylmethylsulfonyl fluoride
PRP – pentapeptide repeat protein
PRR – proline-rich region
RTX – repeats-in-toxins
SA – streptavidin
SD – standard deviation
SDS-PAGE – sodium dodecyl sulfate-polyacrylamide gel electrophoresis
SUV – single unilamellar vesicles
T1SS – type I secretion system
TCEP – tris(2-carboxyethyl)phosphine
TEM – transmission electron microscopy
TFA – trifluoroacetic acid
TIPOC – tip-organizing center
TMH – transmembrane helix
TPase – transpeptidase

Content

1 Introduction

Life on this planet can be divided into three domains, one of which are the Bacteria [1]. Bacteria are mostly single-celled organisms that colonize almost every biological niche on Earth, from land to water, from hot springs to the deep-frozen poles, as well as the bodies of humans and animals. They exhibit an amazing diversity in size, shape and physiology. Studies on bacteria have cast light on so many aspects of life that formerly belonged to the realm of mystery. Some bacteria have emerged as widely studied model organisms because they are easily cultivatable and manipulatable. One example is the dimorphic bacterium *Caulobacter crescentus*. Research on it has deepened our understanding of cellular and molecular biology, for instance, the exquisite intracellular organization that was once thought to be exclusively eukaryotic. Similar to eukaryotes, bacteria employ cytoskeletal elements to spatiotemporally regulate key cellular processes and thus integrate intra- and extracellular cues with developmental programs. This work focuses on a bacteria-specific cytoskeletal protein, bactofilin, in *C. crescentus* and aims to provide insights into its polymerization mechanism as well as its interaction with other proteins.

1.1 *Caulobacter crescentus* as a model organism

C. crescentus is a Gram-negative alphaproteobacterium, thriving in oligotrophic aquatic environments. It was first described in detail by Jeanne Poindexter in 1964 after the isolation from a Californian pond [2]. As indicated by its name, *C. crescentus* has a vibrioid shape and it is characterized by a thin, tubular stalk (*Figure 1A*), like other species in the order of Caulobacterales. The stalk is a polar extension of the cell body with a continuous cell envelope (inner membrane, peptidoglycan, and outer membrane) that is devoid of DNA, ribosomes [2] and the majority of cytoplasmic proteins [2, 3]. It is compartmentalized by crossbands, proteinaceous diffusion barriers, preventing the free exchange of membrane and soluble proteins between the stalk and the cell body [4]. A gelatinous, elastic adhesin known as the holdfast is synthesized at the tip of the stalk, facilitating its irreversible attachment to solid surfaces (*Figure 1A*). The holdfast is polysaccharide-based, containing a 1,4-linked backbone of glucose, mannose, N-acetylglucosamine and xylose [5]. The growth of stalk is regulated by phosphate [6–8]. Under phosphate starvation, cells elongate the stalk dramatically, and the length of stalk can be 30 times longer than that of cells growing in phosphate-rich condition. The development of the stalk confers competitive advantages to *C. crescentus*, as it facilitates the access to nutrients and the release of progeny to environment

when cells are growing in a biofilm [9]. Moreover, *C. crescentus* is well-known for its biphasic cell cycle and asymmetric division. The distinctive features of *C. crescentus* have attracted the attention of scientists since its discovery. Together with its straightforward genetic manipulation and easy synchronization [10], this species has been developed into a model organism within a short time. In the following sections, I will discuss a few representative examples of how studies on *C. crescentus* expand our knowledge on cellular and molecular biology.

1.1.1 The dimorphic lifestyle of *C. crescentus*

C. crescentus is renowned for its specialized dimorphic life cycle. It can divide asymmetrically, yielding two different progenies, a motile swarmer cell and a sessile stalked cell (*Figure 1B*). In contrast to the stalked cell, the swarmer cell is temporarily arrested in G1 phase and incompetent for replication. Equipped with a polar flagellum and several type IVc tight adherence (tad) pili [11], the swarmer cell can move freely in the aquatic environment and explore new niches. Upon surface attachment, it differentiates into a stalked cell by ejecting the flagellum, retracting its pili and forming a stalk at the same pole. Surface sensing through tad pili stimulates this series of transformations [12–14]. DNA replication and chromosome segregation occur in S phase and G2 phase. Before finalizing cell division, a new flagellum and several new pili are built at the pole opposite the stalk. Once these processes are complete, cytokinesis advances, producing two genetically identical daughter cells that differ in physiology and morphology. The stalked daughter cell can enter S phase and reinitiate DNA replication immediately, whereas the swarmer cell first needs to undergo the aforementioned swarmer-to-stalked cell differentiation. The dimorphic life cycle of *C. crescentus* makes this species an indispensable organism to study asymmetric division and cell differentiation, which deepens our knowledge of the related topics.

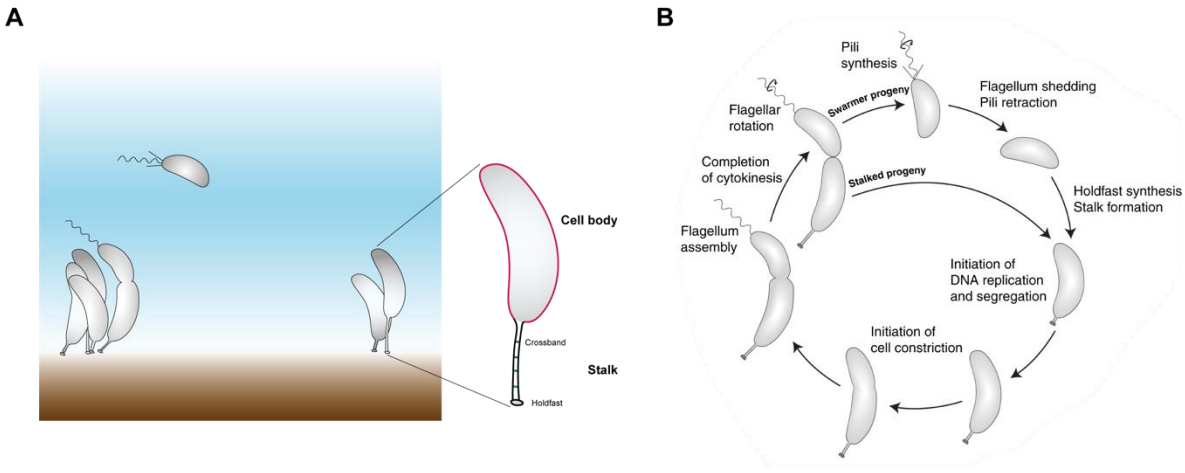

Figure 1 Ecology and dimorphic life cycle of *C. crescentus*. (A) *C. crescentus* lives in fresh water and exists in two states: planktonic or sessile. The surface attachment of *C. crescentus* cells is mediated by the holdfast that locates at the tip of the crossband-compartmentalized stalk. (B) *C. crecentus* divides asymmetrically, producing two progenies with different morphology and replication potential. The stalked cell can enter the new cell cycle instantly, whereas the swarmer cell must undergo the motile-to-sessile transition by replacing the polar flagellum and pili with a stalk before initiating DNA replication. Image taken from [15].

1.1.2 A sophisticated regulation system for cell cycle

The dimorphic life cycle of *C. crescentus* requires precise regulation to guarantee faithful coordination of the developmental programs with the cell cycle progression. Studies have demonstrated that more than 500 genes in *C. crescentus* are regulated as a function of the cell cycle [16], and their expression is mainly governed by four global transcription regulators, DnaA [17], GcrA [18], CtrA [19] and SciP [20], along with a DNA methyltransferase CcrM [21]. Those regulators constitute a cyclical circuit and act in an oscillating and out-of-phase manner to ensure robust cell-cycle control (*Figure 2A*).

In addition to the regulation at the transcriptional level, cell cycle progression is also modulated by phosphorylation, proteolysis, and the second messenger cyclic diguanylate (c-di-GMP), which is best illustrated by CtrA (*Figure 2B*). In the swarmer cell, CtrA mainly exists in the phosphorylated form (CtrA~P) and represses DNA replication [22], whereas it is dephosphorylated in the stalked cell, which promotes its degradation by ClpXP. The phosphorylation state of CtrA as well as another protein, CpdR, which drives ClpXP to the stalked pole [23, 24], is regulated by CckA [25] through the histidine phosphotransferase ChpT [26]. CckA is bifunctional and can act either as a kinase or as a phosphatase. The switch between these two activities is controlled by DivK and c-di-GMP, whose production depends on PleD. DivK and PleD are non-DNA-binding single-domain response regulators. In the swarmer cell, they are dephosphorylated by the pole-localized phosphatase PleC. Dephosphorylated DivK fails to bind to DivL, an atypical histidine kinase that activates CckA [27]. However, DivJ replaces PleC at the stalked cell and phosphorylates both

regulators [28]. DivK~P gains the ability to interact with DivL, which frees CckA from the effect of DivL, and PleD~P elevates the intracellular c-di-GMP level, switching CckA to the phosphatase mode [29]. Meanwhile, the versatile second messenger c-di-GMP can facilitate the proteolysis of CtrA by ClpXP via PopA.

C. crescentus employs various regulatory mechanisms, including oscillatory transcriptional regulators, phosphorelays, second messenger and proteolysis, to accurately control the cell cycle and coordinate it with cellular differentiation and polar morphogenesis. It is instrumental to study this organism, as it sheds lights on how intricate cell cycle regulation can be achieved in bacteria.

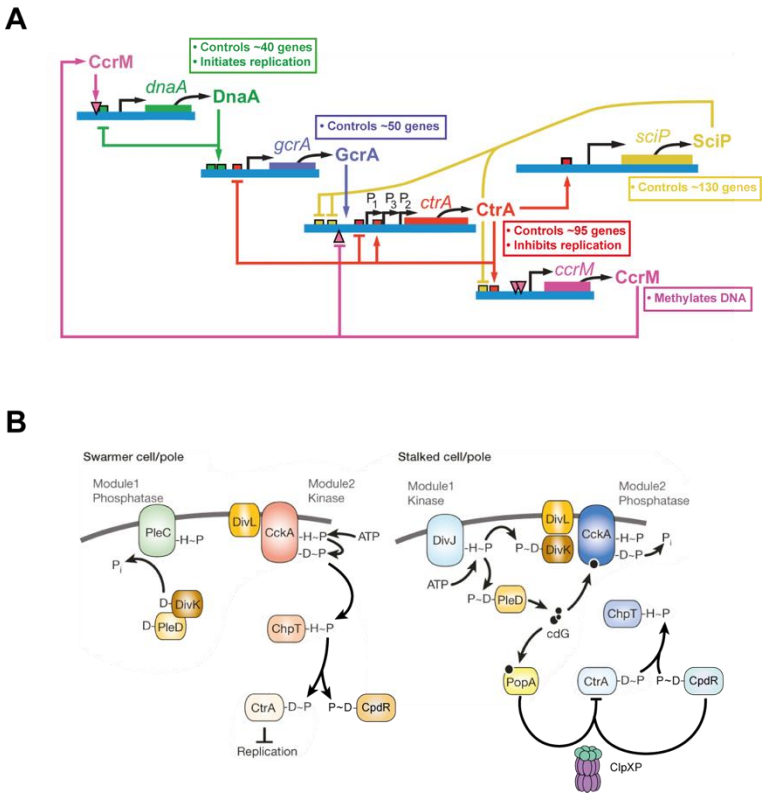

Figure 2 Molecular regulation of the *C. crescentus* cell cycle. (A) The cell cycle of *C. crescentus* is tightly regulated by a self-sustained circuit composed of four transcriptional regulators (DnaA, GcrM, CtrA, and Scip) and a DNA methyltransferase (CcrM). Modified from [30]. (B) CtrA is not only modulated at the transcriptional level but also by phosphorylation, proteolysis and c-di-GMP. The CckA-ChpT-CtrA core phosphorelay system and c-di-GMP production are under the control of another phosphorylation module, composed of PleC, DivJ, DivK and PleD. Phosphorylated CpdR and the elevated concentration of c-di-GMP act in concert to promote the proteolysis of CtrA in the stalked cell. Modified from [29].

1.1.3 An elaborate intracellular organization by cytoskeletal proteins

Bacterial cells are organizationally more complex than they were believed. In addition to temporal regulation, *C. crescentus* leverages precise spatial positioning to establish polarity, create subcellular organization and maintain its morphology, which is pivotal for cell cycle progression. The spatial patterning of effectors and regulatory proteins relies on filamentous

proteins and filament systems that are collectively known as the "bacterial cytoskeleton". There is a large inventory of such specifically located cytoskeletons in *C. crescentus*, making it a powerful model to study bacterial cell biology. In the next sections, a comprehensive summary of current knowledge on cytoskeletal proteins in bacteria will be presented.

1.2 Bacterial cytoskeletal proteins

Similar to their counterparts in eukaryotic cells, bacterial cytoskeletal proteins are essential for the proper temporal and spatial organization of cellular machineries. They not only act as recruiters for functionally related enzymes and regulatory proteins but also provide platforms, allowing the formation of cooperative multi-protein complexes. In bacteria, cytoskeletons have been implicated in a wide range of fundamental processes, such as cell division [31], morphogenesis [32], DNA segregation [33], and polarity establishment [34]. *C. crescentus* harbors a considerable number of cytoskeletons, some of which are structural homologues to eukaryotic cytoskeletons, while the others are bacteria-specific (Figure *3*).

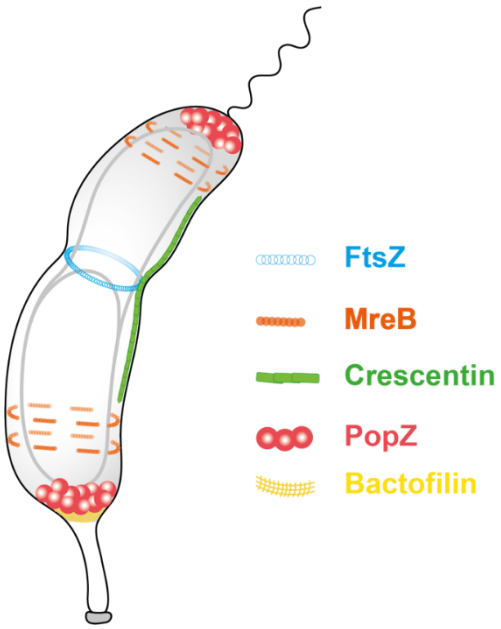

Figure 3 Cytoskeletal elements in *C. crescentus*. *C. crescentus* is a powerful model to study the spatiotemporal organization of cellular components, as it possesses several cytoskeletal elements, including MreB, FtsZ, crescentin, PopZ and bactofilin.

1.2.1 FtsZ and other tubulin homologues

FtsZ is a tubulin homologue [35, 36] in *C. crescentus* and it can self-organize into polymers in a GTP-dependent manner [37–39]. It is widely conserved in bacteria and involved in cell division. *In vivo* studies on several bacteria, such as *C. crescentus* [40, 41], *E. coli* [42–44] and *B. subtilis* [45, 46] have confirmed that it forms a discontinuous, single-layered, loosely packed,

ring-like structure, called the Z-ring, at the incipient division site (*Figure 4*). The formation of the Z-ring at midcell is regulated by the ParA-like protein MipZ in *C. crescentus* [47], as opposed to the Min systems in *E. coli* [48] and *B. subtilis* [49]. MipZ is a negative regulator for the polymerization of FtsZ. It interacts with DNA-bound ParB, consequently creating a bipolar gradient, with the lowest concentration at the midplane, where the assembly of FtsZ is allowed (*Figure 4*). Moreover, the Z-ring is not static but rather dynamic and moves by treadmilling [50–52], which means that FtsZ undergoes polymerization at the plus-end while depolymerizing at the minus-end (*Figure 4*). The treadmilling of FtsZ is determined by GTP hydrolysis, and the movement of a GTPase-deficient variant is much slower than that of the wild-type protein [53]. FtsZ exerts its effect on division in multiple ways. It is the first protein arriving at the future division site and functions as a scaffold for the multiprotein cell division machinery, the divisome [54–56] (*Figure 4*). Dissection of the process of divisome assembly in *C. crescentus* has demonstrated that it can be roughly divided into seven modules [57]. In addition to acting as a marker for the division plane, FtsZ also orchestrates chromosome segregation and cell wall constriction. *C. crescentus* uses the ZapT-ZauP-ZapA system as a molecular bridge between the chromosomal terminus region and the and Z-ring [58, 59], which acts analogously to the MatP-ZapB-ZapA$_{EC}$ system of *E. coli* [60, 61]. Furthermore, studies have revealed that the Z-ring can generate mechanical force that might be necessary for cell wall constriction. Nguyen *et al.* have proposed that force produced by FtsZ can counteract the turgor pressure, allowing the newly synthesized septal peptidylglycan (PG) to be pulled inwards, thereby reducing the circumference of PG gradually [62]. However, if the mechanical force from FtsZ actually drives constriction is controversial [51, 53, 63] and requires further study.

In addition to FtsZ, bacteria also possess other homologues to tubulin. For instance, TubZ is a plasmid-encoded FtsZ/tubulin homologue that plays an important role in the segregation and stability of plasmids [64, 65]. Another example of bacterial tubulin homologue is BtuAB, which are found in a number of *Prosthecobacter* strains. BtuAB are more structurally similar to eukaryotic tubulin than FtsZ and they are able to form small microtubules with unknown function [66–68]. Interestingly, there is also a phage-encoded tubulin-like cytoskeletal protein (PhuZ) that has been described in *Pseudomonas* species. Recent work has shown that PhuZ participates in the formation of a nucleus-like structure surrounding viral DNA and transports the viral capsids from the cytoplasmic membrane to the compartment during the late phase of infection [69, 70].

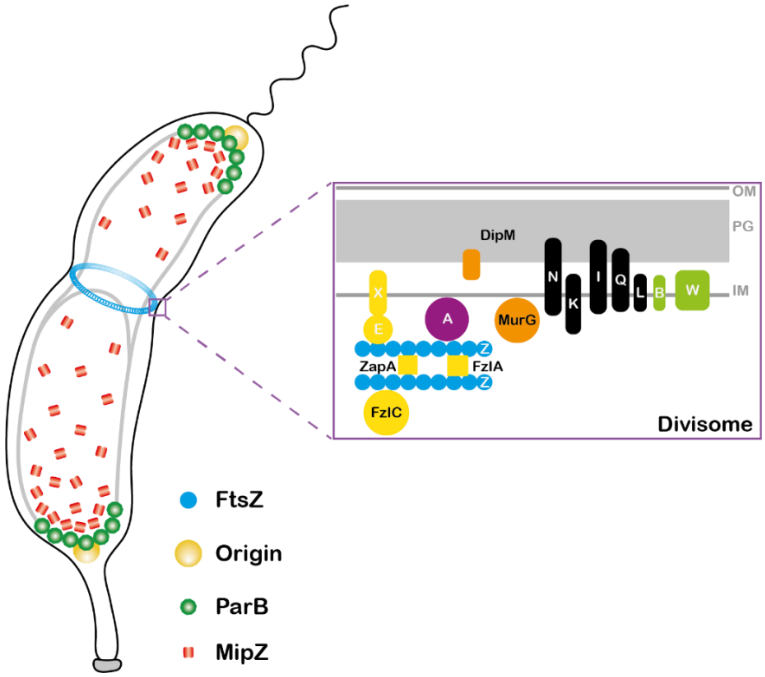

Figure 4 FtsZ is a tubulin homologue in *C. crescentus*, participating in cell division. The polymerization of FtsZ at the incipient division site is controlled by MipZ, which forms a bipolar gradient in the cell with the lowest concentration at the midcell. FtsZ serves as a platform for the assembly of the divisome. The core components of the divisome as well as their localization are dipicted in the box. IM, inner membrane; PG, peptidoglycan; OM, outer membrane; Fts protein names have been abbreviated by excluding 'Fts' from them (e.g. Z = FtsZ, A = FtsA, etc.).

1.2.2 MreB and other actin homologues

Cell shape is crucial for the survival of bacteria; hence, the geometry of the cell should be accurately reproduced during cell division. An actin homologue, MreB, is a vital cell shape determinant in many rod-shaped bacteria, including *C. crescentus* [71–73]. Analogous to its eukaryotic homologues, the polymerization of MreB is ATP-dependent. Nevertheless, studies have demonstrated that GTP can also be accommodated in the catalytic pocket and promote the polymerization of MreB [73, 74]. Structural analyses have substantiated that MreB assembles into membrane-attached [75] antiparallel double filaments [76]. It plays an important role in cell elongation by serving as a scaffold for a multiprotein cell wall biosynthetic complex called the elongasome or the Rod system [77] (*Figure 5*). The core components of elongasome encompass MreC and MreD (cotranscribed with *mreB* in the *mreBCD* operon) [78, 79], the regulatory protein RodZ [80–82] as well as the glycosyltransferase/transpeptidase pair RodA/PBP2 [83]. Furthermore, the discrete, patchy polymer of MreB is cytomotive, moving circumferentially perpendicular to the long axis of cell [84], with its movement powered by cell wall synthesis[84–86]. In addition to its role in cell shape maintenance, MreB has been repurposed during evolution as evidenced by its essentiality to cell division in *Chlamydia* that lacks FtsZ [87] and its involvement in the gliding motility of *Myxococcus xanthus* (*M. xanthus*) [88, 89].

In bacteria, the actin homologues are not restricted to MreB. For example, both ParM [90, 91] and AlfA [92, 93] are actin-like proteins that are implicated in type II plasmid segregation systems. They associate to DNA through accessory proteins, ParR and AlfB, respectively, which stabilize the polymers of ParM and AlfA and promote the directional movement of plasmids. Another noticeable actin-like filament discovered in bacteria is AlpC, which is encoded by prophage CGP3 in *Corynebacterium glutamicum* ATCC 13032 [94]. It has been reported to contribute to the transportation of viral DNA. Moreover, it bears resemblance to ParM and AlfA, as it also has a cognate adaptor, AlpC, with function similar to that of ParR and AlfB.

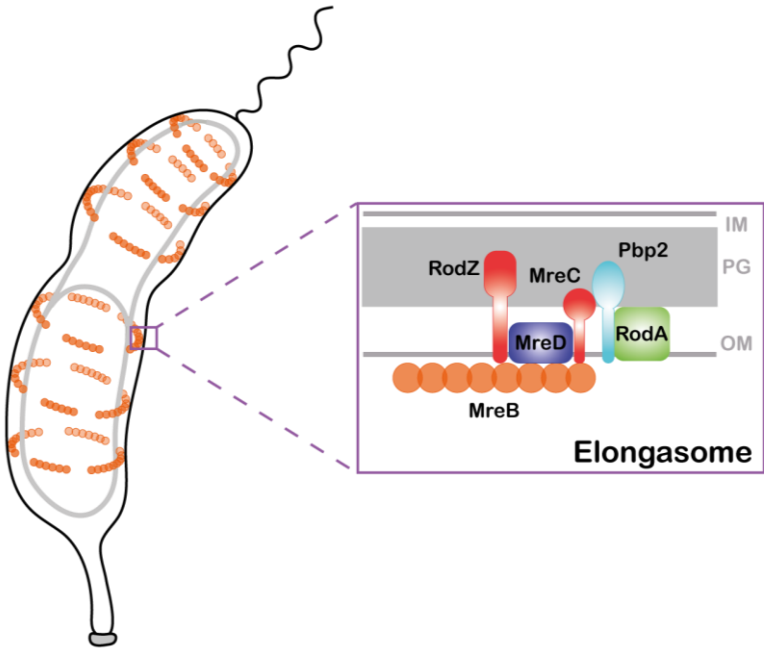

Figure 5 MreB is an actin homologue in *C. crescentus* that maintains cell shape. MreB forms discontinuous patches and moves circumferentially along the cell. It acts as a scaffold for the lateral cell wall biosynthesis complex, the elongasome. A schematic representative of the elongasome is displayed in the box. IM, inner membrane; PG, peptidoglycan; OM, outer membrane.

1.2.3 Crescentin and other intermediate filament-like proteins

Crescentin is an intermediate filament (IF)-like protein discovered in *C. crescentus*, where it plays an important role in the establishment of the distinctive curved shape [95]. It shares similarities with eukaryotic intermediate filament proteins at both sequence and structural levels. Crescentin adopts the typical tripartite architecture of eukaryotic intermediate filaments with a conserved middle part flanked by short head and tail termini (*Figure 6*). The middle part consists of four coiled-coil rod domains (designated 1A, 1B, 2A, and 2B) that are separated by short linkers. Within the fourth domain, there is a conserved phasing discontinuity (stutter) breaking the domain. Due to the abundance of the coiled-coil motif,

crescentin is also known as coiled-coil-rich protein (CCRP). Furthermore, the polymerization of crescentin is nucleotide-independent and biphasic. It first extends longitudinally until it reaches the cell poles and then switches to lateral growth [96]. Microscopic studies in combination with quantitative rheology have suggested that the polymer of crescentin is dynamic and exchanges subunits with the free-moving cytosolic reservoir at a slow rate, which remodels the filamentous structure gradually [97]. The importance of its individual domains in polymerization and function has been analyzed [98]. Collectively, the proper assembly relies on an N-terminal region corresponding to amino acids 28-79 (N28-79) and the rod domains. However, it also requires the first 27 amino acids (N27), the stutter and the tail region to counteract the dissociation triggered by monovalent K^+ ions as well as the L1 linker and stutter to prevent excessive bundling. Moreover, N27 also plays a role in membrane association. How crescentin bends the cell is poorly understood. Nevertheless, it has been proposed that the crescentin filament exerts a mechanical force on the cell envelope that alters the kinetics of peptidoglycan synthesis and hydrolysis [99] (*Figure 6).*

Two other outstanding representatives for bacterial intermediate filament-like proteins are Scy (*Streptomyces* cytoskeletal element) and FilP (filament-forming protein), discovered in *Streptomyces* species. Scy has been confirmed to form long rope-like filaments *in vitro* by negative staining and transmission electron microscope (TEM). It is a component of the tip-organizing center (TIPOC) and functions as a recruiter for the polar growth determinant DivIVA [100]. FilP is involved in apical growth and affects the size and distribution of DivIVA foci [101]. It forms interconnected networks *in vitro* that possibly provide mechanic support for hyphae [102]. Moreover, it has been shown to form a gradient *in vivo* and undergo subunit exchange with the cytosolic pool [101]. Remarkably, it seems that CCRPs have a propensity to polymerize, although not all of them fall into the category of intermediate filament-like proteins, such as the curvature-inducing periplasmic filament CrvAB in *Vibrio cholerae* [103] and four Ccrps in *Helicobacter pylori* (*H. pylori*), which influence cell shape, motility [104] and pathogenicity [105].

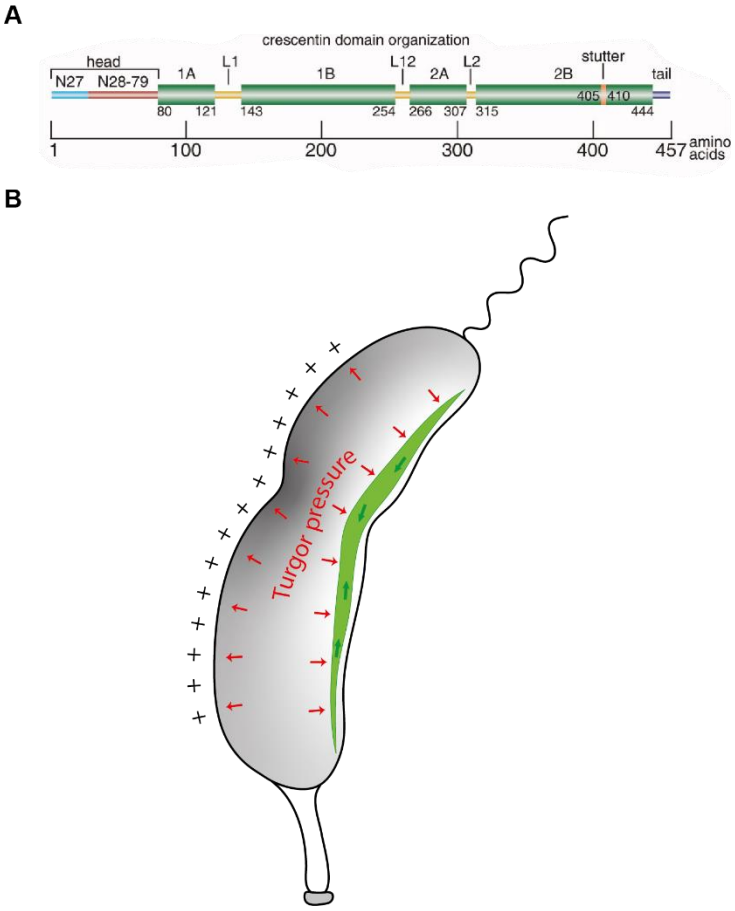

Figure 6 Crescentin is an intermediate filament-like protein in *C. crescentus* that contributes to the curved cell shape. (A) Crescentin has the typical tripartite domain organization of eukaryotic intermediate filament proteins with two short terminal regions flanking four coiled-coil domains that are separated by linkers. The fourth coiled-coil domain is characterized by a stutter. Image taken from [98]. (B) Crescentin provides mechanical support to reduce the strain exerted by the turgo pressure on the side where it locates, which leads to unequal peptidoglycan synthesis rates (the plus sign indicates the side with a faster rate) and eventually leads to cell cuvature.

1.2.4 Cytoskeleton-like scaffolding proteins

In addition to homologues of canonical cytoskeletal proteins, *C. crescentus* harbors a cytoskeleton-like scaffolding protein, namely polar organizer protein Z (PopZ). The analysis of the sequence of PopZ suggests that it can be divided into three parts: a conserved N-terminal domain (NTD), a variable negatively-charged proline-rich region, as well as a conserved C-terminal DUF2497 domain (CTD) that regulates polymerization (*Figure 7A*). PopZ first assembles into an elongated trimer, which further dimerizes through lateral interaction. The final six amino acids of PopZ are indispensable for connecting the hexamers into filaments, which assemble into a loose matrix at the cell poles [106] (*Figure 7B).*

PopZ interacts with several proteins through its disordered N-terminal region (1-133 aa) which contains a MoRF sequence. Such a sequence is a common feature shared by eukaryotic hub proteins, like p53 and BRCA1, and it adopts different structures upon interaction with other proteins [107]. Therefore, PopZ is proposed be a sub-polar hub protein in *C. crescentus*. Because of its multiple effectors, PopZ has pleiotropic effects on polarity, chromosome

segregation and cell cycle progression. Initially, it is located at the stalked pole and anchors the chromosomal origin of replication (*Cori*) via a direct interaction with ParB, which specifically binds to the origin-proximal partitioning sequences (*parS*) [108]. Coincident with chromosome segregation, PopZ travels through the cell and builds a new hub at the opposite pole, which directionally guides the duplicated centromere complex via a Walker-type ATPase, ParA. The ParB-*parS* complex follows DNA-bound ParA progressively and their interaction release ParA from DNA. Ptacin et al. have proposed that the PopZ sub-polar domain can sequester and regenerate the spent ParA at the pole-proximity, which creates a gradient of active ParA and hence prevents the reverse migration of ParB-*parS* [109] (*Figure 7C*). Another important role fulfilled by PopZ is related to cell cycle control. It has been recognized for a long time that PopZ binds to a number of cell cycle regulators such as CckA, ChpT, and DivL [107]. A recent study by Lasker et al. further illustrates how PopZ facilitates the asymmetric distribution of differently phosphorylated CtrA molecules in predivisional cell [110] (*Figure 7D*). It shows that PopZ together with retained DivL increases the concentration of CckA at the new pole, thus switching it into a kinase. In combination with the selective entry into PopZ, the concentrations of CckA, ChpT and CtrA are all elevated in the subdomain, which increases the probability of intermolecular binding and phosphoryl transfer. As a result, CtrA is more likely to exist in the phosphorylated state in the proximity of the new pole.

Although PopZ is restricted to alphaproteobacteria, there is a functionally similar protein, DivIVA, in Gram-positive bacteria. Because it is rich in coiled-coil motif, DivIVA can self-assemble into a polymeric structure and serves as a scaffold [111].

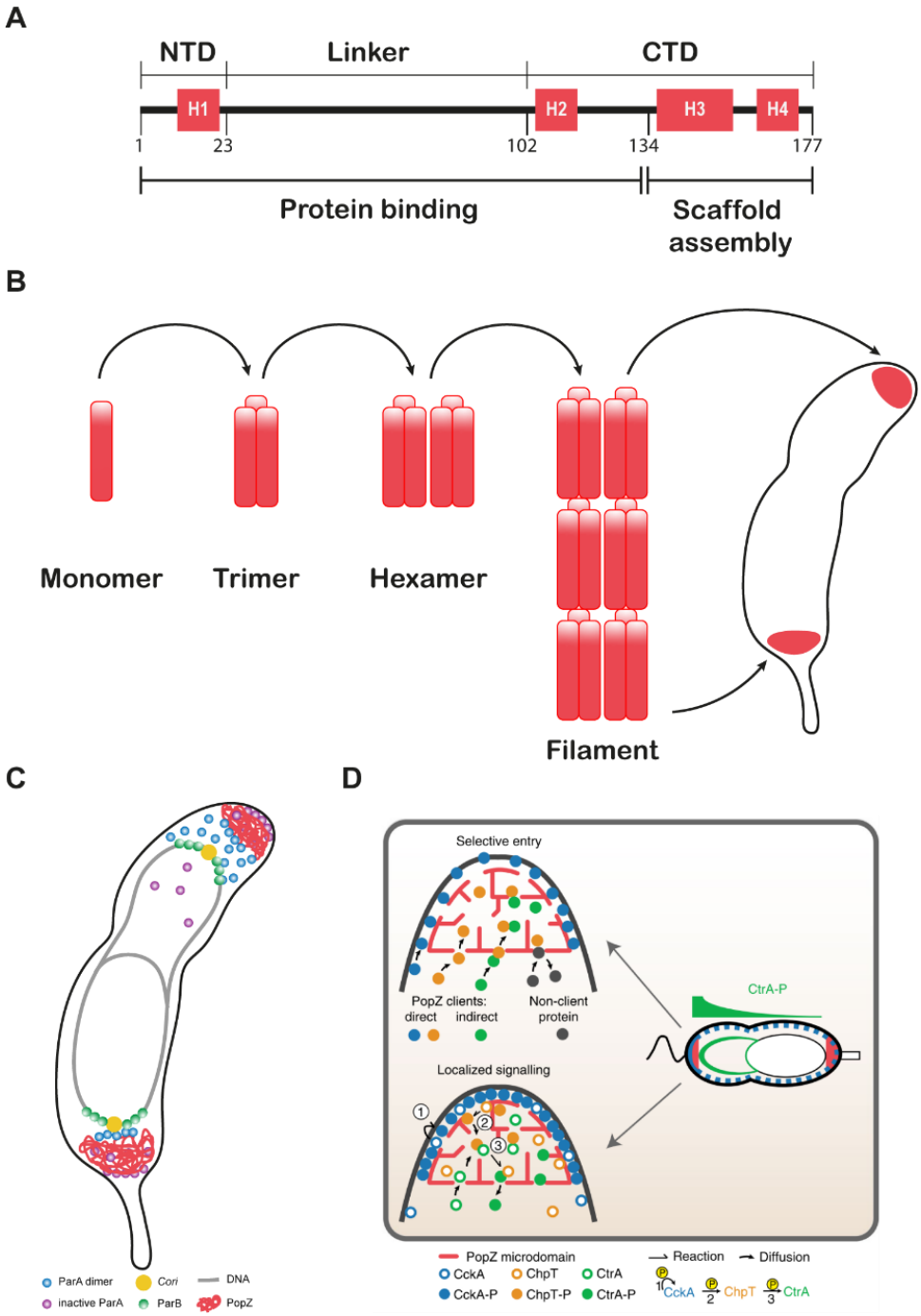

Figure 7 PopZ is a scaffolding protein that is important for cell polarity, chromosome segregation and cell cycle control. (A) PopZ can be divided into three parts: a disordered N-terminal region, a proline-rich linker and a C-terminal region involved in polymerization. There are many proteins interacting with PopZ, which is mediated by the first 133 aa of PopZ. (B) PopZ forms a matrix in *C. crescentus*. It first forms a trimer and then a hexamer through lateral interaction. The hexamer can further assemble into filaments. (C) PopZ is important for chromosome segregation. It anchors the ParB-*parS* complex at the cell poles and regenerates spent ParA to directionally guide the segregation complex to the new pole. (D) PopZ is also implicated in cell cycle progression and polarity establishment by concentrating CckA, ChpT, and CtrA at the new pole. As a result, the distribution of CtrA-P is skewed between two poles. Image taken from [110].

1.3 Bactofilin: a bacteria-specific cytoskeleton

The first member of bactofilin, CcmA, was identified in *Proteus mirabilis* (*P. mirabilis*) through transposon mutagenesis, which suggested that it is a cell shape determinant and affects

swarming motility in this species [112]. Afterwards, Kühn et al. demonstrated that bactofilin is a cytoskeletal protein using the homolog from *C. crescentus* [113]. Different from FtsZ, MreB and crescentin, which are homologues to eukaryotic cytoskeletal proteins, bactofilin is specific to prokaryotes. It is highly conserved and broadly distributed across bacteria, with many species encoding more than one copy of it in their genomes [114, 115]. In the succeeding sections, a compendious summary of our knowledge on bactofilin will be presented.

1.3.1 The structure and polymerization of bactofilin

Bactofilins are characterized by a conserved bactofilin domain (Pfam: PF04519) that is flanked by variable N- and C-terminal tails. The bactofilin domain is involved in filament formation, which is a spontaneous process and does not require any co-factor. Although the flexible terminal regions are not necessary for polymerization, they might engage in protein-protein interactions. Solid-state NMR (ssNMR) analysis has revealed that the bactofilin domain of BacA from *C. crescentus* adopts a right-handed, triangular, β-helical architecture, in which 18 β-strand segments are arranged in six consecutive windings (*Figure 8*) [116, 117]. Although it is rich in β-strands, a study conducted on *H. pylori* bactofilin has shown that it is proteinase K-sensitive and fails to bind to thioflavin T, which indicates that it is fundamentally different from the insoluble, β-sheet-rich amyloid proteins [118]. Moreover, the polymers formed by bactofilin are biochemically inert and resistant to 1 M urea, a broad range of pH values, and non-physiological salt concentrations [119]. The biochemical features of bactofilin as well as its polymerization mechanism have so far remained uncharacterized. Excitingly, a breakthrough was achieved recently in a study solving the structure of bactofilin protofilaments. By employing cryo-EM as well as crystallography, Deng et al. managed to demonstrate that bactofilin monomers assemble into a non-polar protofilament through head-to-head and tail-to-tail association of its subunits (*Figure 8*) [114]. Nevertheless, how protofilaments associate with each other to form higher-order structures, such as bundles and 2D crystalline sheets, requires further investigation.

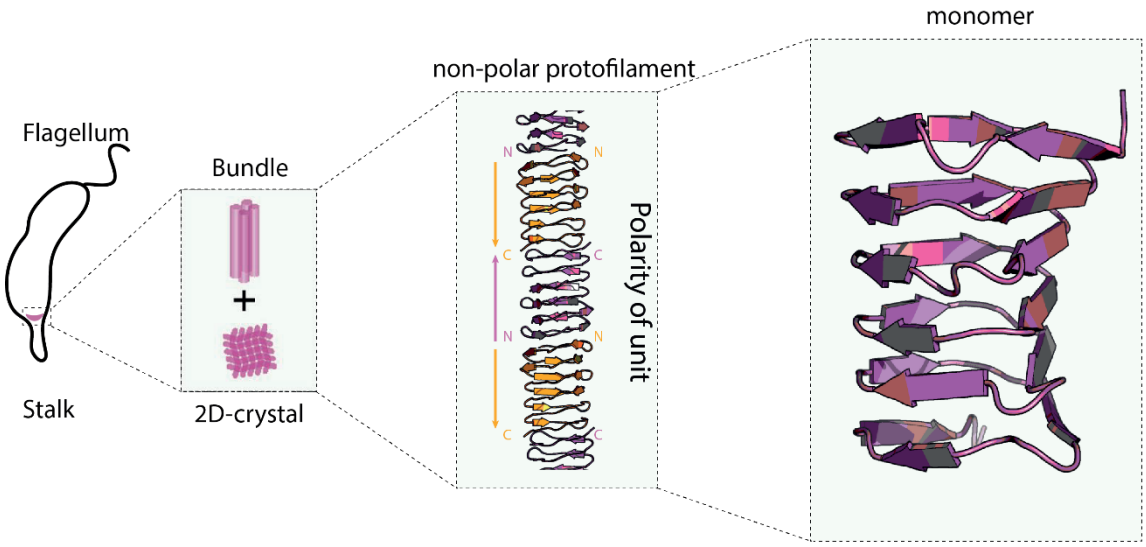

Figure 8 The structure of bactofilin monomer and protofilament. The bactofilin domain of bactofilin adopts a right-handed, triangular, β-helical architecture. It is able to assemble into non-polar protofilaments, which further form higher-order structures, such as bundles and 2D-crystaline sheets. Modified from [116].

1.3.2 Interaction of bactofilins with the membrane

Previously, it has been demonstrated that bactofilins are localized to the vicinity of the cytoplasmic membrane [113, 114, 120]. In *C. crescentus*, for example, both BacA and BacB associate with the cell membrane, as evidenced by cell fractionation and cryo-EM tomography studies. Deng et al. have suggested that within the N-terminal flexible tail of bactofilins, there is a conserved motif mediating the interaction with the cell membrane (*Figure 9*A), which is supported by a surface plasmon resonance study on the bactofilin homologue TtBac from *Thermus thermophilus* (*T. thermophilus*) [114]. Moreover, they hypothesized that this interaction is probably due to the hydrophobicity of the membrane-targeting sequence. A close examination of the identified region shows that it contains a mix of charged and hydrophobic residues. Intuitively, it points to the possibility that bactofilin may employ an N-terminal amphipathic helix to interact with the membrane, a strategy also used by the actin homologues MreB [75] and FtsA [121] (*Figure 9B*). Nevertheless, this hypothesis requires further investigation. It is also possible that the interaction between bactofilin and the membrane is mediated in other ways. According to the literature, peripheral membrane proteins utilize three distinct approaches to interact with biological membranes, namely electrostatic interaction, hydrophobic interaction or post-translational modification [122]. Since phosphatidyglycerol and cardiolipin are two most abundant phospholipids in *C. crescentus*, the cell membrane is overall negatively charged [123]. Hence, it is conceivable that electrostatic forces also contribute to the membrane association of

bactofilin. To obtain a comprehensive understanding of the binding mechanism of bactofilin, additional research is necessary.

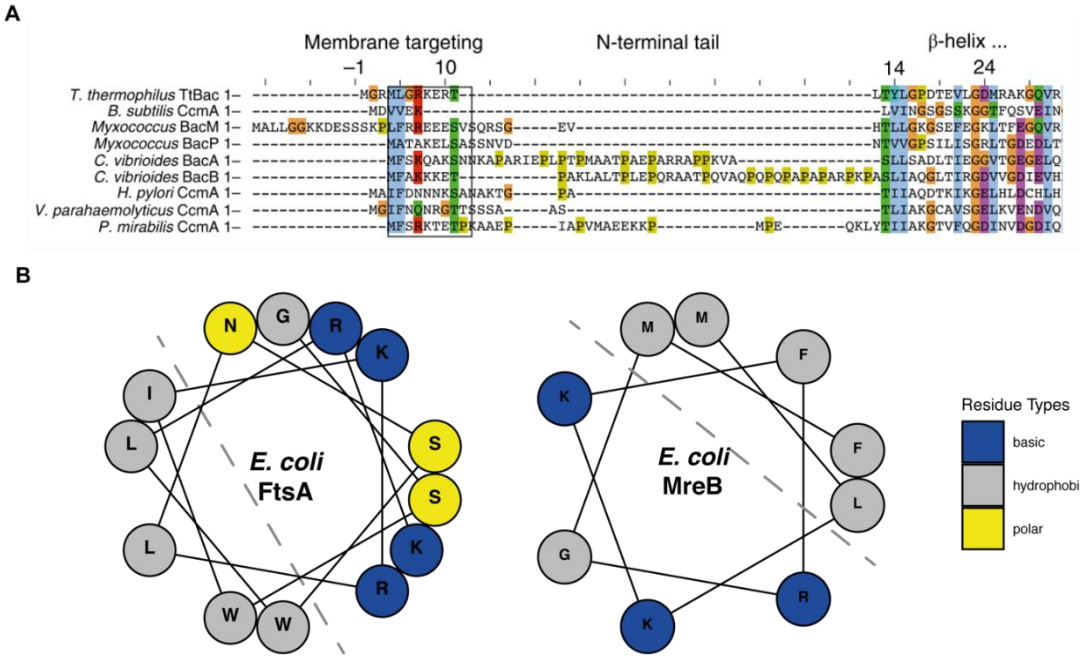

Figure 9 The membrane-targeting regions of bactofilins and other cytoskeletons. (A) A conserved hydrophobic motif was identified in the N-terminal tail of bactofilins, and it is suggested to be involved in membrane binding. Image taken from [114]. (B) Helical wheel view of the membrane-targeting sequences in *E. coli* FtsA (left) and MreB (right). Hydrophobic residues cluster on one side of the helix forming a membrane-interacting surface. Residues are colored by properties: basic, blue; hydrophobic, gray; polar, yellow.

1.3.3 The diverse functions of bactofilin in bacteria

Bactofilin is widespread in bacteria and participates in a variety of cellular processes (*Figure 10A*). In the model organism *C. crescentus*, the two bactofilin paralogues, BacA and BacB, assemble into a sheet-like structure lining the cytoplasmic membrane at the stalked cell pole. The polymer is important for the polar localization of a bifunctional penicillin-binding protein, PbpC, which elongates the stalk [113] (*Figure 10A*). In *Asticcaculis biprothecum* (*A. biposthecum*), a close relative of *C. crescentus*, bactofilin is also involved in stalk biosynthesis [124]. It is initially recruited to the future stalk site by a peptidoglycan (PG) hydrolase homolog, SpmX, and then serves as a scaffold for a PG remodeling complex including SpmX. Without bactofilin, cells produce "pseudostalks" as a consequence of unregulated PG synthesis. However, bactofilin has a different role in *H. pylori* [120], *P. mirabilis* [112], the spirochete *Leptospira biflexa* (*L. biflexa*) [125] and *Myxococcus xanthus* (*M. xynthus*) [126], in all of which it determines cell shape. Take the bactofilin homologue CcmA from *H. pylori* as an instance (*Figure 10B*). According to Taylor *et. al*, it works in concert with MreB to maintain cell shape [120]. CcmA locates preferentially to the cell envelope regions of positive Gaussian curvature, where it orchestrates peptidoglycan synthesis. By contrast, MreB regulates the cell

wall remodeling at regions of Gaussian curvature near or below zero. It has been shown that *H. pylori* cells have a straight-rod-like shape instead of the characteristic helical morphology in the absence of CcmA. Furthermore, bioinformatics analysis has demonstrated that bactofilins are often encoded in an operon with M23 endopeptidases in many species (*Figure 10C*), which is an indication that they might interact with M23 endopeptidases and affect cell morphology through them. However, solid evidence is required to confirm this hypothesis. In *P. mirabilis* [112] and *L. biflexa* [125], bactofilin also affects motility besides functioning as a shape determinant. Bactofilin is even more versatile in *M. xanthus*, where four bactofilin homologues divide the labor and play multiple roles. In addition to the standalone cell shape determinant BacM, the other three homologues, namely BacN, BacO and BacP, form a co-polymer at both cell poles with BacP as the central component. On the one hand, BacP retains the ParAB*S* segregation machinery in the subpolar regions through a ParA-like adapter protein, named PadC [127, 128] (*Figure 11A*). On the other hand, it collaborates with a small GTPase SofG to establish the polar localization of two type IV pili (T4P) motor ATPases PilB and PilT [34] (*Figure 11B*).

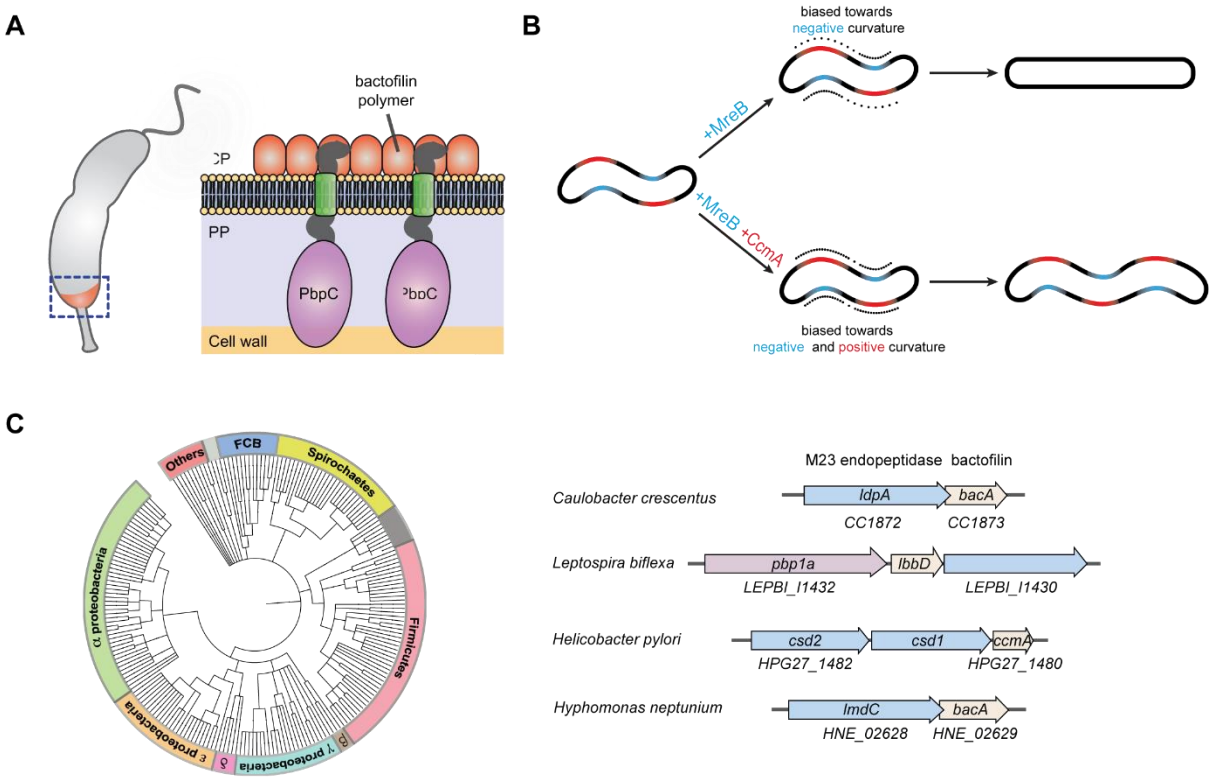

Figure 10 Bactofilins function as scaffolds for cell wall-remodeling enzymes. (A) Bactofilins in *C. cresentus* polymerize into a sheet-like structure recruiting PbpC to the stalked pole, which is important for stalk biogenesis (CP: cytoplasm, PP: periplasm). Image taken from [113]. (B) The bactofilin homologue CcmA works in concert with MreB to maintain the helical cell shape of *H. pylori*. Dots indicate different extents of cell wall remodeling. Regions of positive Gaussian curvature and negative Gaussian curvature are colored blue and red, respectively. Modified from [120]. (D) In many species, bactofilins are encoded in the same operon as M23 endopeptidases (left), as exemplified by *H. neptunium*, *L. biflexa*, *H. pylori* and *C. cresentus* (right) (unpublished data).

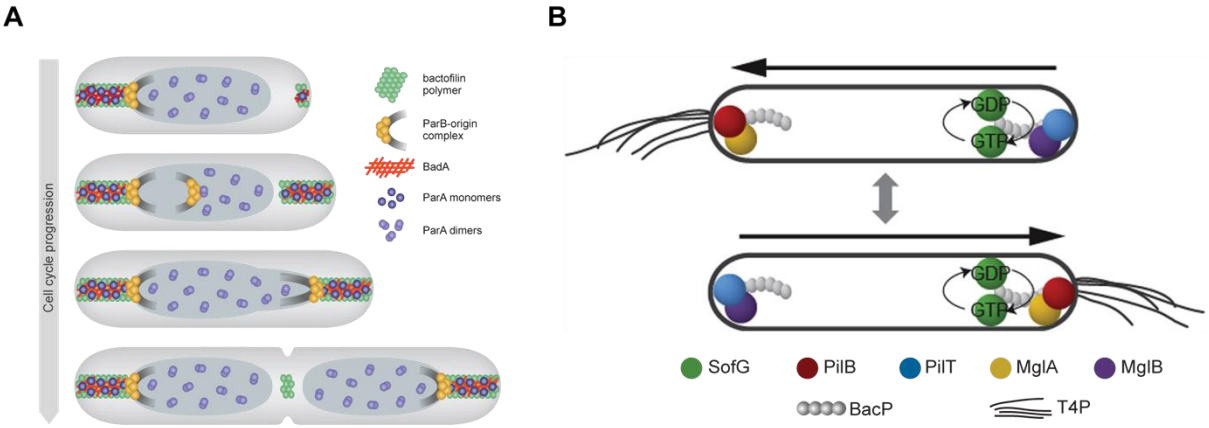

Figure 11 Bactofilin is also involved in cellular processes such as chromosome segregation and polarity establishment. (A) BacP forms sub-polar filaments together with BacN and BacO that anchor the ParB-origin complex through an interaction with the adapter protein PadC. Image taken from [127]. (B) BacP is also implicated in the establishment of the polar localization of the T4P motor ATPases PilB and PilT. Image taken from [34].

1.4 The cell wall of bacteria

Because one of the major functions of bactofilin is to act as scaffold for cell wall-remodeling proteins, which is also the case in the model organism *C. crescentus*, we will spend a few paragraphs to introduce the bacterial cell wall. The main component of the cell wall is peptidoglycan, a mesh-like macromolecule. It is the middle layer of the cell envelope of Gram-negative bacteria, sandwiched between the cytoplasmic membrane and the outer membrane. The peptidoglycan sacculus is the minimal requirement for cell shape and it can retain the cell shape in the absence of other cellular components [129] (*Figure 12*A). Moreover, the peptidoglycan layer prevents cell from bursting due to the turgor pressure [130].

1.4.1 The synthesis of peptidoglycan

Peptidoglycan is a polymer of glycan chains crosslinked by short peptides. The basic building block of PG is *N*-acetyl-glucosaminyl-*N*-acetyl-muramyl-L-alanyl-D-glutaminyl-L-(*meso*)diaminopimelyl-D-alanyl-D-alanine (GlcNAc-MurNAc-L-Ala-D-Glu-L-*meso*DAP-D-Ala-D-Ala), which is synthesized in the cytoplasm and linked to a membrane carrier before its incorporation into existing PG layer [131]. This whole process involves a series of enzymes [132] (*Figure 12B*). To be specific, it starts with the synthesis of MurNAc by MurA and MurB. MurNAc is further modified by MurC, MurD, MurE, MurF and MurI, which adds the peptide stem to it. Afterwards, MurNAc-peptide is linked to the membrane-embedded carrier undecaprenol (UDP) through MraY, producing Lipid I, which is then converted to Lipid II by MurG. At this point, the peptidoglycan precursor linked to UDP is still located in the cytoplasm and it needs the assistance of MurJ to be flipped to the periplasm, where the disaccharide unit forms a β-1,4-glycosidic bond with nascent glycan chains

through the action of glycosyltransferases (GTases). Subsequently, the peptide stems of adjacent glycan chains are interlinked by transpeptidases (TPases), which are also known as penicillin-binding proteins (PBPs), resulting in an elastic sacculus. The extension of PG requires not only synthases but also hydrolases that break down the existing bonds within PG. There are a range of cell wall hydrolases including amidases, glycosidases and peptidases that target different kinds of bonds [133]. Their activities are tightly regulated so that the integrity of cell wall is maintained during its growth and modification.

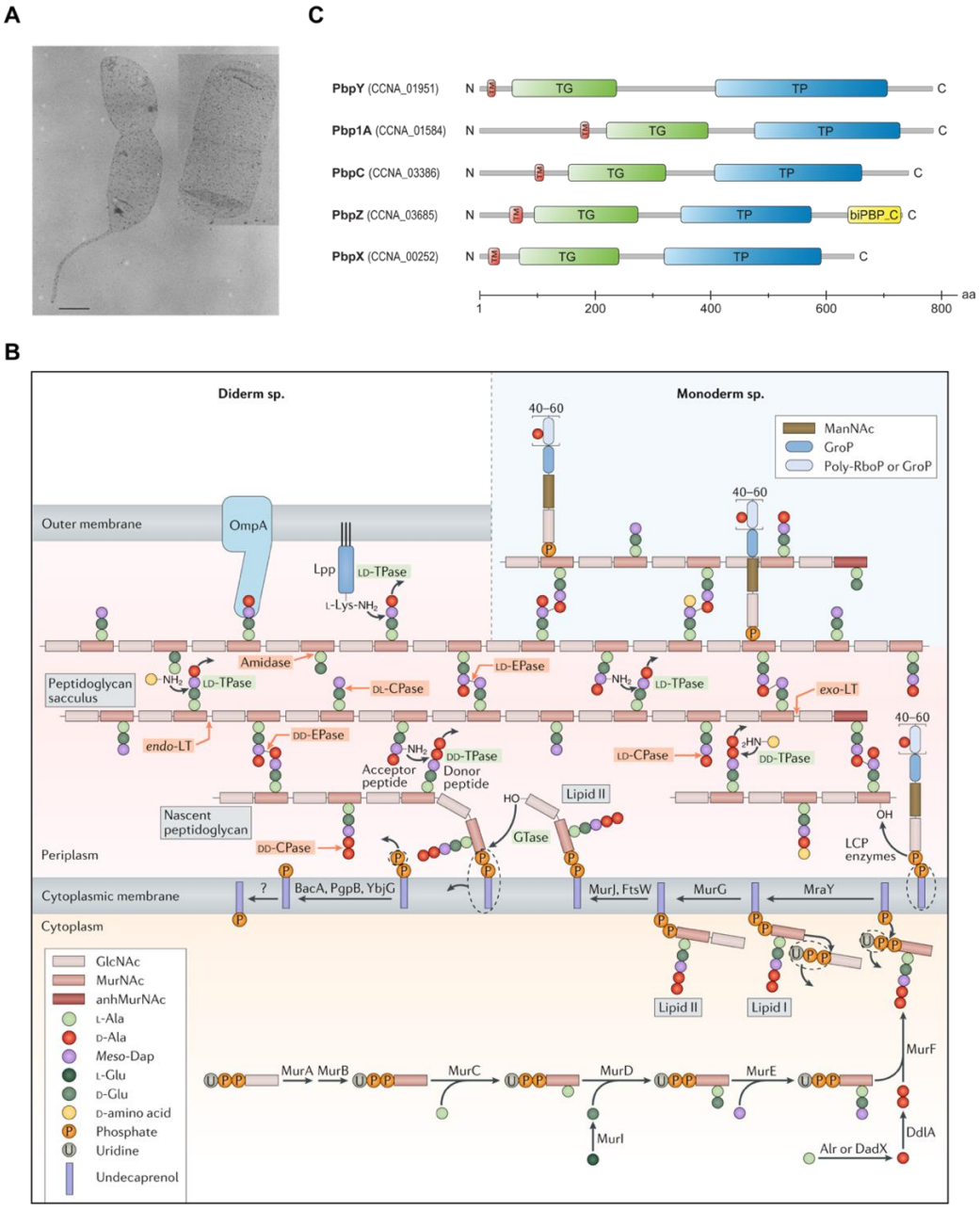

Figure 12 The peptidoglycan layer determines the cell shape and its synthesis is a multi-step process. (A) The cell wall retains its shape even in the absence of other cellular components. Image taken from [129]. (B) The remodeling of the cell wall involves several enzymes. Image taken from [132]. The details of this process can be found in text. (C) Bifunctional PBPs have both GTase and TPase activity. In total, there are five bifunctional penicillin-binding proteins in *C. crescentus*. Image taken from [134].

1.4.2 Penicillin-binding proteins

As mentioned before, penicillin-binding proteins are essential for the growth of the sacculus. They own their name to the fact that they can be inhibited by penicillin, an antibiotic with a structure similar to the D-Ala-D-Ala moiety of the peptide side chain. PBPs can first be classified into two categories based on their molecular weight: the high-molecular-mass (HMM) PBPs and the low-molecular-mass (LMM) PBPs [135]. LMM PBPs are generally peptidases that participate in peptidoglycan maturation and recycling, whereas HMM PBPs are transpeptidases that crosslink the glycan chains. Based on their domain organization, HMM PBPs can be further divided into two types: 1) bifunctional class A PBPs with both GTase and TPase domains and 2) class B PBPs with only transpeptidase activity.

C. crescentus possesses five class A PBPs, namely Pbp1A, PbpX, PbpY, PbpC and PbpZ (*Figure 12C*). Their localization and function have been analyzed comprehensively. These PBPs appear to have distinct but redundant functions, since all paralogues except for PbpZ can sustain the normal growth of cells in the absence of the others [134]. PbpC interacts with the bactofilins through its cytoplasmic tail and it is implicated in the pathway of stalk biogenesis [136]. Moreover, it helps to anchor a stalk-specific protein, StpX, to the outer membrane, which in turn prevents the diffusion of PbpC into stalk [137].

1.4.3 The biosynthesis of stalk

In the majority of rod-shape bacteria, including *C. crescentus*, PG synthesis takes place either along the cell during cell elongation or at the septum upon cell division [138]. The lateral growth mode is regulated by the elongasome which is built on the basis of MreB, whereas pre-septal growth and cytokinesis are mediated by another PG biosynthesis machinery, the divisome, organized by FtsZ. In addition, there is a unique zonal growth mode in *C. crescentus* because of its characteristic stalk [139]. As aforementioned, the extension of the stalk depends on bactofilin homologues and PbpC, but they are not the deterministic factors, as the deletion of them only causes a moderate shortening of the stalk [136, 140]. A systematic analysis of proteins involved in stalk growth has been conducted under phosphate starvation, which revealed a pole-associated machinery composed of several proteins (*Figure 13*). According to Billini et al, the actin homologue MreB is vital for building the stalk and a malfunctional mutant of it produces a completely stalkless morphology regardless of the growth conditions [140]. The other components of elongasome such as the membrane protein RodZ and the transglycosylase/transpeptidase pair RodA/PBP2 also associate with the stalk base and affect the stalk length to different extents. Interestingly, several autolytic proteins related to the divisome contribute to proper stalk growth as well. They include the

catalytically inactive LytM-like protein DipM, the soluble lytic transglycosylases SdpA/SdpB and the carboxypeptidase CrBA. Therefore, it appears that the existing PG remodeling machinery can be redirected and organize into a new functional group to regulate the stalk biosynthesis in the phosphate-limiting condition.

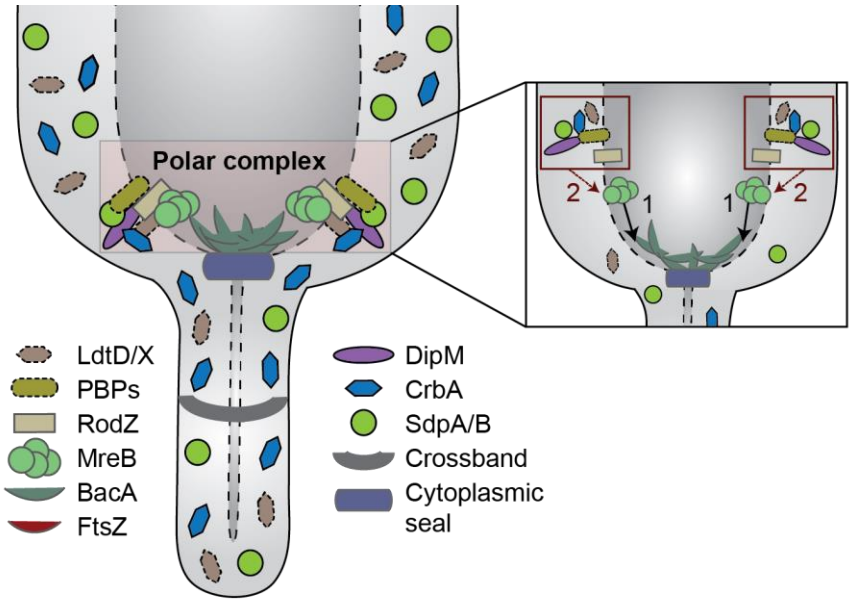

Figure 13 Model of polar stalk biosynthesis in phosphate-limiting condition. The formation of the stalk is determined by the actin homologue MreB. A number of proteins usually associated with elongasome (RodZ, RodA and PBP2) and divisome (DipM, SdpA/B and CbrA) are important for proper stalk length as well. In addition, another cytoskeleton, BacA, and its recruited PbpC constitute an accessory part of the polar complex. Their presence promotes the growth of the stalk but is not decisive. Image taken from [140].

1.5 Scope

Cytoskeletal proteins are vital for bacteria as they are involved in a range of cellular processes, such as chromosome segregation, cell division and cell shape maintenance. Bactofilin polymers are a widespread group of cytoskeletal filaments in bacteria. They are largely limited to prokaryotes without a counterpart in eukaryotes, which highlights their uniqueness. Moreover, it is not possible to obtain insights into their polymerization mechanism, biochemical characteristics and functions from studies on eukaryotic cytoskeletons. Although several breakthroughs have been achieved recently, we still lack a comprehensive view of the biological importance of bactofilins and their mode of action in bacteria. Consequently, this work studies bactofilins in the model organism *C. crescentus* with the intention to provide the missing information. Specifically, the following questions will be addressed: (i) Which residues in bactofilin are crucial for protofilament formation and how do protofilaments further assemble into higher-order structures? (ii) What is the mechanism underlying the membrane association of bactofilin? (iii) How does bactofilin interact with

PbpC? (iv) Are there additional proteins interacting with bactofilins in *C. crescentus* and do they utilize the same mechanism as PbpC to interact with bactofilins?

2 Results

2.1 The polymerization mechanism of bactofilin

Bactofilin is able to polymerize spontaneously, depending on the highly conserved central domain. Solid-state NMR analyses have revealed that the bactofilin domain adopts a right-handed β-helical architecture [116, 117]. Monomers of bactofilin first polymerize into a non-polar protofilament through end-to-end association [114] and then further assemble into higher-order structures, such as bundles and 2D-crystalline sheets [118, 141]. Several lines of evidence have pointed out that the formation of protofilaments appears to be mediated by hydrophobic interaction [114, 119, 141]. Nevertheless, a systematic screening of essential hydrophobic residues at the end of the bactofilin domain is lacking. Moreover, it is still enigmatic how protofilaments interact with each other laterally to form bundles and 2D sheets. Hence, we decided to address these open questions using the bactofilin homologue BacA in *C. crescentus* as a model.

2.1.1 Identification of conserved hydrophobic residues at the end of the bactofilin domain

To identify amino acids at the end of the bactofilin domain responsible for the hydrophobic interaction between monomers, an alignment of bactofilins domain (466 sequences) was retrieved from Pfam database [142]. Based on the alignment, the conservation score of each residue was calculated by the Scorecons server (scoring method: entropic, 21 types) [143]. The analysis uncovered a number of conserved hydrophobic residues at the end of the bactofilin domain. In combination with the structure, we identified several candidates. At the N-terminus, there are L42, L46, I48, and V52, whereas L122, M124, and F130 are identified at the C-terminus (*Figure 14A*). We then attempted to create docking models using the NMR structure of BacA (PDB ID: 2N3D) with the help of ClusPro server [144] by setting these residues to be attractive [145]. Below are two examples, in which two BacA monomers perfectly stack against each other (*Figure 14B*). When no restriction was implemented, we also obtained models in which monomers interact laterally, implying the existence of lateral interactions between protofilaments.

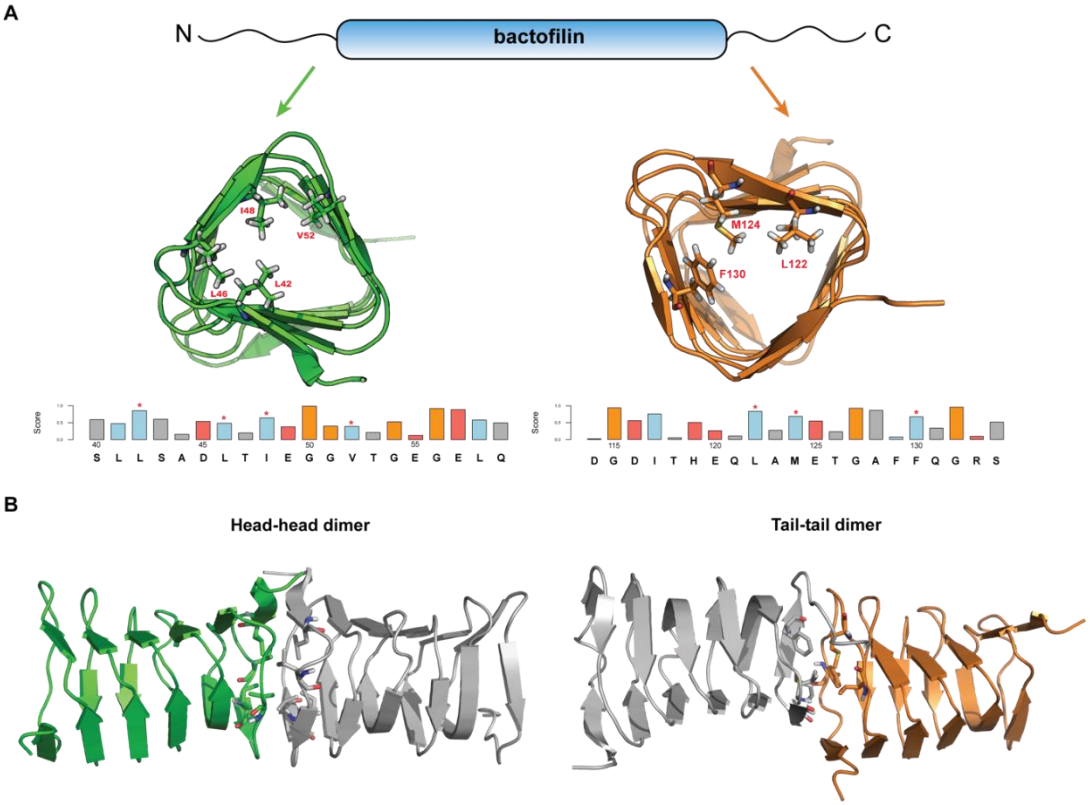

Figure 14 Identification of conserved amino acids at the ends of the bactofilin domain. (A) Based on a sequence alignment (466 sequences), the conservation score for individual residues was calculated, which ranges from 0 (no conservation) to 1 (complete conservation). Numbers give the position of residues in the sequence of BacA from *C. crescentus*. Asterisks denote hydrophobic amino acids that are conserved. (B) Two representative docking models display either the head-head association (left) or the tail-tail association (right). In the predicted models, conserved hydrophobic residues face towards each other.

2.1.2 Point mutation of conserved amino acids delocalizes BacA

To test whether these conserved hydrophobic residues identified in the bioinformatics analysis are crucial for the polymerization of BacA, we mutated them to either polar or charged amino acids. The variants were labeled with the yellow fluorescent protein Venus at the C-terminus for localization studies. If the mutations disrupt the hydrophobic interactions between monomers, the localization behavior of these variants is expected to change. Indeed, all mutants lost their typical polar localization and were diffuse in the cells, which was in sharp contrast to the wild-type protein (*Figure 15*). Immunoblot analysis showed that all fusion proteins were stable (*Figure S1*), excluding the possibility that the diffuse signals were due to the cleavage of fluorescent protein. Noticeably, some variants still formed a few random foci within cells, which could be explained by the high expression level of proteins under the control of the xylose-inducible P*xyl* promoter. Even though mutations weakened the hydrophobic interaction, the overly high concentration of protein may still push variants towards polymerization [114]. In conclusion, these results confirm that the formation of protofilaments is mediated by hydrophobic interactions, and all identified hydrophobic residues contribute to the polymerization.

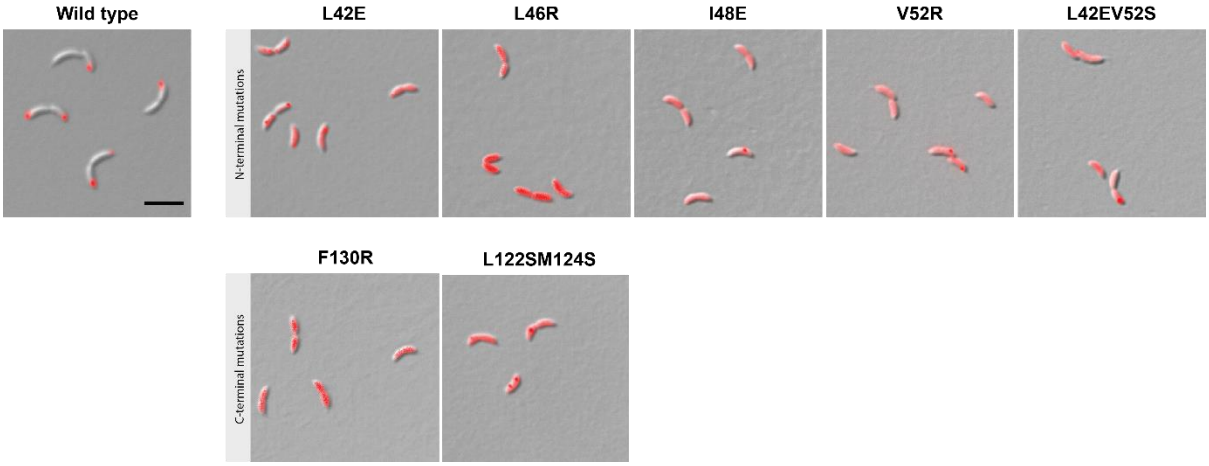

Figure 15 Subcellular localization of BacA variants. BacA variants containing mutations of conserved hydrophobic residues were diffuse within cells, which was different from the polar localization of the wild-type protein. Cells of strain LY1 (Δ*bacAB xylX*::P*xyl-bacA*$_{L46R}$-*venus*), LY2 (Δ*bacAB xylX*::P*xyl-bacA*$_{L42E}$-*venus*), LY3 (Δ*bacAB xylX*::P*xyl-bacA*$_{V52R}$-*venus*), LY4 (Δ*bacAB xylX*::P*xyl-bacA*$_{F130R}$-*venus*), LY5 (Δ*bacAB xylX*::P*xyl-bacA*$_{L122SM124S}$-*venus*), LY6 (Δ*bacAB xylX*::P*xyl-bacA*$_{L42EV52S}$-*venus*) and LY7 (Δ*bacAB xylX*::P*xyl-bacA*$_{I48E}$-*venus*) were grown to late exponential phase and diluted to an OD_{600} of ~0.1. After incubation for another hour, cells were induced with 0.005%xylose for 1 h before visualization by phase contrast (Ph3) and fluorescence microscopy. Scale bar: 3 µm.

2.1.3 The mutant fails to form large polymers *in vitro*

In order to assess the impact of the mutation of hydrophobic residues on the size of bactofilin polymers, we decided to purify one of these mutant variants, namely BacA$_{F130R}$. The corresponding allele was cloned in an overexpression vector fused to a sequence encoding C-terminal hexahistidine (His$_6$) tag. The calculated molecular mass of the recombinant protein is 18.45 kDa. After affinity chromatography, the purified protein was analyzed by size exclusion chromatography (SEC), which functions as a molecular sieve and separates proteins mainly based on their size. According to the elution profile, purified BacA$_{F130R}$-His$_6$ was composed of two species (*Figure 16*). One of them existed as a gigantic polymer of approximately 868 kDa and eluted at an early stage. This species only constituted a small fraction of the purified protein, and it might form due to the high concentration of protein, which favors the polymerization of bactofilin. Nevertheless, the majority protein eluted at a later stage corresponding to a molecular weight about 84.6 kDa, which appears to be a tetramer. Although our initial assumption is that the mutation of phenylalanine (F130) would interfere the interaction between the C-terminal interface of the monomers, resulting in head-head dimers, the estimated molecular mass of the purified protein is larger than expectation. Since the correlation between molecular weight and size (specifically Stokes radius) only holds well for globular proteins but not for proteins of deviant shapes [146, 147], it is possible that the estimated molecular weight of purified BacA$_{F130R}$-His$_6$ is inaccurate and does not properly reflect the actual oligomeric state of the protein. Together with the

localization studies, our results suggest that the mutation of conserved hydrophobic residues at the end of bactofilin domain has negative effects on the polymerization of bactofilin.

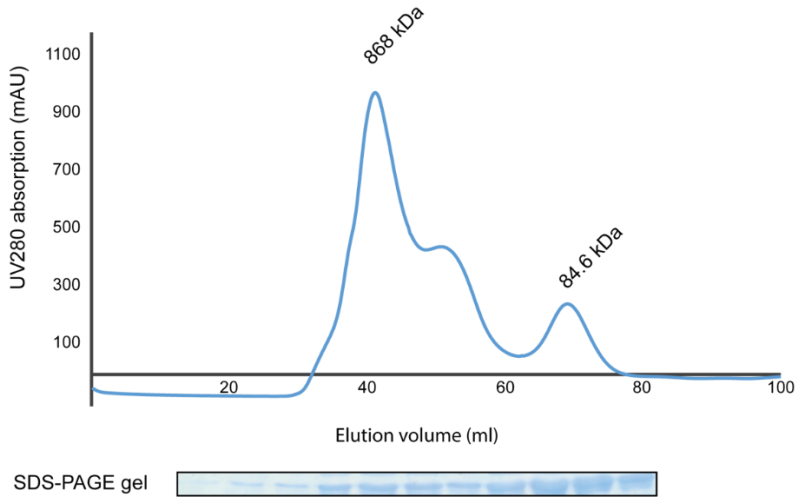

Figure 16 Elution profile of BacA$_{F130R}$-His$_6$ on a HiLoad® 16/200 superdex® 200 pg SEC column. The purified protein was constituted by two distinct species. One of them was a large polymer of about 868 kDa, whereas the other one had a molecular weight of approximately 84.6 kDa. The strip below shows sample from each fraction in an SDS-PAGE gel.

2.1.4 Identification of lateral interaction sites by crosslinking

Bactofilins from phylogenetically divergent species were shown to form bundles or two-dimensional sheets [114, 118, 119, 136], indicating that there may be lateral interfaces between the protofilaments. Although the longitudinal interaction between bactofilin subunits that promotes the formation of protofilaments has been unveiled, we have little information regarding to inter-protofilament interactions. To shed light on the nature of lateral interfaces, a chemical crosslinker bis(sulfosuccinimidyl)suberate (BS^3) was used. BS^3 contains an *N*-hydroxysulfosuccinimide (NHS) ester at each end of its 11.4 Å-long spacer arm (*Figure 17A*), which enables it to react readily with primary amines in the side chain of lysine residue (K) or at the N-terminus of the polypeptide [148]. Purified BacA was mixed with a 10-, 20- and 40-fold molar excess of BS^3 for different period of time and lysines within the length of the spacer arm were crosslinked. The crosslinked species were first separated by gel electrophoresis and then analyzed by mass spectrometry (*Figure 17B*).

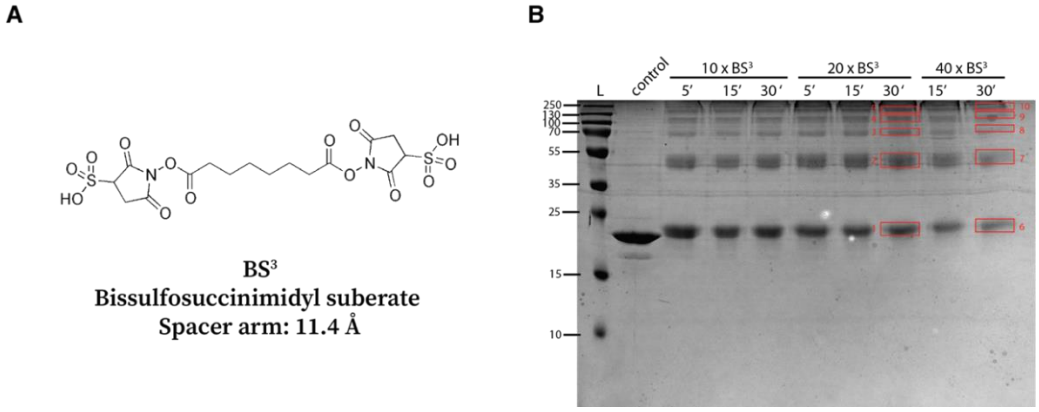

Figure 17 Structure of BS³ and crosslinked species of purified BacA. (A) BS³ is a homobifunctional, water-soluble, amine-to-amine crosslinker with an 11.4 Å-long spacer arm. (B) Purified BacA was incubated with a 10-, 20- and 40-fold molar excess of BS³ for different period of time and then applied to an SDS-PAGE gel to separate differently crosslinked species. Bands highlighted by red boxes were cut out for mass spectrometric analysis.

The mass spectrometry results showed that four out of eight lysines in BacA were crosslinked by BS³. The most frequent crosslinks were at K11-K11, K11-K103, K11-K136, K11-K144 and K103-K103 (*Figure 18*). Given that K11 is located in the N-terminal tail of BacA, we analyzed the impact of the N-terminal region on *in vitro* polymerization by transmission electron microscopy (TEM). A variant lacking N-terminal tail ($BacA_{\Delta N}$) was purified as a fusion protein with a SUMO-tag at its N-terminals. The visualization by TEM demonstrated that BacA retains its bundling property in the absence of the N-terminal region (*Figure 19*). We reasoned that the abundant crosslinking of K11 is due to the fact that it is located in the flexible tail, which makes it more accessible. As for the K103-K103 pair, the likelihood that they were crosslinked by chance is low, because the other lysins (K37, K65 and K137) in the bactofilin domain are also exposed but not crosslinked. Therefore, we concluded that the region containing K103 may be involved in the inter-protofilament interaction. We mapped K103 on models from the docking analysis in order to have a better view of the potential interface. Four out of five models contain K103 in the interface and the distance between neighboring K103 residues is within the length of the spacer arm (*Figure 20*). Nevertheless, the remaining prediction is not necessarily invalid. Because the large assemblies are multi-stranded, there should be more than one interface. The existence of only one interface, which is self-limiting, would only lead to double-stranded filaments. Notably, additional charged amino acids, such as aspartic acid, glutamic acid and arginine, were present in the interface in all predicted models, resulting in surfaces of complementary charge. Thereby, we hypothesized that electrostatic force possibly plays a role in the lateral interaction between BacA protofilaments.

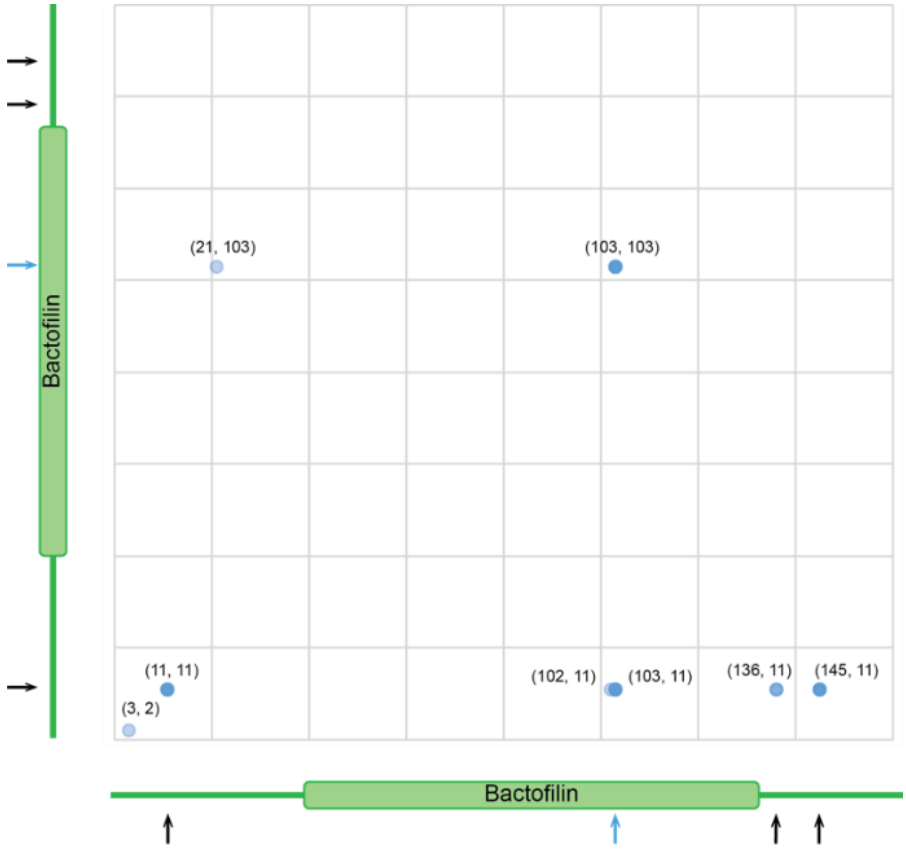

Figure 18 Mass spectrometry analysis of residues crosslinked by BS³. The majority of crosslinked amino acids are lysines except for serine (S) at position 3 and threonine (T) at position 21. Identified lysines are distributed along BacA with K11 in N-terminal tail, K136 and K144 in C-terminal tail, and K103 located on the surface of the bactofilin domain. The number of each hit detected by mass spectrometry is denoted by the opacity of the dots. High opacity means more hits were detected. The position of crosslinked lysines on BacA is indicated by arrows.

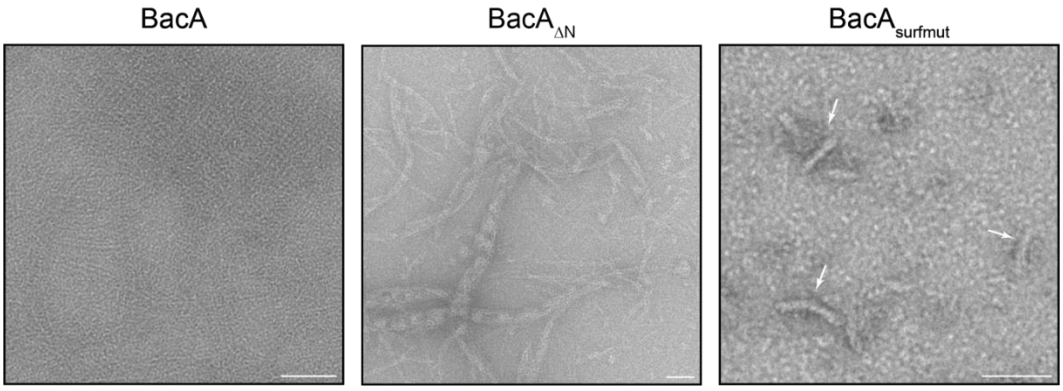

Figure 19 The oligomeric state of BacA variants visualized by TEM. Wild-type BacA (left) and the variant without the N-terminal region (middle) was capable of forming higher-order structures, whereas the variant with exchanges in charged surface residues (right) can only assemble into short fibers (indicated by white arrows). Scale bar: 50 nm.

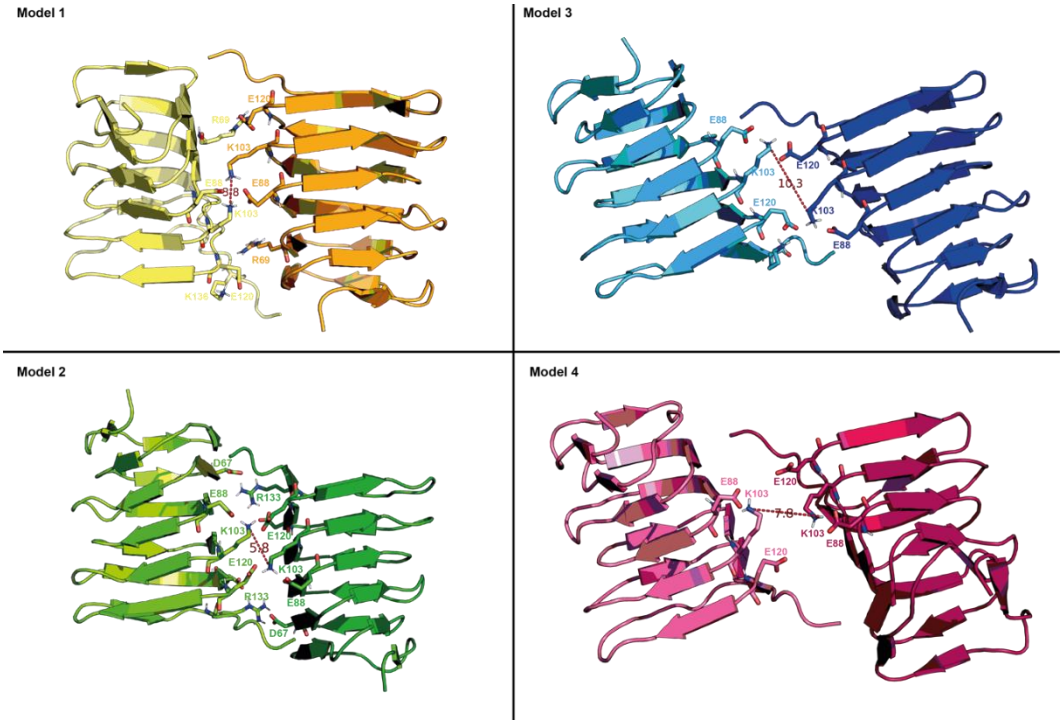

Figure 20 The lateral interaction models for BacA predicted by the ClusPro server. All predications have K103 on the interface and the distance between K103 in each interface is shorter than the spacer arm of BS^3. Additional charged amino acids, such as aspartic acid (D), glutamic acid (E) and arginine (R), are found in the interface as well.

2.1.5 The impact of charged amino acids on the polymerization of bactofilin

Compared with the hydrophobic residues that build the core of the β-helix, charged amino acids are less conserved in bactofilin. They normally face outwards, which generates a charged protein surface (*Figure S2*). To determine if electrostatic forces affect the inter-protofilament lateral interactions, we simultaneously mutated four acidic residues, namely D61, E88, D116 and E120, to threonine. These residues were chosen because they are either more conserved or located in the predicted lateral interaction interface. Although not part of the hydrophobic core of β-helix, their exchange could possibly affect polar contacts between the β-strands and thus destabilize the whole structure. To evaluate the potential effect of the exchange on the structure of the bactofilin domain, we compared the polar contacts of the wild-type protein with those of the mutant protein (referred as $BacA_{surfmut}$ in the following text). The analysis showed that there is no major alteration except for one contact that is missing when D61 is converted to threonine (Figure *21A*). We therefore conclude that bactofilin could fold properly despite the simultaneous introduction of four mutations.

In the next step, the variant was fused to a C-terminal mVenus fluorescent protein and was expressed in a Δ*bacAB* strain under the control of the xylose-inducible P*xyl* promoter. In contrast to the polar localization of the wild-type protein, $BacA_{surfmut}$-mVenus was evenly

distributed within cells (*Figure 21B*). The Western blot analysis (*Figure S3*) showed that the fusion protein was relatively stable, indicating that the fluorescence signal was representative of the subcellular localization of $BacA_{surfmut}$. In order to provide direct experimental evidence that exchanges negatively affect the polymerization of BacA into macromolecular structures, the mutant protein was purified as a fusion protein with a Strep-II tag at its C-terminus and was further analyzed by transmission electron microscopy. It appeared that the $BacA_{surfmut}$ retained the ability to polymerize. However, it only formed short fibers that were 30-40 nm long and ~9 nm wide (*Figure 19*). In comparison, the wild-type protein assembled into either extended bundles or 2D sheets consisting of multiple protofilaments (*Figure 19*), which is consistent with previous observations [141]. In brief, these data indicate that the charged amino acids on the surface of BacA may contribute to the lateral interaction, which may in turn be required for efficient longitudinal polymerization.

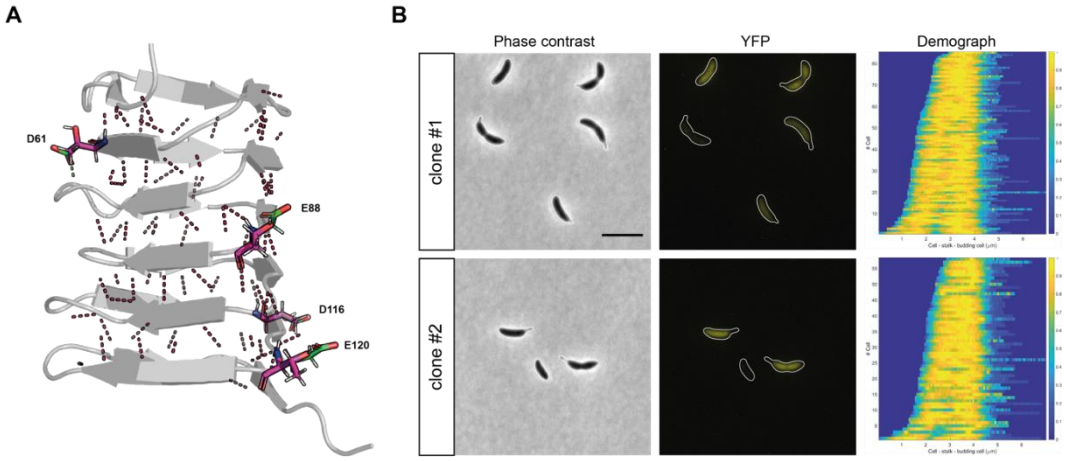

Figure 21 Effect of the exchange of charged surface residues on BacA. (A) When the acidic amino acids D61, E88, D116 and E120 (colored in green) were mutated to threonine (colored in magenta), the majority of polar contacts within the structure was unaltered, except for the one involved in the side chain of D61. Unchanged polar contacts are colored in red, whereas the missing one is green. (B) $BacA_{surfmut}$-mVenus lost the typical polar localization. Cells of strain LY83 (Δ*bacAB xylX*::P*xyl-bacA*$_{surfmut}$-*mvenus*) were grown to late exponential phase and diluted to an OD600 of ~0.1. After incubation for another hour, cells were induced with 0.3% xylose for 1 h before visualization by phase contrast (Ph3) and fluorescence microscopy. Demographs summarizing the single cell fluorescence profiles are given at the bottom (n = 85 cells for clone 1 and 58 cells for clone 2). Scale bar: 3 µm.

2.2 The membrane association of bactofilin

Several lines of evidence indicate that bactofilins associate closely with the cytoplasmic membrane [114, 120, 136]. However, the membrane binding mechanism remains unclear. One possibility is that bactofilin interacts with yet unidentified membrane proteins. Alternativelly, it could interact directly with the membrane. According to Deng et al., the latter hypothesis is more likely, as they revealed a conserved motif with a conspicuous

phenylalanine residue located at the N-terminus of bactofilins, which was required for membrane binding *in vitro* [114].

2.2.1 BacA interacts with membrane through the N-terminal motif

To confirm whether the proposed region at the N-terminal end is essential for the membrane targeting of BacA, we deleted it and fused the fluorescent protein mVenus to the C-terminus of the mutant protein. The localization of the resulting fusion, $BacA_{\Delta 2\text{-}8aa}$-mVenus, was different from that of the wild-type protein, as it displayed uniformly diffuse signal (*Figure 22A*), which suggests that the deleted region is essential for membrane localization. Immunoblot analysis (*Figure S4*) confirmed that the protein was stable, eliminating the possibility that the even distribution of $BacA_{\Delta 2\text{-}8aa}$-mVenus was due to the cleavage of fluorescent tag. However, when the identified membrane-targeting sequence was analyzed carefully, it did not appear to be very hydrophobic. Actually, charged amino acids intermix with hydrophobic ones, which gives rise to the possibility that the suggested region folds into an amphipathic helix when it binds to the cytoplasmic membrane. There are a few cases of cytoskeletal proteins interacting with the lipid membrane via an amphipathic helix, for instance, MreB [75] and FtsA [121]. To investigate the possibility, we arranged a few proposed membrane-targeting sequences of bactofilins into helical wheels, which can reveal if hydrophobic residues concentrate on one side of the helix, usually with polar and hydrophilic residues on the other side, indicating the formation of an amphipathic helix. Nevertheless, none of the sequences displayed a typical amphipathic-helix arrangement (*Figure 22B*). Moreover, it was noticeable that a number of positively charged amino acids were present in the N-terminal region of bactofilin. Because the membrane of *C. crescentus* is negatively charged [123], it is reasonable to assume that electrostatic forces also play a role in the membrane interaction.

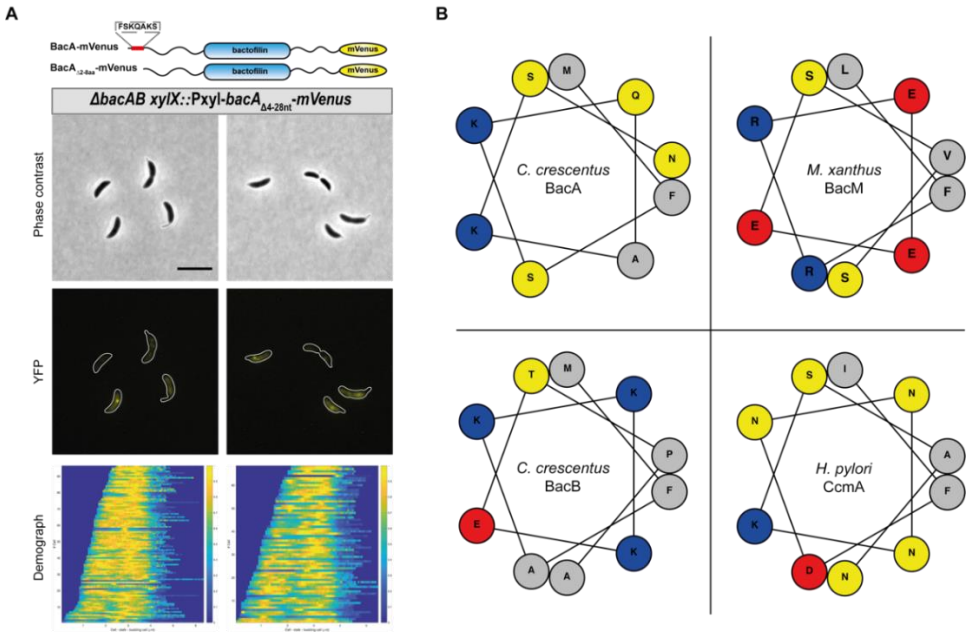

Figure 22 The proposed membrane-targeting motif of BacA appears to be essential for the membrane association of BacA but it does not fold into an amphipathic helix. (A) The schematic representation of fusion protein and its localization pattern. Cells of strain LY84 (Δ*bacAB xylX*::P*xyl-bacA*$_{\Delta 4\text{-}32nt}$-*mvenus*) were grown to late exponential phase and diluted to an OD600 of ~0.1. After incubation for another hour, cells were induced with 0.3% xylose for 3 h before visualization by phase contrast (Ph3) and fluorescence microscopy. Demographs summarizing the single cell fluorescence profiles are given at the bottom (n = 96 cells for clone 1 and 68 cells for clone 2). Scale bar: 3 µm. (B) Helical wheel diagrams of suggested membrane-targeting sequences of bactofilins. Charged and hydrophilic residues intersperse among hydrophobic ones, which indicates that the identified region does not fold into an amphipathic helix. Residues are colored by properties: basic, blue; acid, red; hydrophobic, gray; polar, yellow.

2.2.2 Screening for critical residues mediating membrane association

In order to gain insight into the mechanism underlying the membrane binding of bactofilin, we systematically mutated each residue within the membrane-targeting sequence and analyzed the subcellular localization of the mutant proteins. Except for the variant with the mutation of serine (S) at position 8, the others could be readily expressed under the control of xylose-inducible promoter. Based on their subcellular localization, the mutants can be classified into three categories. The first group behaved similarly to wild-type BacA and displayed polar localization in most cases (*Figure 23*). It consists of two variants, one of which has the mutation of serine at position 3 (BacA$_{S3A}$), while the other one carries an exchange of glutamine (Q) at position 5 (BacA$_{Q5A}$). The second group, which is composed of BacA$_{K4S}$, BacA$_{A6S}$ and BacA$_{K7S}$, by contrast, had a localization pattern between the wild type and the deletion mutant BacA$_{\Delta 2\text{-}8aa}$ (*Figure 24*). They were still able to form foci, but not necessarily at the stalked pole. BacA$_{K4S}$ and BacA$_{A6S}$ had the tendency to form an additional focus at the midcell, whereas the localization of BacA$_{K7S}$ was more random and unpredictable. Analogues to the varaiant lacking the whole membrane-targeting sequence, the third group, BacA$_{F2Y}$ and BacA$_{K4SK7S}$, were diffuse within cells (*Figure 25*), indicative of a complete loss of membrane binding or a great reduction in the affinity. The localization behavior of the

variant lacking two lysine residues appears to be the result of an additive effect of the single mutations. The stability of fusion proteins was confirmed by immunoblots (*Figure S5*), indicating that the observed signal can reflects the real localization of the BacA variants.

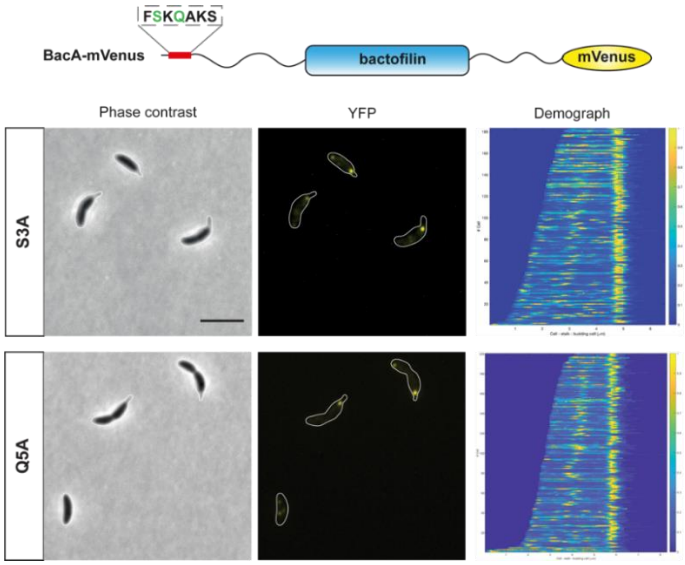

Figure 23 BacA$_{S3A}$ and BacA$_{Q5A}$ localize to the stalked pole as the wild type protein. Cells of strain LY95 (Δ*bacAB xylX*::P*xyl-bacA*$_{S3A}$*-mvenus*) and LY96(Δ*bacAB xylX*::P*xyl-bacA*$_{Q5A}$*-mvenus*) were grown to late exponential phase and diluted to an OD600 of ~0.1. After incubation for another hour, cells were induced with 0.3% xylose for 1.5 h before visualization by phase contrast (Ph3) and fluorescence microscopy. Demographs summarizing the single cell fluorescence profiles are given at the bottom (n = 183 cells for LY95 and 200 cells for LY96). Scale bar: 3 µm.

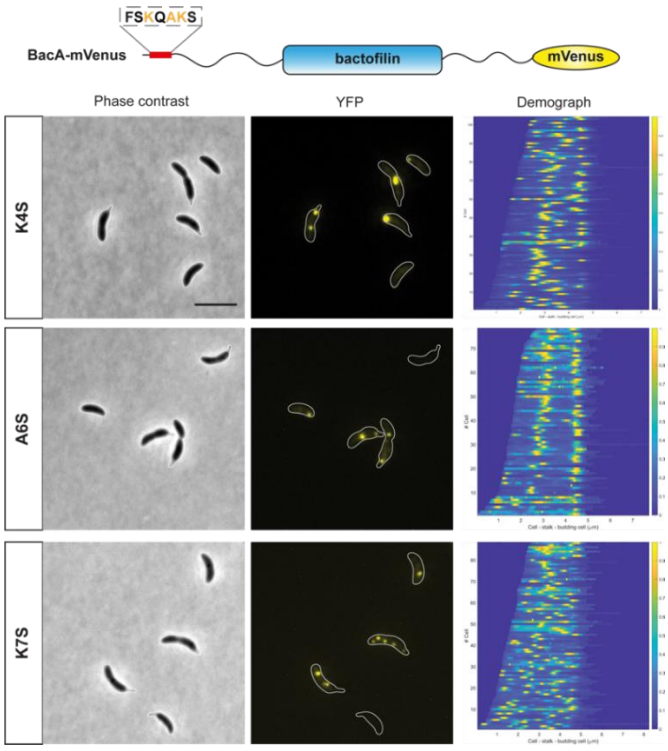

Figure 24 The localization pattern of BacA$_{K4S}$, BacA$_{A6S}$ and BacA$_{K7S}$ is between that of BacA and BacA$_{Δ2\text{-}8aa}$. Cells of strain LY88 (Δ*bacAB xylX*::P*xyl-bacA*$_{K4S}$*-mvenus*), LY91(Δ*bacAB xylX*::P*xyl-bacA*$_{A6S}$*-mvenus*) and LY92 (Δ*bacAB xylX*::P*xyl-bacA*$_{K7S}$*-mvenus*) were grown to late exponential phase and diluted to an OD600 of ~0.1. After incubation for another hour, cells were induced with 0.3 %xylose for 1.5 h before visualization by phase contrast (Ph3) and fluorescence microscopy. Demographs summarizing the single cell fluorescence profiles are given at the bottom (n = 64 cells for LY88, 78 cells for LY91 and 88 cells for LY92). Scale bar: 3 µm.

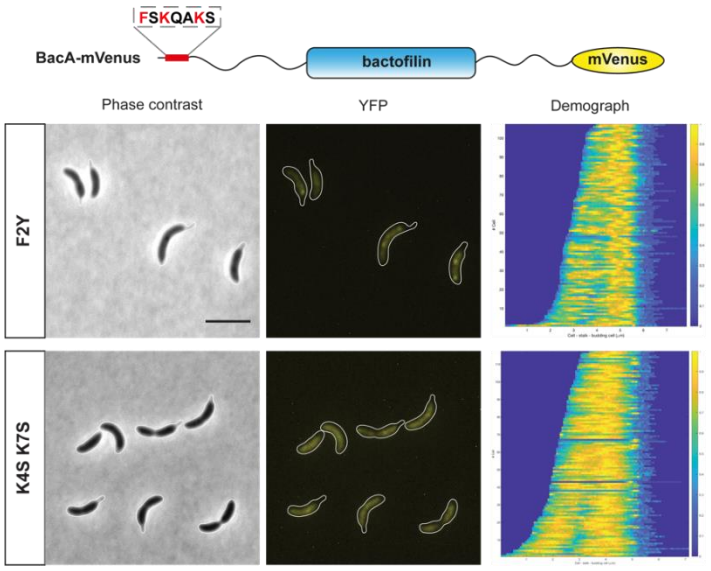

Figure 25 BacA$_{F2Y}$ and BacA$_{K4SK7S}$ show the same diffuse localization as the variant BacA$_{\Delta 2\text{-}8aa}$. Cells of strain LY97 (Δ*bacAB xylX*::P*xyl-bacA*$_{F2Y}$-*mvenus*) and LY89(Δ*bacAB xylX*::P*xyl-bacA*$_{K4SK7S}$-*mvenus*) were grown to late exponential phase and diluted to an OD600 of ~0.1. After incubation for another hour, cells were induced with 0.3% xylose for 1.5 h before visualization by phase contrast (Ph3) and fluorescence microscopy. Demographs summarizing the single cell fluorescence profiles are given at the bottom (n = 107 cells for LY97 and 117 cells for LY89). Scale bar: 3 µm.

Next, we performed single-particle tracking analyses on the deletion mutant (Δ2-8aa) and the above-described two mutants (F2Yand K4SK7S) showing similar localization pattern to the deletion mutant. Calculating the average mean squared displacement (MSD) of the fusion proteins, we found that Δ2-8aa was significantly more mobile than wild-type BacA. Although the mobility of K4SK7S and F2Y variants was also higher than that of the wild-type protein, the difference was not as pronouced as for the deletion variant (*Figure 26A*). Furthermore, the distribution of step sizes in the single particle tracks suggests that the existence of two distinct diffusion regimes, a mobile and a static population. For wild-type BacA, the mobile fraction comprised only 34.6% of the total population (*Figure 26B*). In contrast, approximately three quarters of the population of the deletion varaint were mobile. The proportion of mobile molecules was 57.1% and 63.7% for the F2Y and K4SK7S variants, respectively. These results support the finding of our localization study and provide additional information regarding to the affinity of different mutants to the lipid membrane. As expected, the absence of the whole membrane targeting sequence has the greatest impact on the association to the membrane. The decrease in the binding affinity is not identical for the other two variants, with the double mutation being more dramatic.

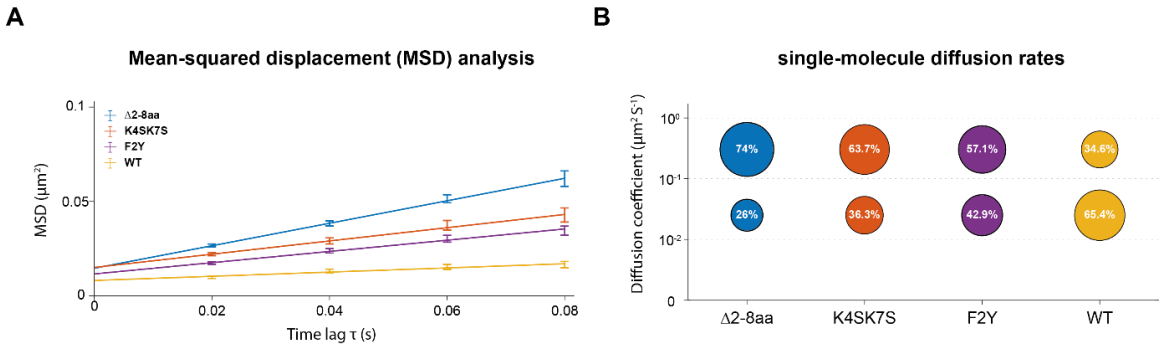

Figure 26 The dynamics of identified membrane-binding impaired mutants. (A) Mean-squared displacement analysis of the mobility of the indicated BacA-mVenus fusions based on live-cell single-molecule localization microscopy data. Error bars indicate the SD. (B)Bubble plots showing the single-molecule diffusion rates of the indicated BacA-mVenus fusions. The values were obtained by fitting the probability distributions of the frame-to-frame displacements from (A) to a two-component Gaussian mixture model assuming that the populations are composed of a mobile (top) and a static (bottom) fraction.

2.2.3 Interaction of membrane-binding impaired BacA variants with liposomes

In light of the above results, we wondered if the mutants behave consistently *in vitro*. To this end, we mixed purified BacA variants with liposomes and then separated liposome-bound from unbound protein by ultracentrifugation (*Figure 29A*). The liposomes were made of negatively charged phosphatidyglycerol to mimic the charge of the cytoplasmic membrane of *C. crescentus* [123]. In the absence of liposomes, the majority of proteins stayed in the supernatant fraction, regardless of the nature of protein. However, the variants sedimented to the bottom to different degrees when liposomes were added. As expected, nearly all wild-type BacA was found in the liposome pellet. The co-sedimentation with liposomes was reduced to the largest degree for Δ2-8aa variant. Approximately 40% of protein was found in the unbound state. As for the K4SK7S variant, the soluble fraction was lower with only 20% of total protein remaining in the supernatant. Strikingly, the supernatant/pellet distribution of the F2Y varaint was similar to that of the wild-type protein. We additionally performed a vesicle flotation assay, in which liposomes and associating protein migrate up a sucrose gradient to the topmost fraction rather than down into the pellet to substantiate our findings from the co-sedimentation assay (*Figure 29B*). There was a basal level of around 15% total protein in the top fraction for all variants when liposomes were omitted. In the presence of liposomes, we again observed the same association pattern as in the pelleting assay. More than 95% of wild-type BacA and F2Y was detected in the top layer. In contrast, only 78% of K4SK7S and 20% of Δ2-8aa co-floated with liposomes to the topmost fraction. Collectively, the *in vitro* results demonstrate that the removal of the whole membrane-targeting sequence and the exchange of two lysine residues diminished the affinity of bactofilin to lipid membrane, which is in line with the data from the single-particle tracking analysis. However, a few questions still need to be clarified: 1) Why does the mutant lacking

the proposed membrane-binding motif still interact with liposomes to some extent? 2) Given the even distribution of the F2Y variant in *C. crescentus* cells, why does it still interact with liposomes *in vitro*?

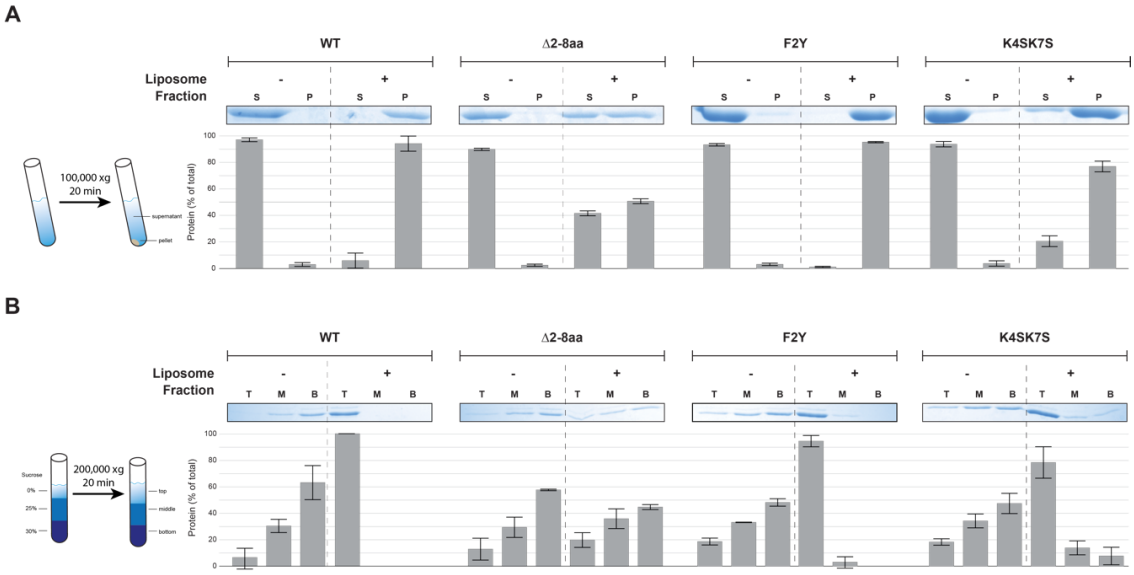

Figure 27 The identified BacA varaints bind to liposomes to different degrees in *vitro*. (A) Co-sedimentation analysis of the association of BacA variants to liposomes. A premix of 20 μM BacA variants ± 1.0 mg/mL liposomes was incubated at room temperature for 20 min before ultracentrifugation. The resulting supernatant (S) and pellet (P) fractions were analyzed on a 15% SDS-PAGE gel. A quantification of the BacA variants in each fraction is shown below each representative image. Error bars represent SD from three replicates. (B) Analysis of the membrane binding activity of BacA variants by a liposome flotation assay. A premix of 20 μM BacA variants ± 1.0 mg/mL liposomes was incubated at room temperature for 20 min before mixing with an equal volume of 60% sucrose binding buffer. Buffer with 25% sucrose and 0% sucrose were subsequently layered on top sequentially. During centrifugation, liposomes and associated protein migrate along the sucrose gradient to the uppermost fractions. The resulting fractions (Top T, Middle M and Bottom B) were analyzed by a 15% SDS-PAGE gel. A quantification of the BacA variants is shown below each representative image. Error bars represent SD from two replicates.

2.2.4 The polymerization of BacA may be provoked by membrane association

Given the discrepancy between the *in vivo* localization pattern and the *in vitro* interaction with liposomes observed for the F2Y variant, we hypothesized that even moderate changes in membrane affinity may have dramatic effects on the assembly of BacA structure. It is generally accepted that membrane recruitment increases the local concentration of the protein and protein interactions because the diffusion of the recruited protein is now confined to a two-dimensional surface. Due to the deficiency in membrane binding, the local concentration of F2Y *in vivo* may be too low to assemble into higher-order polymers, as evidenced by the evenly distributed yellow fluorescence signal. However, transmission electron microscopy confirmed that when the concentration of purified F2Y variant was high enough, it was still able to form large polymers *in vitro* (*Figure 28*). Compared with the monomers or short filaments, the large assemblies, in particular 2D-sheets, can provide more membrane binding sites, which can overcome the impaired affinity due to exchange of

phenylalanine, hence restoring the membrane association property. Therefore, we envisaged that if a membrane-targeting sequence is fused to $BacA_{\Delta 2\text{-}8aa}$, we may be able to observe foci *in vivo* again, given the coupling of membrane binding and polymerization. To this end, we fused two amphipathic helixes (1-11 aa) of *E. coli* MreB (EcMreB) in tandem to the N-terminus of the deletion variant (referred as chimera in the following text). The interaction between the lipid membrane and the amphipathic helix of EcMreB has been substantiated in a previous study [75] and by us in *E. coli* (*Figure S6*). As expected, the chimera fused to mVenus was able to form bright foci within *C. crescentus* cells (*Figure 29A*). The stability of the fusion was also confirmed by immunoblot to exclude the possibility that the fluorescent protein was cleaved off (*Figure S7*). Additionally, we noticed that these foci were distributed along the cell membrane. This was illustrated even better by the single-molecule tracking. An Overlay of all single molecule tracks from a typical time-lapse series revealed that the chimeric protein prefers to stay in the vicinity of the membrane (*Figure 29B*). Further analyses demonstrated that the chimera could not fully restore the polar localization of wild-type BacA but it was less mobile compared to the deletion mutant (*Figure 29C*). In brief, these results support the notion that the polymerization and membrane binding are intertwined and promote each other.

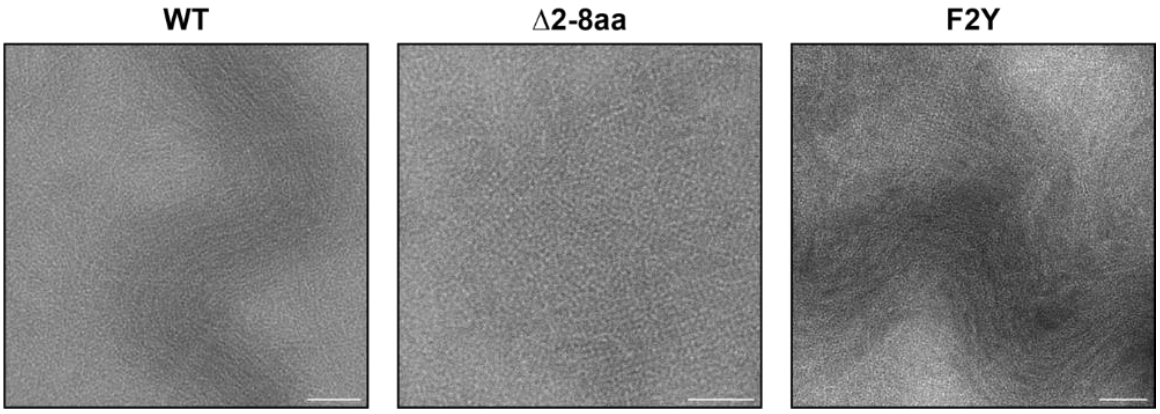

Figure 28 The polymerization of membrane-binding-impaired BacA variants is unaffected *in vitro*, as visualized by TEM. All BacA variants were able to form large assemblies such as 2D sheets or spiral-shaped bundles *in vitro*. Scale bar: 50 nm.

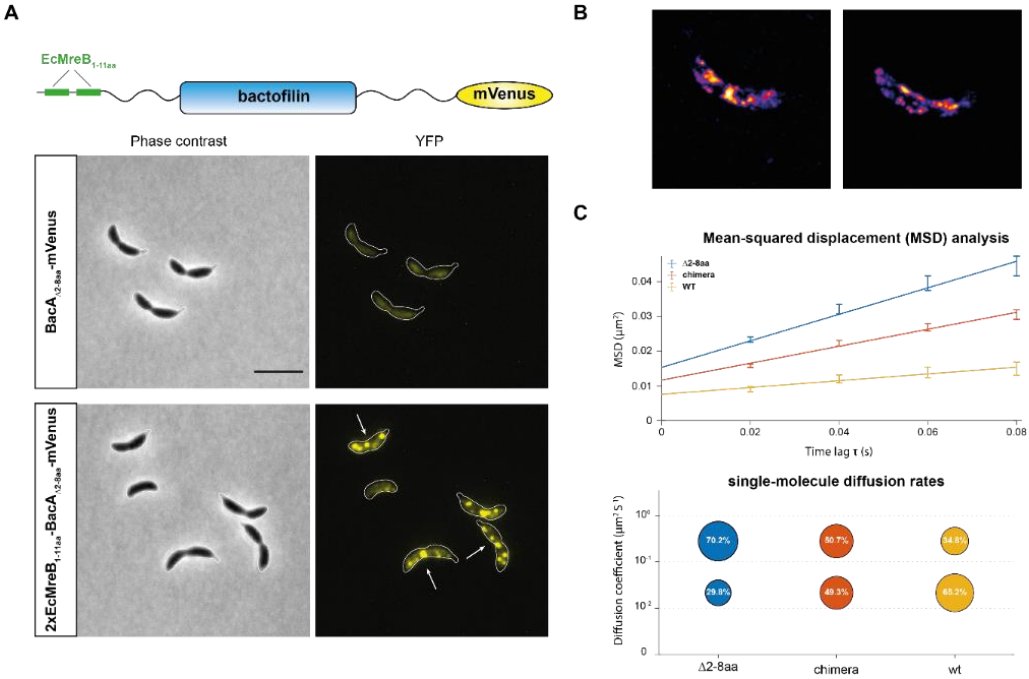

Figure 29 The fusion with amphipathic helixes from *E. coli* MreB restores the polymerization of BacA$_{\Delta 2\text{-}8aa}$ *in vivo*. (A) The chimeric protein formed randomly distributed foci within *C. crescentus* cells. Cells of strain LY84 (Δ*bacAB xylX*::P*xyl-bacA*$_{\Delta 4\text{-}32nt}$-*mvenus*) and LY103 (Δ*bacAB xylX*::P*xyl*-2x *mreB*$_{EC\ 1\text{-}33nt}$-*bacA*$_{\Delta 4\text{-}32nt}$-*mvenus*) were grown to late exponential phase and diluted to an OD600 of ~0.1. After incubation for another hour, cells were induced with 0.3% xylose for 2 h before visualization by phase contrast (Ph3) and fluorescence microscopy. Scale bar: 3 µm. (B) Sum of single-molecule tracks from movies of exponentially growing cells expressing 2xEcMreB$_{1\text{-}11aa}$-BacA$_{\Delta 2\text{-}8aa}$-mVenus. (C) Analyses of the mobility of the indicated BacA-mVenus fusions. Top: mean-squared displacement analysis based on live-cell single-molecule localization microscopy data. Error bars indicate the SD. Bottom: bubble plots showing the single-molecule diffusion rates. The values were obtained by fitting the probability distributions of the frame-to-frame displacements to a two-component Gaussian mixture model, assuming that the populations are composed of a mobile (top) and a static (bottom) fraction.

2.3 The interaction between PbpC and BacA

It has been shown previously that the bifunctional penicillin-binding protein PbpC interacts with bactofilins in *C. crescentus* through its cytoplasmic tail [136]. However, it is unclear whether both BacA and BacB are involved in the interaction, as the localization of PbpC was only investigated in cells lacking both paralogues. Moreover, the precise binding interface between bactofilin and PbpC is undetermined. Hence, we decided to elaborate the interaction between PbpC and bactofilin.

2.3.1 Only BacA interacts with PbpC

Although both bactofilins localize to the pole, it is possible that only one of them directly interacts with PbpC. We first strived to clarify this by studying the localization of PbpC in the presence of only one bactofilin paralogue. It turned out that PbpC exclusively interacted with BacA, as polar foci made of mVenus-PbpC were visible as long as BacA was present but not when only BacB was available (*Figure 30A*). Because a previous study found that a PG hydrolase (SpmX) in *A. biprosthecum* plays a critical role in recruiting bactofilin to the stalk

base and bactofilin in turn stabilizes SpmX at this location and acts as a platform for other PG remodeling enzymes [124], we wondered if this kind of interplay also exists for PbpC and BacA in *C. crescentus*. Therefore, the localization of BacA was examined in the absence of PbpC. It appeared that the subcellular localization of Venus-BacA was not influenced by PbpC, because the fusion persisted at the stalked pole regardless of the presence of PbpC (*Figure 30B*). In conclusion, these results indicate that BacA plays a decisive role in recruiting PbpC to the stalked pole, whereas its own localization is independent of PbpC.

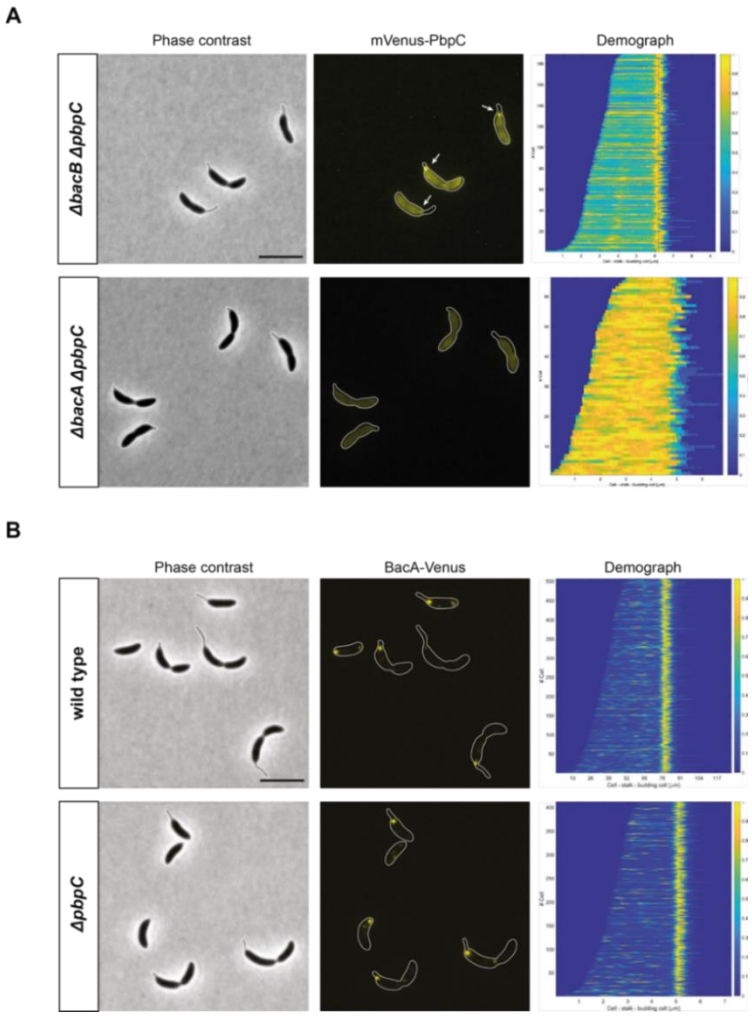

Figure 30 The polar localization of PbpC is determined by BacA, but PbpC does not affect the localization of BacA. (A) PbpC was able to localize to the stalked pole only when BacA was available, but not in the sole presence of BacB. (B) The localization of BacA was unaffected by PbpC. Cells of strains LY75 (Δ*bacB* Δ*pbpC xylX*::P*xyl-mvenus-pbpC*), LY72 (Δ*bacA* Δ*pbpC xylX*::P*xyl-mvenus-pbpC*), MT256 (*xylX*::P*xyl-bacA-venus*) and JK136 (Δ*pbpC xylX*::P*xyl-bacA-venus*) were grown to late exponential phase and diluted to an OD600 of ~0.1. After incubation for another hour, cells were induced by 0.3 % xylose for 1 h and analyzed by phase contrast (Ph3) and fluorescence microscopy. Scale bar: 3 µm. Demographs summarizing the single cell fluorescence profiles observed for the four strains are given on the right (n = 189 cells for LY75, 66 cells for LY72, 506 cells for MT256 and 412 cells for JK136).

2.3.2 Sequence alignment of the cytoplasmic tail of PbpC

It has been shown that the localization of PbpC to the stalked pole depends on the interaction between its cytoplasmic tail and bactofilin [136]. In order to further pinpoint

residues critical for this interaction, we performed a bioinformatics analysis on the cytoplasmic tail of PbpC. According to the annotation in the Pfam database [142], the cytoplasmic tail (aa 1-83) plus the transmembrane helix (aa 84-109) of PbpC constitute a domain called PBP_N, which is exclusively distributed in *Caulobacter* species. The sequence alignment of the PbpC cytoplasmic tail revealed that it is composed of two conserved regions (C1 and C2), a proline-rich region (PRR) and a positively charged region following the conserved region 2 (*Figure 31*). It is not uncommon to have a positively charged region immediately preceding the transmembrane helix (TMH) at the cytoplasmic side, which has been confirmed by a plethora of analyses [149, 150]. As for the proline-rich region, it has been implicated in protein-protein interactions [151]. Interestingly, the tails of BacA are also characterized by proline-rich regions, which makes it reasonable to conject that bactofilin and PbpC could interact via proline-rich regions. The two conserved regions, C1 (aa 2-13) and C2 (aa 63-70), also attracted our attention. Their importance in the recruitment of PbpC to stalked pole was assessed in the following section.

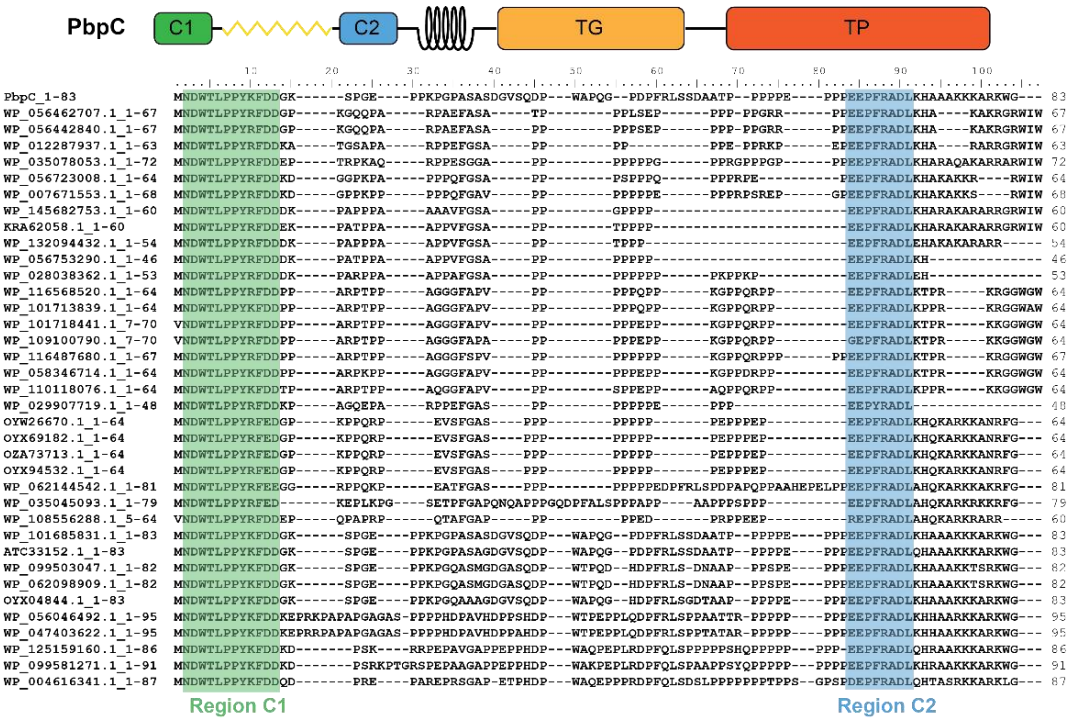

Figure 31 Sequence alignment of the PbpC cytoplasmic tail. The cytoplasmic part includes two conserved regions (C1 and C2), a proline-rich region and a positively charged region.

2.3.3 PbpC interacts with BacA through its first thirteen amino acids

Based on the sequence alignment, we designed two variants of PbpC that allowed us to study the involvement of different parts of its cytoplasmic tail in the interaction with bactofilin. The first construct lacks conserved region C1 (aa 2-13) but retains the rest of PbpC

cytoplasmic tail, whereas the second variant is a chimera of conserved region C1 and an unstructured periplasmic stretch of DipM (aa 224-396) (*Figure 32A*). Subsequently, we produced these PbpC variants fused to mVenus in a Δ*bacB* Δ*pbpC* strain to study their localization pattern. Notably, the two variants exhibited distinct localization patterns. In the absence of conserved region C1, the polar localization of PbpC was abolished, while the replacement of proline-rich region and conserved region C2 had no obvious impact (*Figure 32B*). The stability of the fusion proteins was also examined to exclude the possibility that the observed signal is due to cleavage of the fluorescent protein (*Figure S8*). Collectively, the *in vivo* localization studies suggest that the conserved region C1 (aa 2-13) plays an essential role in the interaction between PbpC and BacA.

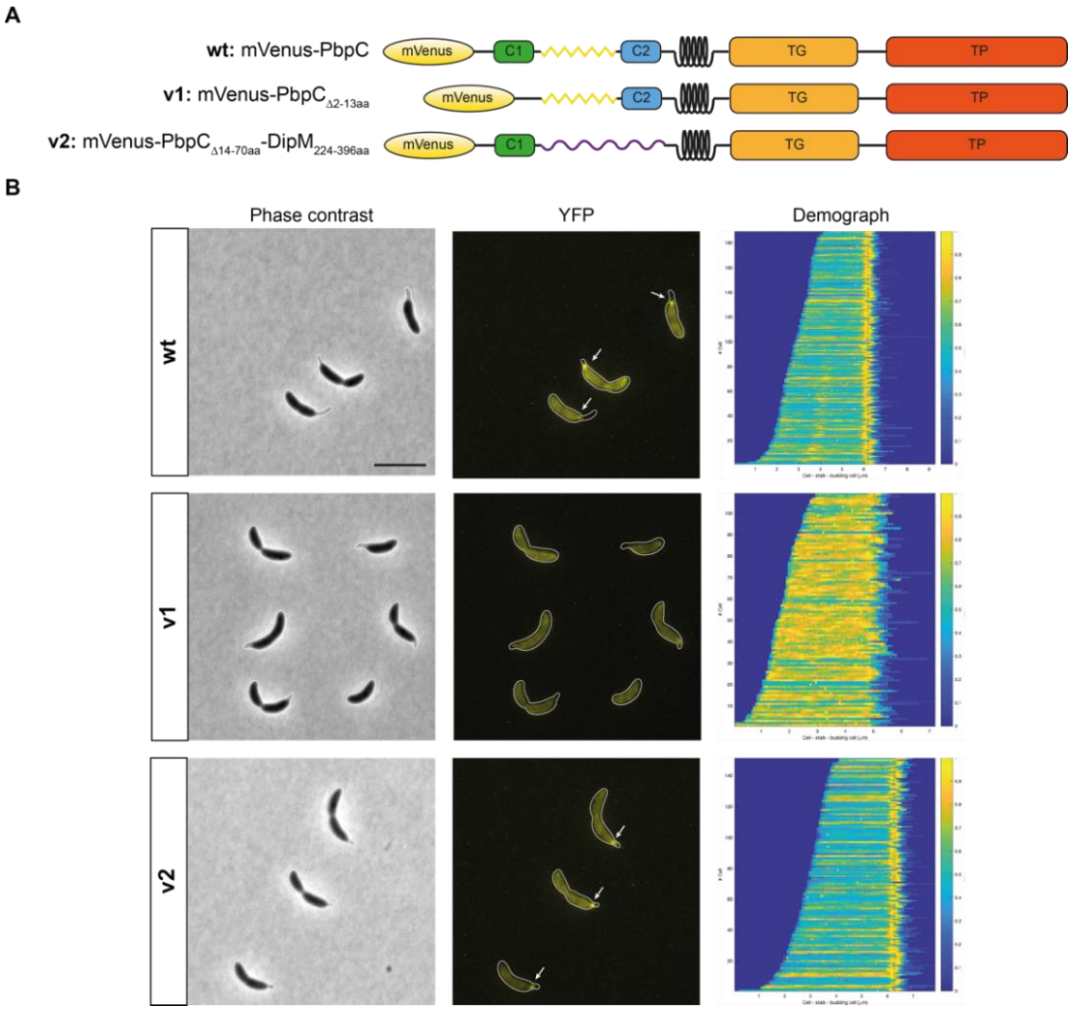

Figure 32 The recruitment of PbpC to the stalked pole depends on the interaction between conserved region C1 (aa 2-13) and BacA. (A) Schematic representation of PbpC variants fused to mVenus. (B) The localization pattern of PbpC variants in the presence of BacA. Cells of strains LY75 (Δ*bacB* Δ*pbpC xylX*::P*xyl-mvenus-pbpC*), LY76 (Δ*bacB* Δ*pbpC xylX*::P*xyl-mvenus-pbpC*$_{\Delta 4\text{-}39nt}$) and LY77 (Δ*bacB* Δ*pbpC xylX*::P*xyl-mvenus-pbpC*$_{1\text{-}39nt}$-*dipM*$_{670\text{-}888nt}$-*pbpC*$_{249\text{-}2199nt}$) were grown to late exponential phase and diluted to an OD600 of ~0.1. After incubation for another hour, cells were induced by 0.3% xylose for 1.5 h and analyzed by phase contrast (Ph3) and fluorescence microscopy. Scale bar: 3 µm. Foci are indicated by white arrows. Demographs summarizing the single cell fluorescence profiles observed for three strains are given at the bottom (n = 189 cells for LY75, 109 cells for LY76, and 151 cells for LY77).

To corroborate this finding, we further employed bio-layer interferometry (BLI) to evaluate the interaction between $PbpC_{aa1\text{-}13}$ and BacA *in vitro*. BLI is a technique that can probe the interaction between biomolecules in real-time by measuring the interference pattern of white light reflected from a biolayer and an internal reference surface (*Figure 33A*). It utilizes a biosensor whose tip can be coated with bait molecules. The subsequent binding of analytes to the immobilized baits induces the change of interference pattern and the shift of wavelength directly correlates to the change in thickness (nm) of the biological layer. The biotinylated $PbpC_{aa\ 1\text{-}13}$ peptide was first immobilized on the tip of a streptavidin (SA) biosensor. Consistent with the *in vivo* study, the addition of BacA increased the thickness of biolayer as evidenced by a shift in the wavelength (*Figure 33B*). The degree of change was positively correlated to the concentration of BacA. Furthermore, the apparent equilibrium dissociation rate constant (K_D) was obtained by analyzing a titration series, yielding a value of 4.9 µM. In summary, both *in vivo* and *in vitro* results have substantiated that PbpC interacts with BacA through the first thirteen amino acids of its cytoplasmic tail.

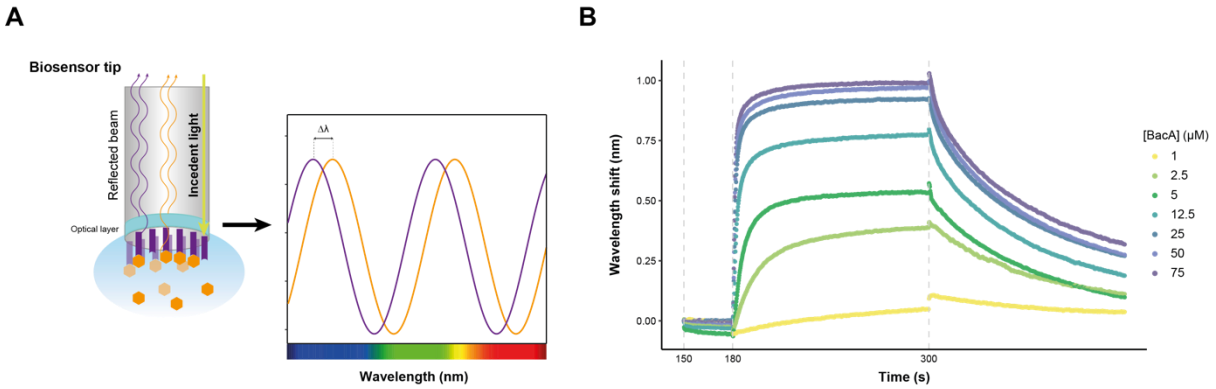

Figure 33 The N-terminal peptide of PbpC interacts with BacA *in vitro*. (A) The principle of bio-layer interferometry. (B) Bio-layer interferometric analysis of the interaction between PbpC and BacA. Streptavidin sensors coated with biotinylated $PbpC_{aa\ 1\text{-}13}$ were probed with indicated concentrations of BacA. The interaction kinetics were followed by monitoring the wavelength shifts resulting from changes in the optical thickness of the sensor surface during association or dissociation of the analyte.

2.3.4 BacA interacts with PbpC via the last winding of its core

We were interested in the interaction site not only on PbpC but also on BacA. To gain that information, we applied hydrogen-deuterium exchange mass spectrometry (HDX-MS). HDX measures the rate at which backbone hydrogens are exchanged for deuterium, reflecting the solvent accessibility, based on which the information about protein conformation and iteraction sites can be derived [152, 153]. Overall, the addition of $PbpC_{aa\ 1\text{-}13}$ only caused moderate changes in the HDX pattern of BacA. The most pronounced change occured in the last winding (aa 106 – 129) close to the C-terminus of the β-helical bactofilin domain (*Figure 34B*). The mass spectrometry analysis demonstrated that the

presence of the $PbpC_{aa1-13}$ peptide protected that region (*Figure 34A*). Although the change was subtle, it is not likely due to non-specific interaction, as no obvious difference was observed for other parts of BacA. In conclusion, the result of the HDX-MS analysis indicates that the C-terminal region (aa 106-129) of bactofilin domain may participate into the interaction with PbpC.

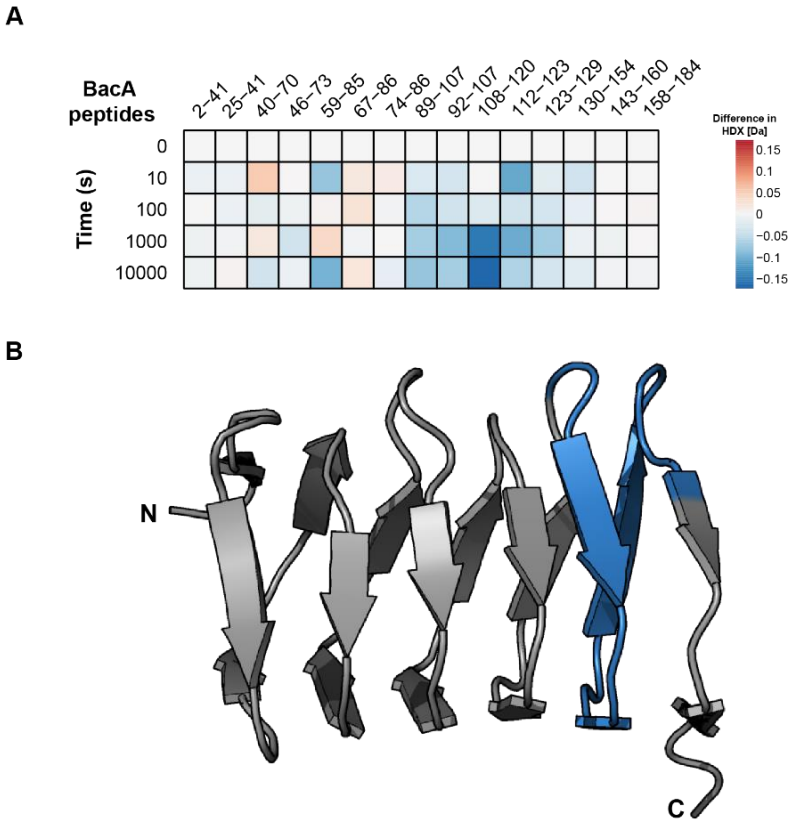

Figure 34 The interaction with PbpC is mediated by residues 106-129 of BacA, which constitute the last winding of the β-helical bactofilin domain. (A) The heat plot shows the differences in deuterium uptake between the apo-state and the bound-state at different incubation times. (B) The observed changes (t = 1000 s) were mapped onto the structure of BacA. The color code is identical to the one used in the heat plot.

2.4 Discovering the protein interactome of bactofilins

The bifunctional penicillin-binding protein PbpC is heretofore the only identified protein interacting with bactofilin in *C. crescentus*. Compared with the well-studied cytoskeletal proteins MreB and FtsZ, which serve as scaffolds for PG remodeling complexes, the study of the interactome of bactofilins is still in its infancy and requires further investigation. Moreover, it appears that the polymerization of bactofilins is precisely controlled *in vivo*, as they only form foci at the stalked-cell stage, although its expression level is constant throughout the cell cycle [136]. Moreover, the mechanism regulating the polymerization remains unclear. Therefore, we decided to explore the protein-protein interaction network for bactofilins in *C. crescentus* by co-immunoprecipitation (Co-IP) and mass spectrometry

analysis with the aim to gain insight into the regulation of bactofilin polymerization as well as the potential additional roles undertaken by bactofilins.

2.4.1 Numerous proteins interact with bactofilins in *C. crescentus*

Co-immunoprecipitation is a commonly used technique to unravel protein-protein interactions that occur *in vivo*. It utilizes an antibody to specifically recognize and isolate complexes containing the bait protein. In combination with mass spectrometry, the identity of interactomes can be determined. In order to perform Co-IP on BacA and its paralogue BacB, an HA-tag, derived from human influenza hemagglutinin, was fused to the C-terminus of target proteins [136]. The mass spectrometry-based proteomics revealed that a variety of proteins interacted with bactofilins in *C. crescentus* in addition to PbpC. In the case of BacA-HA, two additional proteins, CC1891 and CC3376, were identified (*Figure 35A* and *Table S4*). Interestingly, the interactome of BacB-HA was larger, including components of lipoprotein transport system (LolD and LolE) [154, 155], ATP-binding proteins of ATP-binding cassette (ABC) transporter, components of the Tol-Pal system (TolQ and TolR) [156], TonB-dependent receptors, sirohydrochlorin ferrochelatase, as well as the pole-localized proteins StpX [137], DivJ [28] and PopZ [106] (*Figure 35B* and *Table S5*). The longer tails of BacB might account for the greater number of binding partners. Furthermore, BacB appeared to be implicated in membrane integrity, as many of its partners are either membrane proteins or involved in membrane transportation [157–159]. Among the newly identified interaction partners, CC1891 and CC3376 gained our attention, because they interacted with both BacA and BacB. Therefore, we initiated preliminary studies on them.

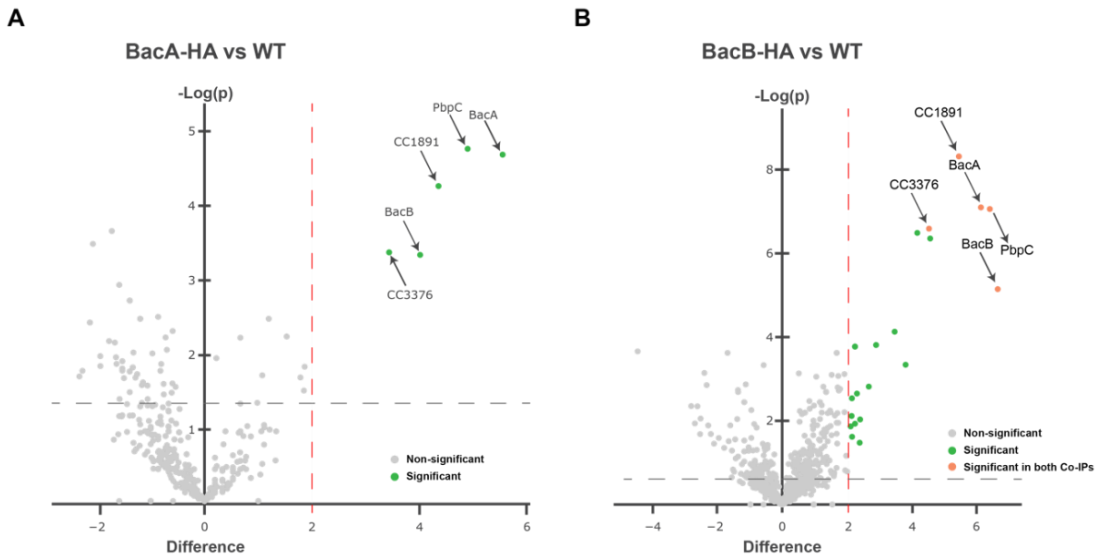

Figure 35 Co-immunoprecipitation identified novel interaction partners for bactofilins. (A) Volcano plot of proteins interacting with BacA-HA. (B) Volcano plot of proteins interacting with BacB-HA. Significant hits are defined as proteins that are enriched at least 2-fold compared to the controls and show a p-value < 0.05.

2.4.2 The localization of bactofilin is independent of CC3376

CC3376 is a 141 amino acid-long protein. It is annotated to be an uncharacterized protein with a DUF2385 domain that is conserved in a number of alpha-proteobacteria (*Figure 36A*). According to the domain organization provided in Pfam, CC3376 also contains an N-terminal signal peptide and a disordered C-terminal region (*Figure 36A*). The signal sequence is predicted to be a substrate for the general secretion (Sec) pathway by SignalP 6.0 [160] and its cleavage is supposed to take place at amino acid +21 by signal peptidase I (SPase I) (*Figure 36B*). Since CC3376 is an exocytoplasmic protein, the interaction between it and bactofilins should either be transient in cytosol or indirect through a transmembrane protein spanning the inner membrane. One candidate for such an adaptor is PbpC, because it straddles the three layers of the cell envelope. To confirm our assumption, another Co-IP was conducted for BacA-HA in a Δ*pbpC* background. The result revealed that the hits for CC3376 have decreased substantially when PbpC was absent (*Figure 37* and *Table S6*), which indicates that PbpC bridges the gap between bactofilin and CC3376.

In order to get a glimpse of the function of CC3376, we examined the genetic context of its gene which is orientated reversely in *C. crescentus* genome. A search with CauloBrowser [161] showed that it is located in an operon with *CC3374* and *CC3375* (*Figure 36C*). CC3374 is an NfeD-like protein containing an NfeD domain at its C-terminus. The NfeD-like proteins can be classified into three groups: an ancestral group NfeD1b with additional N-terminal protease, truncated NfeD1b as well as NfeD1a with membrane-spanning domains [162]. CC3374 appears to belong to NfeD1a group, because it is of comparable length to other NfeD1a proteins and contains two transmembrane regions preceding the NfeD domain. Since NfeD1a proteins exclusively associate with paraslipin, a conserved protein found in all three domains of life, we assumed CC3375, which is annotated as a stomatin-like protein, is actually a paraslipin. The function of NfeD-like proteins is diverse. Hence it is difficult to predict the role played by CC3374. Nevertheless, it is possible that CC3376, CC3374 and CC3375 act in a coordinated fashion.

Furthermore, we tried to localize CC3376 in *C. crescentus* cells either by fusing the red fluorescent protein mCherry to its C-terminus or by inserting mCherry between the signal peptide and the transmembrane helix (*Figure S9*). However, neither of the constructs was functional. To assess the effect of CC3376 on the localization of bactofilins, we produced bactofilins fused to fluorescent proteins in a Δ*CC3376* strain. The subcellular localization study shows that both BacA and BacB can localize to the stalked pole as usual regardless of the absence of CC3376 (*Figure 38*). Moreover, the Δ*CC3376* mutant did not show obvious

morphology defects. So far, the relationship between CC3376 and bactofilins as well as the physiological function of CC3376 remains elusive and requires further investigation.

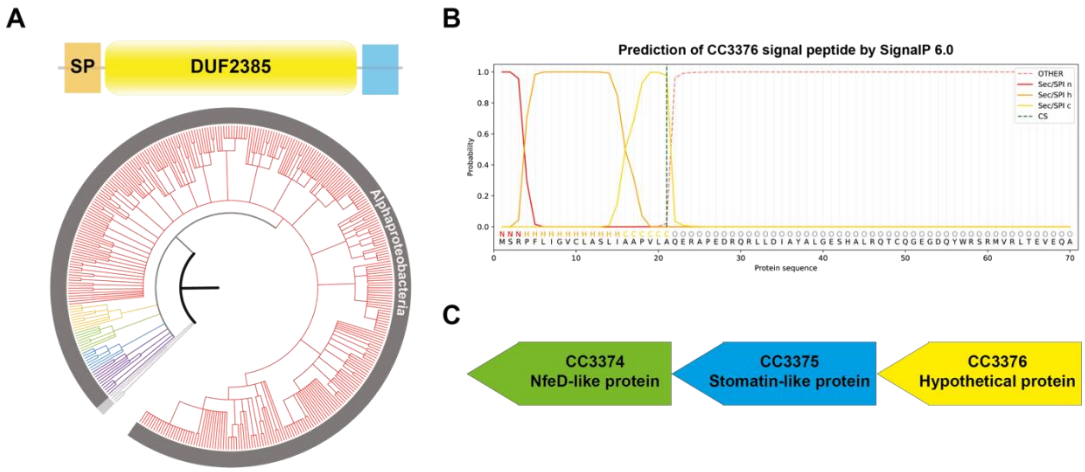

Figure 36 Bioinformatic analysis of the uncharacterized protein CC3376. (A) Domain organization of CC3376 and distribution of DUF2385. CC3376 is composed of an N-terminal signal sequence, a DUF2385 domain and a low-complexity C-terminus. The DUF2385 domain is widely conserved in several orders of the alphaproteobacteria, such as *Hyphomicrobiales* (red), *Maricaulales* (yellow), *Hyphomonadales* (green) and *Caulobacterales* (blue). (B) The signal sequence of CC3376 was predicted to be targeted to the Sec pathway and the processing of preprotein is through signal peptidase I at position +21. (C) *CC3376* is annotated to be in the same operon as *CC3374* and *CC3375*.

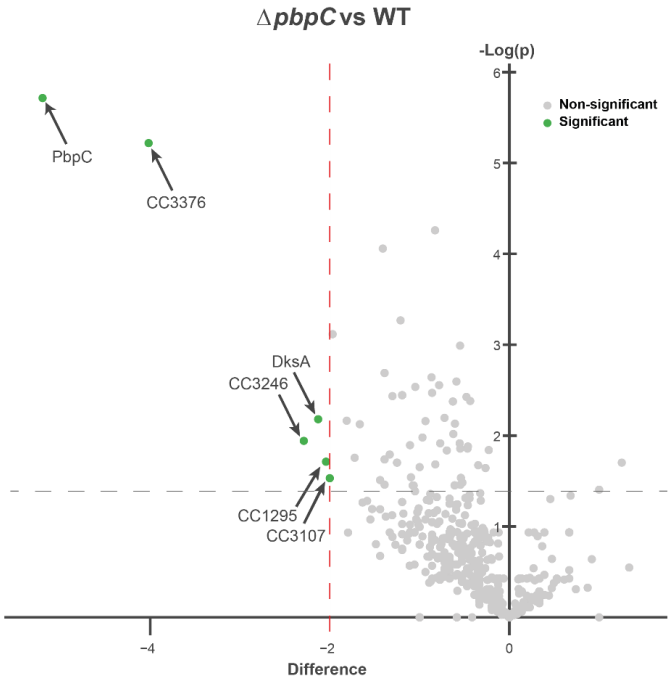

Figure 37 Co-immunoprecipitation with BacA-HA in the absence of PbpC confirms that the interaction between BacA and CC3376 is mediated by PbpC. Significant hits are defined as proteins that are at least 2-fold less than controls and with a p-value < 0.05.

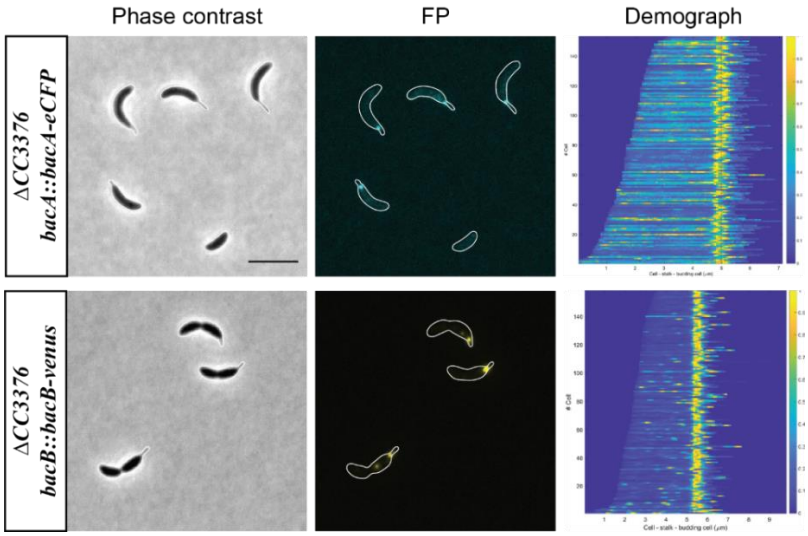

Figure 38 The deletion of *CC3376* influences neither the localization of bactofilins nor the morphology of the cells. Cells of strain LY42 (Δ*CC3376 bacA::bacA-ecfp*) and LY61 (Δ*CC3376 bacB::bacB-venus*) were imaged by phase contrast (Ph3) and fluorescence microscopy. Scale bar: 3 µm. Demographs summarizing the single cell fluorescence profiles observed for two strains are given at the bottom (n = 153 cells for LY42 and 158 cells LY61).

2.4.3 CC1891 is a pentapeptide repeat protein

According to the information on UniProt, CC1891 is a 250 amino acid-long pentapeptide repeat protein (PRP), which is characterized by tandem pentapeptide repeats. Proteins belonging to the PRP family are versatile, playing a variety of roles, such as glycolipid transporter [163] and topoisomerase poison resistant factor [164]. The center position (denoted as position i) of the pentapeptide is highly likely to be a hydrophobic residue (leucine or phenylalanine), as the amino acids at this position build the hydrophobic core of the β-helical structure. Residues N-terminal to residue i are residues i-1 and i-2, accordingly, residues C-terminal to residue i are denoted i+1 and i+2. The side chains of residues i-1, i+1 and i+2 are commonly positioned away from the interior. Hence, these positions can accommodate polar and charged amino acids. Sequence analysis of CC1891 showed that it encompasses 36 tandem pentapeptide repeats which are arranged in 9 consecutive coils (*Figure 39A*). Moreover, it is predicated to be a right-handed quadrilateral β-helix by the I-TASSER server [165] similar to other PRPs (*Figure 39B*). Noticeably, a 7 amino acid-long loop between face 3 and face 4 of coil 6 interrupts the consistency of the β-helix, which is not uncommon. PRPs involved in quinolone resistance are also discontinued by loops which appear to be important for the function of those proteins [164]. Another feature of CC1891 is the low-complexity, proline-rich C-terminal tail. Bactofilins and PbpC are both characterized by proline-rich termini; thus, we assumed that the proline-rich region might be important for the interaction between bactofilins and their interaction partners.

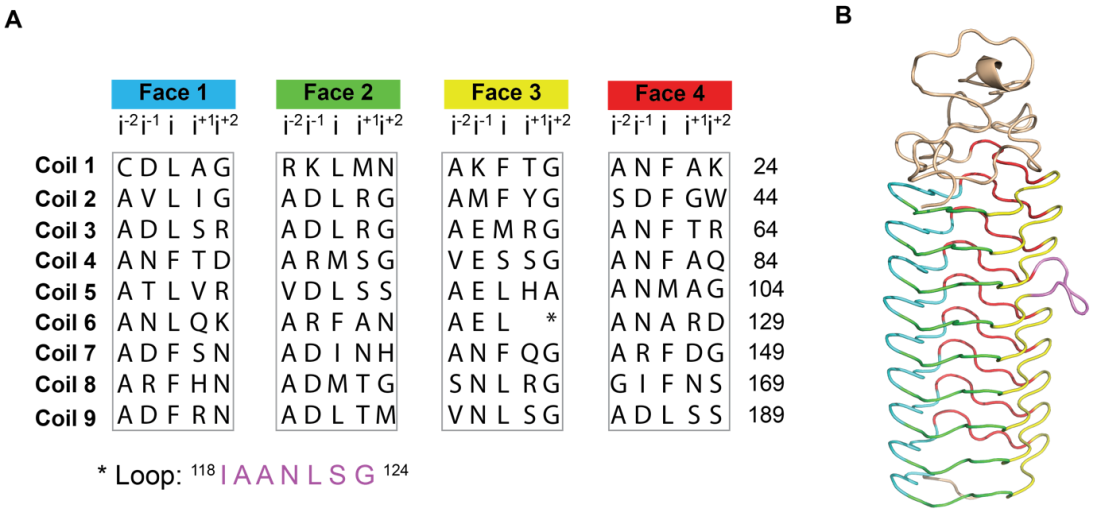

Figure 39 Sequence alignment of the 36 tandem pentapeptide repeats of CC1891 and predicted structure of CC1891. (A) The sequence of CC1891 core is segmented into four columns, representing the four faces of the right-handed quadrilateral β-helix. The color of each face is indicated at the top and has also been used for coloring predicted structure. The loop is displayed by an asterisk and the sequence is listed below. (B) The structure of CC1891 was predicted by the I-TASSER server. The C-terminal proline-rich region is colored in wheat.

2.4.4 Characterization of the interaction between CC1891 and bactofilin

To shed light on the interaction between the pentapeptide protein CC1891 and bactofilin, we decided to identify the interface between them. Genes encoding those two proteins were cloned into a co-expression vector with a hexahistidine-tag fused to the N-terminus of BacA. Interestingly, we noticed that the solubility of BacA increased greatly when it was co-expressed with CC1891 (*Figure 40A*). This observation can be explained either by an interaction with CC1891 or by the fusion to the His_6-tag. We reasoned that the N-terminal tag may interfere with the binding of BacA to the membrane, thereby reducing the fraction of proteins pelleting together with membrane debris. Nevertheless, the purification was difficult, as the sample became viscous after cell disruption, which was also observed for the co-purification of BacP, a bactofilin homologue from *M. xyanthus*, and its interaction partner PadC (unpublished). Due to the blocking of chromatograpy column and high back pressure, we switched from an automated system to gravity-flow column to purify the protein. The yield of the purification was low, but there was a protein approximately the size of CC1891 co-eluted with His_6-BacA (*Figure 40B*). That was confirmed to be CC1891 by mass spectrometry. In summary, the co-purification data suggests that CC1891 and BacA might also interact *in vitro*.

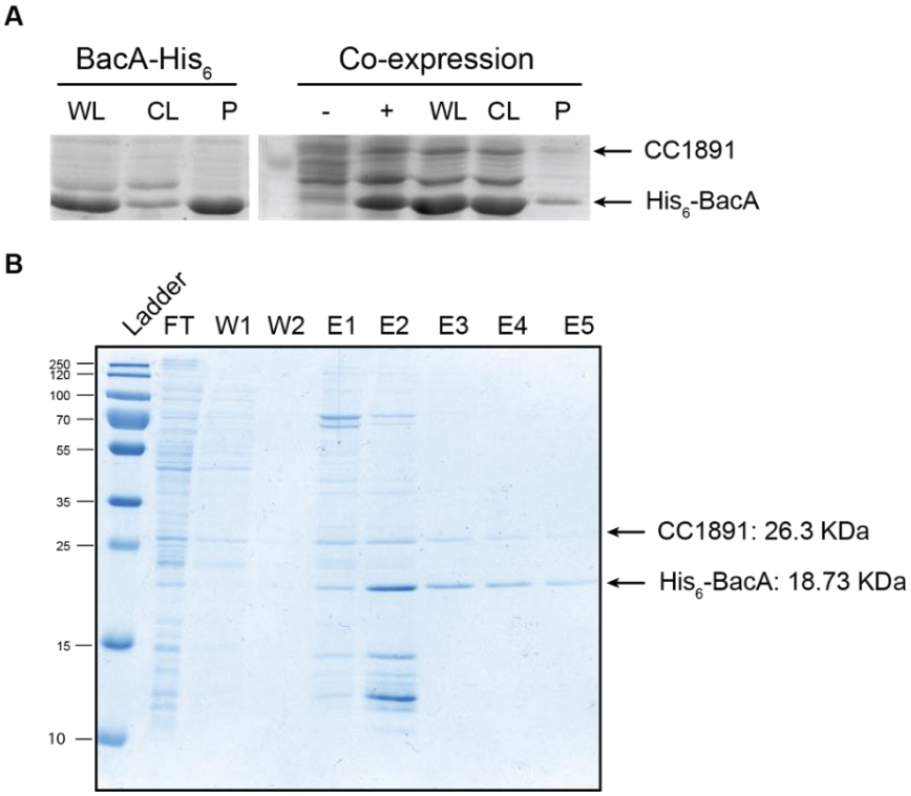

Figure 40 CC1891 and BacA appears to interact with each other *in vitro.* (A) The solubility of His_6-BacA was improved when co-expressed with CC1891. (B) CC1891 co-eluted with His_6-BacA from an Ni-NTA matrix.

In order to localize CC1891 in *C. crescentus*, the red fluorescent protein mCherry was fused to either the N-terminus or the C-terminus of CC1891. The genes encoding these constructs were then integrated at chromosomal *xylX* locus. Strikingly, CC1891 did not localize to the stalked pole, as the bactofilins did, but was rather evenly distributed throughout the cells (*Figure 41A*), which was contradictory to our expectation. The stability of the fusion proteins was also examined to exclude the possibility that the observed signal is due to cleavage of the fluorescent protein (*Figure S10*). A literature search revealed that there was a study on CC1891, according to which CC1891 is actually an outer membrane protein that may function as a receptor for the contact-dependent toxins CdzC/D [166]. Although results from that study can explain why the mCherry signal was diffuse, it raises more questions: 1) How does an outer membrane protein interact with cytoplasm-located bactofilins? 2) Does CC1891 actually interact with bactofilins? Or are our Co-IP and *in vitro* results artifacts due to the structural similarity of CC1891 and bactofilins? To answer these questions, we started a bioinformatic analysis of the sequence of CC1891. If CC1891 is indeed an outer membrane protein, it needs to be transported across two layers of membrane. There are several secretion systems available for protein translocation to the outermembrane in Gram-negative bacteria, which can be divided into two groups: Sec-dependent and Sec-independent [167]. Proteins

exported through the Sec-dependent pathways utilize a common machinery, the Sec translocase, to move across the inner membrane, whereas substrates for the Sec-independent pathway can be transported from the cytosol to the outer membrane in a single step via the double-membrane spanning apparatus. In order to be translocated via the Sec apparatus, CC1891 should contain a signal peptide at its N-terminus. However, no such sequence was detected by the SignalP 6.0 server, which indicates that the transportation of CC1891 is possibly not through the Sec secretion system. One of the Sec-independent pathways present in *C. crescentus* is the type I secretion system (T1SS), which is generally constituted by three parts: an ABC transporter in the inner membrane, a periplasm-spanning membrane fusion protein (MFP) and an outer membrane protein. It has been implicated in the secretion of the paracrystalline surface layer (S-layer) protein RcsA [168] and the contact-kill bacteriocin CdzC/D [169]. The secretion signal recognized by T1SS locates at the extreme C-terminus of the protein [170–173], but no universal code has been identified. In addition to the secretion signal, some proteins also contain an aspartate and glycine-rich motif termed "repeats-in-toxin" (RTX) [174] that facilitates the passage of the translocon. Moreover, the substrates for T1SS are generally acidic with an isoelectric point (pI) frequently below pH 5 [175]. However, CC1891 neither possesses an RTX motif nor has a low pI value (the theoretical pI is 8.78). In conjunction with the proposal by García-Bayona *et al.* that CC1891 bears an N-terminal signal sequence [166], we concluded that CC1891 is not likely to be a substrate for the T1SS. We resorted to a β-lactamase assay to determine the localization of CC1891. To this end, we fused β-lactamase to its C-terminus and integrated the corresponding allele at the *xylX* locus of the *C. crescentus* chromosome. However, CC1891-Bla was unable to grow on ampicillin plates despite the addition of inducer, which contrasted with the positive controls StpA-Bla and StpB-Bla, a pair of previously identified periplasmic proteins (*Figure 41B*). This result does not eliminate the possibility that CC1891 is an outer membrane protein, as it may be associated to the outer leaflet of membrane or the orientation of the construct positioned β-lactamase away from periplasmic space. Overall, we cannot make any conclusion about the localization of C1891 based on the β-lactamase assay and many questions still surround the interaction between CC1891 and bactofilin.

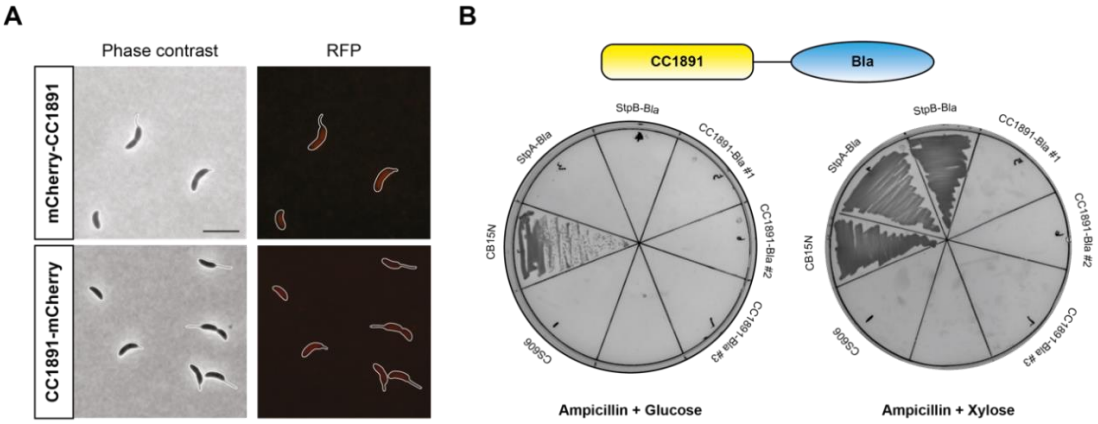

Figure 41 CC1891 was diffuse in *C. crescentus* and the C-terminal fusion to β-lactamase cannot support the growth in the presence of ampicillin. (A) Regardless of the position of mCherry, the fusion proteins were evenly distributed within cells. Cells of strains LY25 (*xylX*::P*xyl-mCherry-CC1891*) and LY34 (*xylX*::P*xyl-CC1891-mCherry*) were induced by 0.03% xylose for 1 h and photographed by phase contrast (Ph3) and fluorescence microscopy. Scale bar: 3 μm. (B) The TEM-1 β-lactamase gene (*bla*) was fused to the 3' end of *CC1891*. The gene fusions were placed under the P*xyl* promoter in a β-lactam-sensitive reporter strain. Cells of different strains CB15N, CS606 (Δ*CC2139*), SS165 (Δ*CC2139 xylX*::P*xyl-stpB-bla*), SS172 (Δ*CC2139 xylX*::P*xyl-stpA-bla*) and LY49 (Δ*CC2139 xylX*::P*xyl-CC1891-bla*) were plated on PYE agar containing 50 μg/ml ampicillin and either 0.2% glucose or 0.3% xylose.

3 Discussion

Bacteria possess a variety of filament-forming proteins termed cytoskeletons, which play fundamental roles in spatiotemporally organizing the cellular components and orchestrating cellular processes. Among the bacterial cytoskeletons discovered so far, some are homologous to their eukaryotic counterparts and share similar polymerization mechanisms and structures, such as FtsZ [35, 36], MreB [71–73]. and crescentin [95]. However, there are also bacteria-specific cytoskeletal proteins, as exemplified by bactofilin, which has been identified around a decade ago [136]. Numerous studies have been dedicated to the polymerization [114, 117, 119, 141] and functions [34, 120, 126, 127, 136] of bactofilin in various species. However, compared with the well-studied FtsZ and MreB, the research on bactofilin is still in its infancy and there are many unresolved questions surrounding bactofilin. In order to obtain the missing information, this work focused on the bactofilin homologue BacA in the model organism *C. crescentus*.

3.1 The polymerization mechanism of bactofilins

The collective data from several studies have suggested that hydrophobic patches at the termini of the bactofilin domain may account for the interaction between neighboring bactofilin monomers [119, 141], which can assemble into non-polar protofilaments [114] and then higher-order structures. However, the identity of these hydrophobic residues as well as their importance in polymerization is undetermined. Therefore, we decided to initiate a systematic analysis of BacA from *C. crescentus* in this work. Based on the calculated conservation scores and the structure of the bactofilin domain, several conserved hydrophobic residues were identified, including L42, L46, I48 and V52 at the N-terminus and L122, M124 and F130 at the C-terminus (*Figure 14A*). These identified amino acids were predicted to mediate the interaction between monomers in a template-based docking study (*Figure 14B*). Furthermore, the importance of individual residues or combinations were examined by subcellular localization studies, which confirmed that their exchange disrupts the formation of polymers *in vivo* (*Figure 15*). Among those mutant variants, we analyzed the oligomeric state of $BacA_{F130R}$ by size exclusion chromatography. The elution profile revealed that the majority of $BacA_{F130R}$ had an apparent molecular mass of 84.6 kDa (*Figure 16*). The estimated size is approximately four times larger than the theoretical molecular weight of a BacA monomer, which differs from our expectation. We originally assumed that the introduction of the F130R mutation would lead to dimers. Nevertheless, given the fact that SEC separations are not dependent on

the molecular mass but rather on the hydrodynamic radius of the protein of interest and potentially affected by non-ideal interactions with the stationary phase [146, 147], the value obtained might be imprecise. In order to determine the molar mass and oligomeric state more accurately, multi-angle light scattering (MALS) can be coupled to size exclusion chromatography. The combination of size exclusion chromatography and multi-angle light scattering has been routinely used in protein characterization and quality control [176, 177]. Basically, MALS measures the scattering of incident beam by the sample from different angles simultaneously. The intensity of the scattered light correlates to the absolute molar mass of particles in solution [178]. In summary, we have identified several conserved hydrophobic residues at the ends of the bactofilin domain and their importance in polymerization has been determined experimentally.

In this work, we also investigated the lateral interaction between bactofilin protofilaments. It is a common characteristic of bactofilin protofilaments to further coalesce into large assemblies such as bundles or 2D sheets [114, 118, 119, 136]. In order to uncover the mechanism governing this process, we resorted to the chemical crosslinker BS^3, which can readily react with primary amines in proteins. Mass spectrometry was employed to identify the crosslinked sites, which revealed that K11-K11, K11-K103, K11-K144 and K103-K103 were enriched. Except for K103, the other lysines are on the flexible tails of BacA. Because of the exceptional high frequency of crosslinked K11, we examined the influence of the N-terminal region on the polymerization of BacA *in vitro*. The purified fusion protein lacking the N-terminal tail was analyzed by transmission electron microscopy. The acquired image shows that $BacA_{\Delta N}$ was still capable of forming filaments and thick bundles (*Figure 19*), indicating that the bundling property is not altered. As for the lysine detected on the central bactofilin domain, we do not consider its crosslinking is due to chance, as more than one lysine is located on the surface of bactofilin domain, but only K103 was crosslinked. Moreover, we noticed that the lateral interfaces in the docking predictions are charge-complementary (*Figure 20*). Consequently, we decided to explore the possibility that electrostatic forces mediate the inter-protofilament interaction. To this end, a variant ($BacA_{surfmut}$) containing four mutations of acidic amino acids (D61, E88, D116 and E120) was created and its localization pattern as well as polymerization state was probed. In stark contrast to the wild-type protein, $BacA_{surfmut}$ was diffuse within cells (*Figure 21*) and only formed short needles approximately 30-40 nm long and 9 nm wide (*Figure 19*). Collectively, the findings imply that electrostatic interaction may be crucial for BacA to polymerize into large assemblies, in line with a previous study on BacM from *M. xanthus*. In that study, glycine in alkali buffer has been shown to act as a counterion disrupting the bundles

of BacM [119]. Lateral interactions through charged amino acid pairs have also been implicated in FtsZ assembly, which is proved to be functionally important [179]. Nevertheless, our study on the lateral interaction between BacA protofilaments is preliminary. There are many other questions that need to be clarified in the future research, such as the precise nature of the interface and the potential cellular factors regulating lateral interaction. Bactofilin has a high propensity to assemble into higher-order structures *in vitro*. However, this process appears to be deliberately controlled *in vivo*, because the visible foci of bactofilin only occur at the stalked-cell stage despite a constant expression level [136]. It is not uncommon for cytoskeletal proteins to have highly controlled polymerization mechanism, as exemplified by the tubulin-homologue FtsZ, whose polymerization is extensively regulated by both positive [180–182] and negative regulators [183, 184].

3.2 The membrane association of bactofilin

Several lines of evidence have demonstrated that bactofilin is located in the proximity of cell membranes [114, 120, 136], which could possibly be explained by hydrophobic interactions mediated by a relatively conserved region at the N-terminus of the protein. The suggested sequence was experimentally confirmed to be functional for bactofilin from *T. thermophilus* [114]. However, it is unknown if that region is universal for other bactofilins. Therefore, we removed it from BacA and observed the localization of the mutant protein ($BacA_{\Delta 2\text{-}8aa}$). Consistent with the result obtained for *T. thermophilus* bactofilin, the membrane-binding capacity of the mutant appeared to be impaired, as evidenced by the loss of the characteristic polar localization (*Figure 22A*). Of note, the suggested region (*Figure 9A*) has a high proportion of charged and polar amino acids, which casts doubt on the hypothesis by Deng et al. [114] that the hydrophobicity of the membrane targeting sequence is crucial for the interaction. One possibility is that, despite being unstructured, the sequence may form an amphipathic helix upon contact with a lipid membrane, which is a common strategy employed by cytoskeletal proteins, such as MreB [75] and FtsA [121]. However, the membrane-targeting sequences of bactofilin do not display the typical features of an amphipathic helix when arranged into a helical wheel (*Figure 22B*). To further illustrate the mechanism underlying the interaction between bactofilin and membrane, we decided to systematically mutate individual residues within the membrane-targeting sequence. The resulting variants can be classified into three categories based on their localization pattern. The first group, consisting of the S3A and Q5A variants, formed foci at the stalked pole like the wild-type BacA (*Figure 23*), whereas the second group, composed of the K4S, A6S and K7S variants, retained the ability to form foci *in vivo*,

but the distribution of foci was random (*Figure 24*). Because the cell membrane of *C. crescentus* is negatively charged [123] and there is a preponderance of basic residues, we postulated that the interaction between bactofilin and the membrane is probably due, at least in part, to electrostatic interaction, which has also been implicated in lipid-binding of eukaryotic cytoskeletons [185]. Therefore, we simultaneously mutated the two lysine residues in the mortif. The resulting K4SK7S variant as well as the F2Y variant constitutes the third category and both displayed the localization pattern similar to that of Δ2-8aa variant (*Figure 25*). We further analyzed the mobility of wild-type BacA and the membrane-binding impaired variants in *C. crescentus* cells. Single-molecule tracking revealed that all three variants were more mobile than the wild-type protein. As expected, the Δ2-8aa variant was the most mobile one, followed by K4SK7S and F2Y variants. Taken together, it appears that both hydrophobic and positively charged residues play significant roles in the interaction with the membrane. In many cases, the membrane association of peripheral membrane proteins is dependent on more than one mechanism. It has been shown that electrostatic interactions and hydrophobic interactions can work cooperatively to facilitate membrane targeting. In this process, long-range non-specific electrostatic interactions allow the adsorption of positively charged amino acids to lipids of complementary charge, followed by slower hydrophobic interactions with the lipid core through a hydrophobic loop or an amphipathic helix [186].

Next, we examined the membrane binding ability of the mutant proteins *in vitro* by two different assays. In the co-sedimentation assay, liposome and its associated proteins are pelleted by ultracentrifugation. By contrast, the co-flotation assay utilizes a sucrose gradient, and thus the liposome-protein complex moves along the sucrose gradient to the uppermost layer instead of going down. The distribution of protein in different fractions for wild-type BacA and the two variants, Δ2-8aa and K4SK7S, is consistent with the *in vivo* study (*Figure 27*), but surprisingly, the Δ2-8aa variant still possessed residual membrane-binding ability, indicative of additional binding region or non-specific binding. One option is to include BSA into the reaction in terms of the latter reason, so that the non-specific interaction between proteins and liposomes can be blocked. Alternatively, we could adjust the concentration of liposome used for the reaction to avoid excessive binding sites. Strikingly, nearly all of F2Y variant associated with liposomes in both assays (*Figure 27*), which we assumed to be related to the oligomeric state of F2Y *in vitro*. TEM demonstrated that F2Y as well as the deletion variant (Δ2-8aa) polymerized as effectively as the wild-type protein, producing macrostructures (*Figure 28*). Compared with monomers and short filaments, the large assemblies may provide more binding sites, which we hypothesize can overcome the reduction in affinity due to the

single exchange. To better characterize the interaction between the F2Y variant and the cell membrane, one alternative is to fractionate *C. crescentus* cells and quantify the percentage of F2Y in each fraction. The other option is to mutate the phenylalanine to a more distinctive residue. Although tyrosine is a polar amino acid because of the hydroxyl group, it shares similarity to phenylalanine in terms of the aromatic ring. Previously, aromatic amino acids have been shown to be favored at the interface of lipid membrane and protein [186, 187]. Hence, a radical change of phenylalanine may generate a more pronounced difference from the wild type. Since neither the K4SK7S nor the F2Y variant recapitulates the behavior of the deletion variant in the liposome binding assay, it would be necessary to test a variant with triple exchanges in the future.

Furthermore, data from both *in vivo* and *in vitro* experiments suggest that the membrane association and polymerization of BacA may be coupled. To clarify this, we fused two amphipathic helixes from *E. coli* MreB in tandem to the Δ2-8aa variant. In line with our expectation, the chimeric protein regained the ability to form foci *in vivo* (*Figure 29A*), and the foci were preferentially distributed along the cell membrane (*Figure 29B*). This is not the first instance, in which the polymerization of bacterial cytoskeletal protein is shown to be driven by membrane association. The actin homologue MreB has the same property [75, 188]. Compared with free movement in a 3D space, the constrained movement on a 2D surface increases the local concentration of cytoskeletal proteins, thereby favoring a polymerization. However, there are remaining questions that need to be addressed in the future. For example, it is still unclear whether the membrane binding of bactofilin is regulated or not and which factor could regulate this process. It has been shown recently that the ATP-bound state of MreB allosterically affects the association to the liposome, which ultimately influences the lateral interaction between MreB protofilaments [189]. It would be interesting to study if such factors also exist for bactofilin.

3.3 Interaction between PbpC and BacA

PbpC is a bifunctional penicillin binding protein that has both transglycosylase and transpeptidase activity. It localizes to the stalked pole of *C. crescentus*, promoting stalk biogenesis. The polar localization of PbpC relies on the interaction of its N-terminal cytoplasmic tail with bactofilin(s) [136]. However, neither the division of labor between BacA and BacB in recruiting PbpC nor the precise nature of the interface between bactofilin and PbpC is clear. Therefore, we first examined the localization of mVenus-PbpC in the presence of only one bactofilin paralogue to differentiate between the functions of BacA and BacB. Strikingly, mVenus-PbpC

was only able to localize to the stalked pole when BacA was present (*Figure 30A*). We then went on to study the dependence of BacA localization on PbpC. Cytoskeletal proteins generally serve dual roles as both recruiters and organizers for their respective PG synthesis machinery, as observed for FtsZ [190], MreB [86] and DivIVA [191]. However, the order can be reversed as shown in alphaproteobacterium *A. biprosthecum*, in which the PG hydrolase SpmX first marks the position for future stalks and recruits bactofilin, which then in turn functions as a scaffolding protein to anchor PG remodeling complex including SpmX to the stalk base [124]. When we examined the subcellular localization of BacA in the Δ*pbpC* background, we revealed that BacA can invariantly localize to the stalked pole regardless of the absence of PbpC (*Figure 30B*).

Subsequently, we strived to elucidate the interaction between PbpC and BacA. The cytoplasmic region of PbpC was compared against the protein sequence database using the PSI-BLAST algorithm [192]. The resulting homologous sequences are mostly distributed in *Caulobacter* species and are part of a domain named PBP_N. The sequence alignment revealed that the cytoplasmic tail of PbpC includes two conserved motifs, a proline-rich region that separate these two motifs and a positively charged region immediately preceding the transmembrane helix (*Figure 31*). To assess the function of different regions, we constructed two PbpC variants (*Figure 32A*). The first one lacks the conserved region C1 corresponding to aa 2-13, whereas in the second one, the region of the cytoplasmic tail following motif C1 was replaced by an unstructured region of the periplasmic protein DipM. The localization study has demonstrated that the conserved region C1 was essential for the protein-protein interaction, since the absence of that region abolished the recruitment of PbpC to the stalked pole by BacA (*Figure 32B*). The result from the *in vivo* study was further substantiated by bio-layer interferometry. We derived an apparent equilibrium dissociation constant of 4.9 μM for the interaction of PbpC and BacA. Additional effort was also made to identify the interaction interface on BacA by HDX-MS. It appears that BacA interacts with PbpC via the C-terminal of its bactofilin domain. Of note, the difference in HDX between the bound state and the apo state was small, but it could be rationalized by the facts that either the interaction region is blocked by the polymerization of BacA or the interaction between BacA and peptide is transient and thus difficult to capture.

In conclusion, our data has clarified the interaction between BacA and PbpC, which may provide insight into the interaction between bactofilin and its binding partners in other bacterial species. Heretofore, bactofilin homologues have been demonstrated to interact with several different peptidylglycan remodeling proteins, such as the PG hydrolase SpmX in *A.*

biprosthecum [124] and the M23 endopeptidase LmdC in *H. neptunium* (unpublished), but the detail regarding the interaction has never been investigated.

3.4 Novel interaction partners for bactofilins

In this study, we also screened for novel interaction partners of bactofilins in *C. crescentus*. The motivation is twofold: firstly, studying the interactome can provide a better view of the biological function of bactofilin; secondly, a potential new interaction partner may regulate the polymerization of bactofilin, which is a missing puzzle piece. Hence, we used co-immunoprecipitation followed by mass spectrometry. For BacA-HA, two additional proteins were discovered except for PbpC, namely CC1891 and CC3376 (*Figure 35A*). Interestingly, there were 21 proteins in total significantly enriched in the Co-IP for BacB-HA (*Figure 35B*), which is much more than the number of proteins identified for BacA. We reasoned that the longer tails of BacB may account for that. The functions of these proteins are diverse, but nearly half of them are directly or indirectly related to membrane-associated proteins. For instance, there are proteins involved in lipoprotein transportation, ABC transporters, components of Tol-Pal system and TonB-dependent transporters, which indicates that BacB potentially plays an important role in the integrity of the cell envelope. Since CC1891 and CC3376 interact with both BacA and BacB, we decided to first focus on them.

CC3376 is annotated as an uncharacterized protein with a central DUF2385 domain. There is little information about this protein, making it hard to infer the function. A phylogenetic analysis of the DUF2385-containing proteins showed that this domain is primarily distributed in the alphaproteobacteria (*Figure 36A*). Further analyses demonstrated that CC3376 possesses an N-terminal signal peptide and is a substrate for the Sec-dependent secretion pathway (*Figure 36B*), which raises questions about how CC3376 as an exocytoplasmic protein can interact with bactofilin. One of our hypotheses is that the interaction is mediated by an adaptor protein. Because PbpC spans the cell envelope, we re-examined the interaction between CC3376 and BacA in the absence of PbpC. The data from the Co-IP showed that the number of hits for CC3376 was significantly reduced in that condition (*Figure 37*), which implies that our hypothesis is correct. Nevertheless, the physiological relevance of the interaction between PbpC and CC3376 remains unclear and requires further study. Moreover, we noticed that gene encoding CC3376 is located in an operon with *CC3374* and *CC3375* (*Figure 36C*). CC3374 is a NfeD-like protein that is normally associated with a stomatin-like protein, in this case, CC3375. They are homologues to the *E. coli* YbbJ and YbbK proteins, which were shown to suppress the sensitivity of a Δ*ftsH* strain to high temperature [193]. If CC3374 and CC3375 play the

similar roles as their homologues in *E. coli* and CC3376 indeed interacts with these two proteins, it will support the notion that bactofilins are also crucial for cell envelope homeostasis in *C. crescentus*. To investigate the function of CC3376, we constructed deletion strains. However, the deletion affected neither the cell morphology nor the localization of bactofilins (*Figure 38*). Since *CC3376* is in an operon, the deletion of the whole operon may provide more insights. Furthermore, we tried to localize CC3376 in *C. crescentus* by fusing it to the red fluorescent protein mCherry. However, no fluorescent signal could be detected, which is possible that the tag interferes with protein function. An alternative approach could be use immunofluorescence to visualize CC3376.

As for the other candidate CC1891, it is annotated to be a pentapeptide repeat family protein. The first pentapeptide repeat protein HglK was identified in the cyanobacterium *Anabaena* sp. strain PCC 7120 in 1995 [163]. It contains 36 degenerated pentapeptide repeats at its C-terminus preceded by four transmembrane-spanning regions and it is suggested to function as a glycolipid transporter. With the development of a search algorithm and the increase in the number of sequenced species, a great variety of pentapeptide repeat proteins were discovered and they are distributed across the bacterial lineages and also present in several eukaryotic species, such as *Plasmodium falciparum*, *Arabidopsis*, zebrafish, mouse, and human. The consensus sequence of the pentapeptide repeat was proposed to be [S,T,A,V][D,N][L,F][S,T,R][G] [194], which, however, has been updated recently after analyzing more sequences. The possible candidate at each position is expanded [195]. The structures of several PRPs have been solved, which all are characterized by a right-handed quadrilateral β-helix [164, 196–198]. Moreover, studies have shown that when a pentapeptide repeat protein acts as a topoisomerase poison resistance factor, it generally contains a C-terminal β /α/ β structure, through which the protein can dimerize [199]. A sequence alignment and structure prediction demonstrate that CC1891 shares the common features of pentapeptide repeat proteins. Its 36 repeats are segmented into 9 coils (*Figure 39A*) and there is a loop between face 3 and face 4 of coil 6, which breaks the consistency of the structure (*Figure 39B*). The interruption in pentapeptide repeat proteins is ubiquitous, especially in the class conferring quinolone resistance [164]. The function of PRPs is diverse. For instance, HetL from cyanobacterium *Nostoc* sp. PCC 7120 is implicated in heterocyst differentiation [197], and MfpA from *Mycobacterium tuberculosis* inhibits the activity of DNA gyrase conferring resistance to ciprofloxacin and sparfloxacin [200]. Thereby, it is hard to infer the role of CC1891. To illustrate the interaction between CC1891 and BacA, we decided to co-purify the two proteins with a hexahistidine tag fused to the N-terminal end of BacA. Of note, the solubility of BacA was improved upon co-expression

(*Figure 40A*). On the one hand, this could be due to the presence of CC1891. On the other hand, we cannot exclude a possible negative impact of the N-terminal His_6-tag on the membrane association. Non-tagged CC1891 co-eluted with His_6-BacA (*Figure 40B*), indicating an interaction between these two proteins *in vitro*. We further studied the localization pattern of CC1891 in *C. crescentus*. Contradictory to our expectation, mCherry-tagged CC1891 was diffuse within the cells instead of co-localizing with BacA at the stalked pole (*Figure 41A*). We found a possible explanation for this observation through literature searches. According to a previous study, CC1891 is an outer membrane protein and it may function as a receptor for the contact-dependent toxins CdzC/D [166]. Nevertheless, more questions regarding the interaction between BacA and CC1891 arise. Our primary aim was to clarify the localization of CC1891, for which we employed bioinformatics tools and β-lactamase assay. Sequence analyses detected no signal peptide in CC1891 that may facilitate its translocation from the cytosol to the outer membrane. Moreover, the CC1891-Bla fusion did not enable growth on ampicillin plates, unlike the positive controls StpA-Bla and StpB-Bla (*Figure 41B*). Since the subcellular localization of the fused β-lactamase affects the result of the assay, the negative result does not necessarily mean that CC1891 is not exported. To precisely localize CC1891, it is better to repeat the fractionation experiment as performed in the paper. Because *C. crescentus* encodes six pentapeptide repeat proteins (CC0350, CC0587, CC1890, CC1891, CC2259 and CC2260), but only CC1891 was enriched in the Co-IP for both BacA and BacB, it is unlikely that the interaction between bactofilins and CC1891 is non-specific. If CC1891 is indeed an exocytoplasmic protein, there are two possible explanations for the Co-IP results. Either the crosslinking by formaldehyde captured the transient interaction between these two proteins before the transportation of CC1891, or there is a linker protein bridging the two proteins, analogously to the interaction seen for BacA and CC3356. Overall, more evidence is required to support the interaction between bactofilins and CC1891.

In brief, the co-immunoprecipitation analysis detected a number of potential binding partners for bactofilins in *C. crescentus*. We do not yet know their biological functions and cannot explain the biological importance of their interaction with bactofilins. However, the identification of novel interaction partners implies that bactofilins might be more physiologically important than previous thought. Despite the fact that bactofilins are dispensable in standard laboratory condition, they may be crucial in oligotrophic environments or under other conditions.

3.5 Concluding remarks

In this work, the polymerization mechanism of bactofilin and the interaction between bactofilin and other protein have been studied using the bactofilin homologue in *C. crescentus*. Collectively, several conserved hydrophobic residues at the ends of the bactofilin domain were identified to be vital for the formation of the non-polar protofilaments. The further assembling into marcostructures, such as bundles and 2D crystalline sheets, appears to be mediated by the electrostatic forces. Moreover, the investigations on the membrane association, which is a universal property of bactofilin, has suggested that it plays an important role in the polymerization. Apparantly, restriction of bactofilin in 2D-space by membrane binding increases the local protein concentration, which favors the polymerization. In addition, we elucidated the interaction between BacA and the bi-functional penicillin-binding protein PbpC. The interfaces on both proteins were pinpointed and the binding affinity between them was derived. We also performed co-immunoprecipitation to explore the interatome of bactofilins with the aim to identify potential regulators for the polymerization and other interaction partners. Numerous proteins were identified, however, their biological relevances remain largerly unresolved. It will be an important aspect of subsequent research to elucidate the interaction between bactofilins and these proteins. Furthermore, there are other theories about the regulation of bactofilin polymerization, for instance, the membrane curvature was hinted in this process. It would be intriguing to explore those possibilities in the future.

4 Material and Methods

4.1 Materials

4.1.1 Chemicals and enzymes

Reagents used in this work were obtained from the following manufacturers: Abcam (UK), Analytical Jena (Germany), Avanti® Polar Lipids (USA), Becton Dickinson (USA), Bio-Rad (USA), Biotium (USA), Carl-Roth (Germany), ChromoTek (Germany), Difco (Spain), GE Healthcare (UK), GenScript (USA), Invitrogen (Germany), Merck Millipore (Germany), PerkinElmer (USA), Sigma-Aldrich (USA), and Thermo Fisher Scientific (USA).

Restriction enzymes were obtained from New England Biolabs (USA) or Thermo Fisher Scientific (USA). The polymerase chain reaction (PCR) was performed either with KOD Hot Start DNA polymerase (Merck Millipore, Germany) or with Biomix™ Red (Bioline, Germany). The ligation of two DNA molecules was catalyzed by T4 DNA ligase (Thermo Fisher Scientific, USA).

4.1.2 Kits

Table 1 Commercial kits used in this study

Kit	Application
GenElute™ Gel Extraction Kit (Sigma-Aldrich, USA)	Extraction of DNA fragments from agarose gel
GenElute™ PCR Clean-Up Kit (Sigma-Aldrich, USA)	Purification of PCR amplicons
GenElute™ Plasmid Miniprep Kit (Sigma-Aldrich, USA)	Isolation of plasmids
Illustra bacteria genomicPrep Mini Spin Kit (GE Healthcare, Germany)	Isolation of chromosomal DNA
Q5® site-directed mutagenesis kit (New England Biolabs, USA)	Introduction of point mutations
Western Lightening™ Chemiluminescence Reagent Plus kit (PerkinElmer, USA)	Detection of chemiluminescence

4.1.3 Buffers and solutions

All standard buffers and solutions were prepared according to previously published protocols [201, 202]. The chemical components were dissolved in de-ionized water (Purelab Ultra water purification systems, ELGA, Germany) and sterilized either by autoclaving (20 min at 121 °C, 2 bar) or by filtration (pore size 0.22 µm, Sarstedt, Germany). Specific buffers and solutions are listed in the respective method sections.

4.1.4 Media and additives

All media were prepared with de-ionized water. Complex media were sterilized by autoclaving at 121 °C and 2 bar for 20 min, whereas heat-sensitive minimal medium (M2G) and additives such as antibiotics and inducers were sterilized by filtration (pore size 0.22 µm, Sarstedt, Germany). For solid media, 1.5 % (w/v) agar was added prior to autoclaving. The additives were added to pre-cooled media (below 60 °C) when required. The final concentration of antibiotics and other additives used in this study is listed in *Table 2*.

LB (Luria-Bertani) broth:

1% (w/v) Tryptone
0.5% (w/v) Yeast extract
1% (w/v) NaCl

PYE (peptone-yeast-extract):

0.2% (w/v) Peptone
0.1% (w/v) Yeast extract
1 mM $MgSO_4$
0.5 mM $CaCl_2$

M2G (M2 minimal medium with glucose):

6.1 mM Na_2HPO_4
3.9 mM KH_2PO_4
10 mM NH_4Cl
0.5 mM $MgSO_4$
0.5 mM $CaCl_2$
0.2% (w/v) Glucose
0.1% (v/v) $FeSO_4$/EDTA-solution (Sigma-Aldrich, F0518)

Table 2 The final concentration of additives added into media

Additives [stock concentration]	**Final concentration** [μg/ml]			
	***E. coli* liquid**	***E. coli* solid**	***C. crescentus* liquid**	***C. crescentus* solid**
Ampicillin [100 mg/ml]	200	200	10	50
Kanamycin [20 mg/ml]	30	50	5	25
Chloramphenicol [10 mg/ml]	20	30	2	2
Gentamycin [1 mg/ml]	15	20	0.5	5
Spectinomycin [20 mg/ml]	50	100	25	50 + 5 streptomycin
Streptomycin [10 mg/ml]	30	30	5	5
D(+)-glucose [20%]	-	-	0.2%	0.2%
D(+)-sucrose [30%]	-	-	3%	3%
D(+)-xylose [20%]	-	-	0.005%/0.3%	0.3%
Vanillate [0.5 M]	-	-	0.5 mM	0.5 mM
IPTG [1 M]	1 mM	1 mM	-	-

4.2 Microbiological methods

4.2.1 Bacterial strains and growth condition

All *C. crescentus* strains were derived from the wild-type strain NA1000 (CB15N) and grown either in liquid media (PYE or M2G) or on PYE agar plates at 28 ˚C. *E. coli* strains were cultivated in LB medium or on LB agar plates. *E. coli* TOP10 was used for general cloning purposes and grown at 37 ˚C. *E. coli* Rosetta(DE3)/pLysS (Invitrogen, Germany) was used for protein overproduction. It was inoculated at 18 ˚C or 37 ˚C. Liquid cultures were shaken at agitation speed of 220 rpm. When required, antibiotics and other additives were supplemented according to *Table 2*. A complete list of the bacterial strains (*Table S1*) used in this study is found in the appendix.

4.2.2 Storage of cells

For long-term storage of bacterial strains at -80 ˚C, overnight cultures were mixed with 20% (v/v) sterilized DMSO. The pre-sterilized cryo vials (Thermo Fisher Scientific, USA) were used as containers.

4.2.3 Measurement of cell density

The optical density (OD_{600}) of bacterial cultures was measured photometrically using a Ultrospec™ 2100 pro UV/Visible spectrophotometer (Amersham Phamarcia Biotech, UK) at a wavelength of 600 nm. The corresponding culture media were used as blanks.

4.2.4 Preparation of *E. coli* competent cells

To prepare chemically competent cells, an overnight *E. coli* culture was diluted 1:100 in 250 ml LB medium. Cells were grown to the mid-exponential phase (OD_{600} ~0.6) before cooling down on ice. After 10 min of cooling, cells were collected by centrifugation (5000 ×g, 4 °C, 10 min). The pellet was resuspended in 15 ml ice-cold 0.1 M $CaCl_2$ and incubated on ice for 30 min. Afterwards, cells were centrifuged again as specified above and resuspended in 4 ml of ice-cold buffer composed of 0.1 M $CaCl_2$ and 10% (v/v) glycerol. The competent cells were split into 80 µl aliquots and stored at -80 °C for later use.

4.2.5 Transformation of *E. coli*

The frozen competent cells were first thawed on ice and then mixed with 1 µl plasmid, 5 µl ligation product or 5 µl Gibson assembly product. The mixture was incubated for 30 min on ice before a heat shock at 42 °C for 45 sec. After 2 min of cooling on ice, 1 ml LB medium was added to cells. Subsequently, the cells were grown at 37 °C for at least 30 min to allow expression of the selection marker before plating on LB agar plates supplemented with selective antibiotics.

4.2.6 Preparation of *C. crescentus* competent cells

Electrocompetent cells of *C. crescentus* were prepared by following a previously established protocol [203]. Cells were grown in PYE media until the late exponential phase (OD_{600} ~1.0) and then cooled down on ice. Afterwards, they were collected by centrifugation (12,000 ×g, 4 °C, 10 min). The cells were resuspended in the same volume of ice-cold 10% (v/v) glycerol and centrifuged again (6500 ×g, 4 °C, 10 min). This step was repeated twice, but in the last round 1/10 of the original volume was used. Finally, cells were resuspended in 1/50 volume of ice-cold 10% (v/v) glycerol and split into 80 µl aliquots, which were snap-frozen in liquid nitrogen and stored at -80 °C until use.

4.2.7 Electroporation of *C. crescentus*

To electroporate *C. crescentus* competent cells, a frozen aliquot of competent cells was first thawed on ice and then mixed with 10 µl of purified plasmid. After 5 min of incubation on ice,

the mixture was transferred into a pre-cooled electroporation cuvette (0.1 cm electrode; Bio-Rad, USA), which was subjected to a pulse of 1500 V, 400 Ω, 25 μF (Gene Pulser Xcell, Bio-Rad, USA) and immediately mixed with 900 μl of ice-cold 2xPYE. Subsequently, cells were incubated at 28 °C for 2 h before plating on PYE agar plates containing suitable antibiotics.

4.2.8 β-lactamase assay

To assess if CC1891 is exported, the *bla* gene was fused to the 5' end of the gene encoding CC1891 and the construct was integrated at the *xylX* locus of CS606 strain (Δ*bla*). Cells of strain LY49 (Δ*bla xylX*::P*xyl-cc1891-bla*), SS165 (Δ*bla xylX*::P*xyl-stpB-bla*), SS172 (Δ*bla xylX*::P*xyl-stpA-bla*), CS606 (CB15N Δ*bla*) and CB15N were patched on PYE agar containing 50 μg/ml ampicillin and inducer (0.2% glucose or 0.3% xylose). The plates were incubated at 28 °C for two days and imaged with a Gel Doc XR+ system (Bio-Rad, USA).

4.3 Molecular cloning

4.3.1 Construction of plasmids

Plasmids used in this study were designed via SnapGene® (Version 3.3.4; Dotmatics, USA) and validated by sequencing the resulting constructs. Oligonucleotides for molecular cloning were synthesized by Eurofins Genomics (Germany) or Microsynth (Germany). The Sanger sequencing of PCR products and plasmids was performed by Microsynth (Germany) and the preparation of samples was according to the user guide. The detail of the plasmids (*Table S2*) and oligonucleotides (*Table S3*) used in this study can be found in the appendix.

4.3.2 Isolation of DNA

DNA fragments from PCR or restriction digestion were purified by using either GenElute™ PCR Clean-Up Kit (Sigma-Aldrich, USA) or GenElute™ Gel Extraction Kit (Sigma-Aldrich, USA) following the manual. Plasmids were extracted from *E. coli* cells using the GenElute™ Plasmid Miniprep Kit (Sigma-Aldrich, USA). Genomic DNA of CB15N was isolated using the NucleoSpin® Microbial DNA Kit (Macherey-Nagel, Germany).

4.3.3 Polymerase chain reaction

PCR for general purpose

To amplify DNA fragments for cloning purposes, KOD Hot Start DNA polymerase (Merck Millipore, USA) was used. The standard reaction setup and cycling conditions are listed in *Table 3*.

Table 3 The standard setup and cycling conditions for PCR amplification using KOD Hot Start DNA polymerase

The composition of reaction		Cycling conditions		
Components	**Volume**			
10x KOD buffer	5 µl	Polymerase activation	95 ˚C for 2 min	
DMSO	5 µl			
dNTPS (2mM each)	5 µl	Denaturation	95 ˚C for 30 s	35x
25 mM $MgSO_4$	3 µl	Annealing	Lowest primer Tm ˚C for 30 s	
Forward primer (10 µM)	1.5 µl	Extension	70 ˚C for 30 s/kb	
Reverse primer (10 µM)	1.5 µl			
Template DNA (10 ng/µl)	1 µl	Final extension	70 ˚C for 10 min	
KOD polymerase (1 U/µl)	1 µl			
ddH_2O	27 µl	Hold	10 ˚C for ∞	
Total volume	50 µl			

Colony PCR

To perform PCR analyses on cells, colonies were picked from the agar plate using sterilized toothpicks and transferred into 15 µl aliquots of BioMix™ Red (Bioline, Germany). The components of the reaction mixture and cycling conditions are listed in *Table 4*.

Table 4 The standard setup and cycling conditions for colony PCR using BioMix™ Red

The reaction mixture (10 x 15 µl)		Cycling conditions		
Components	**Volume**	Polymerase activation	95 ˚C for 5 min	
2x BioMix™ Red	75 µl			
DMSO	7.5 µl	Denaturation	95 ˚C for 30 s	35x
Forward primer (10 µM)	0.75 µl	Annealing	58-65 ˚C for 30 s	
Reverse primer (10 µM)	0.75 µl	Extension	72 ˚C for 30 s/kb	
ddH_2O	66 µl			
Total volume	150 µl	Final extension	72 ˚C for 4 min	
		Hold	10 ˚C for ∞	

Mutagenesis PCR

To introduce desired mutations into the target gene, KOD Hot Start polymerase (Merck Millipore, USA) or the Q5® site-directed mutagenesis kit (New England Biolabs, USA) was used. For the mutagenesis with KOD polymerase, the protocol is similar to the one used for general DNA amplication, except for the number of cycles, which was reduced to 20. To remove the template DNA, PCR products were treated with 1 µl *Dpn*I at 37 ˚C for 1 h before transformation.

When the mutagenesis kit was used, the primers were designed using online NEBaseChanger® tool. The composition and thermocycling conditions were listed in *Table 5*. The resulting products were treated with the provided multi-enzyme KLD mix at room temperature for 5 min to remove the template DNA and cyclize the PCR products. The setup of the reaction can be found in *Table 6*.

Table 5 Reaction mixture for Q5® site-directed mutagenesis and the cycling conditions

The composition of reaction		Cycling conditions		
Components	**Volume**	Polymerase activation	98 °C for 2 min	
2x Master mix	12.5 µl			
Forward primer (10 µM)	1.25 µl	Denaturation	98 °C for 10 s	25x
Reverse primer (10 µM)	1.25 µl	Annealing	50-72 °C* for 30 s	
Template DNA (1-25 ng/µl)	1 µl	Extension	72 °C for 30 s/kb	
ddH_2O	9 µl			
Total volume	25 µl	Final extension	72 °C for 4 min	
		Hold	10 °C for ∞	

* The Tm is calculated by NEBaseChanger®

Table 6 The setup for KLD reaction

Components	Volume
PCR product	1 µl
2x KLD reaction buffer	5 µl
10x KLD enzyme mix	1 µl
ddH_2O	3 µl
Total volume	10 µl

4.3.4 Agarose gel electrophoresis

To determine the size of DNA fragments or purify the fragment of interest, DNA products were first mixed with 6x DNA gel loading dye (Thermo Fisher Scientific, USA) if needed and then applied to a 1 % agarose gel supplemented with GelRed® nucleic acid gel stain (Biotium, USA). GeneRuler 100 bp or 1kb DNA Ladder (Thermo Fisher Scientifc, USA) served as a size standard. Gels were immersed in 0.5x TAE running buffer (20 mM Tris/HCl, pH 8, 0.175 % acetic acid, 0.5 mM EDTA, pH 8.0) and run at a constant voltage of 160 V for 25 min. The separated DNA fragments were visualized with a UV-Transilluminator (UVP-BioDoc-ITTM Imaging System; UniEquip, Germany).

4.3.5 Restriction digestion

Restriction digestion was performed at 37 °C overnight following the instructions provided by the manufacturers. Afterwards, the sample was cleaned either with the GenElute™ PCR Clean-Up Kit (Sigma-Aldrich, USA) or the GenElute™ Gel Extraction Kit (Sigma-Aldrich, USA).

Table 7 The protocols for restriction digestion

Restriction enzymes from NEB		FastDigest® enyzmes from Thermo Fisher Scientific	
10x NEB buffer	5 µl	10x FastDigest® buffer	2 µl
Enzyme A	1 µl	Enzyme A	1 µl
Enzyme B	1 µl	Enzyme B	1 µl
DNA	1 µg	DNA	1 µg
ddH_2O	Up to 50 µl	ddH_2O	Up to 20 µl

4.3.6 Ligation

Two DNA fragments were ligated using T4 DNA ligase (Thermo Fisher Scientific, USA) according to the manual. The molar ratio of insert and vector was 3:1. The reaction mixture (*Table 8*) was incubated at room temperature for 1 h.

Table 8 The reaction mixture for ligation

Components	Volume
10x T4 ligase buffer	2 µl
Linearized vector DNA	x µl (20 to 100 ng)
Insert DNA	y µl (3:1 molar ratio over the vector)
T4 DNA ligase	1 µl
ddH_2O	Up to 20 µl

4.3.7 Gibson assembly

Gibson assembly was performed as an alternative to restriction cloning. A total volume of 5 µl of linearized vector and DNA insert (molar ratio 1:1) was added to 15 µl ready-to-use Gibson assembly master mix. The reaction mixture was incubated at 50 °C for 1 h. The composition of the master mix and 5x isothermal reaction buffer can be found below (*Table 9*).

Table 9 The composition of Gibson assembly master mix and 5x isothermal reaction buffer

Master mix of Gibson assembly		5x isothermal reaction buffer	
5x isothermal reaction buffer	320 µl	PEG 800	25% (w/v)
T5 Exconuclease (10 U/µl)	0.64 µl	Tris-HCl, pH 7.5	500 mM
Phusion DNA polymerase (2U/µl)	20 µl	$MgCl_2$	50 mM
Taq DNA ligase (40 U/µl)	160 µl	DTT	50 mM
ddH_2O	699.36 µl	NAD	5 mM
Total volume	1200 µl	dNTPs	1 mM

4.4 Microscopic methods

4.4.1 Light microscopy and fluorescence microscopy

To prepare samples for microscopy, overnight cultures were diluted to an OD_{600} of 0.1 and grown for another 1 h before adding 0.005% or 0.3% xylose. After a few hours (the exact induction time are indicated in respective figure legend), cultures were diluted 10 times and 1.5 µl of dilutions were spotted on 1% agarose pads prepared with ddH_2O.

Images were taken with an Axio Observer. Z1 microscope (Zeiss, Germany) equipped with a Plan Apochromat 100x/1.45 Oil DIC, a Plan Apochromat 100x/1.4 Oil Ph3 phase contrast objective, and a pco.edge sCMOS camera (PCO, Germany). The X-Cite® 120PC metal halide light source (EXFO, Canada) and appropriate filter cubes (ET-CFP, ET-YFP or ET-TaxasRed; Chroma, USA) were used for fluorescence detection. Images were recorded with VisiView 3.3.0.6 (Visitron Systerms, Germany) and processed with Fiji [204] and Adobe Illustrator CS6

(Adobe Systems). The subcellular distribution of fluorescence signals was analyzed with BacStalk [205].

4.4.2 Transmission electron microscopy

Protein samples of appropriate concentrations were applied to carbon-coated copper grids (400 mesh) that were hydrophilized by glow discharging (PELCO easi-Glow, Ted Pella, USA). Subsequently, the samples were stained with 2% uranyl acetate after a short washing step with H_2Obidest. Images were acquired with a JEOL JEM-2100 transmission electron microscope equipped with a F214 FastScan CCD camera (TVIPS, Germany), using an acceleration voltage of 120 kV.

4.4.3 Single-molecule tracking

Cells for single-molecule tracking were grown in M2G minimal media at 28 °C. 0.3% xylose was supplemented in the early exponential phase. After a 3-hour induction, cells were spotted on coverslips (diameter: 25 mm; Menzel Gläser, Germany) and covered with 1% agarose pads prepared with ddH_2O. All coverslips were cleaned before use by sonication in 1% (v/v) Hellmanex II solution for 15 min, followed by rinsing in distilled water and a second round of sonication in double-distilled water. The excitation laser beam was directed to underfill the back aperture of the objective lens, generating a concentrated parallel light source, which leads to a strong excitation followed by rapid bleaching of the fluorophores. Only unbleached molecules as well as newly synthesized and folded fluorophores can be tracked. When an observed molecule is bleached in a single step during imaging, it is assumed to be a single molecule [206]. Images were acquired with an Olympus IX71 microscope (Olympus, Japan) equipped with a UAPON 100×OTIRF objective (Olympus, Japan) and an electron-multiplying CCD (EMCCD) camera iXon Ultra (Andor Technology, Belfast, UK). A 514-nm laser diode was used as the excitation light source, and the band corresponding to the fluorophore was filtered out. A total of 2500 frames were taken per movie with an exposure time of 20 ms (23 fps). The acquired streams were loaded into Fiji [204] for analysis and the automated tracking of single molecules was performed by the MATLAB-based software u-track 2.2.0 [207].

4.5 Biochemical methods

4.5.1 Protein overproduction

To overproduce proteins for purification, Rosetta(DE3)/pLysS cells with appropriate plasmids were grown overnight at 37 °C and diluted 100 folds on the following day. 1 mM isopropyl β–D-1-thiogalactopyranoside (IPTG) was added to the fresh culture when the OD_{600} reached approximately 0.6. All proteins were produced at 37 °C for 4 h, except for $BacA_{surfmut}$-StrepII, whose overproduction was conducted at 18 °C overnight. Afterwards, cells were harvested by centrifugation and stored at -80 °C.

4.5.2 Protein purification

Purification of BacA variants by affinity chromatography and SEC

$BacA_{F130R}$-His_6 and His_6-SUMO-$BacA_{37\text{-}161aa}$ were purified by affinity chromatography followed by size exclusion chromatography. For this two-step purification, cell pellets were re-suspended in B1 buffer (50 mM HEPES/NaOH pH7.2, 300 mM NaCl, 5 mM $MgCl_2$, 0.1 mM EDTA, 5% glycerol and 20 mM imidazole) supplemented with 10 µg/mL DNase I and 100 µg/mL phenylmethylsulfonyl fluoride (PMSF) and lysed by three passages through a French press at 16,000 psi. The crude cell extract was centrifuged at 16,000 rpm, 4 °C for 30 min to remove the insoluble fraction. The cleared lysate was loaded onto an equilibrated 5 ml HisTrap™ HP affinity column (GE Healthcare, USA). The column was first washed with 10 column volumes (CVs) B1 buffer followed by elution of the protein with a linear gradient of 20 – 250 mM imidazole over 10 CVs. The fractions containing a high amount of the protein of interest were concentrated using Amicon® Ultra Centrifugal Filters (Merke Millipore, Germany) and then applied to HiLoad® 16/600 Superdex® 200 prep grade size exclusion column (GE Healthcare, USA) that had been equilibrated with B2 buffer (50 mM HEPES/NaOH pH7.2, 300 mM NaCl, 5 mM $MgCl_2$, 0.1 mM EDTA and 5% glycerol). The column was washed with 1.5 CVs B2 buffer to separate the loaded proteins. Buffers used for purifying His_6-SUMO-$BacA_{37\text{-}161aa}$ were additionally supplemented with 1 M urea, which was subsequently removed by overnight dialysis in B2 buffer. After analysis on a 15% SDS-PAGE gel, fractions containing the protein of interest were concentrated using Amicon® Ultra Centrifugal Filters (Merke Millipore, Germany) and sent for TEM analysis when necessary.

Two-step affinity chromatography for proteins with SUMO tag

Four BacA variants, namely the wild type, Δ2-8aa, F2Y and K4SK7S, were purified as N-terminal His_6-SUMO fusions. In the first step of purification with a 5 ml HisTrap™ HP affinity column (GE Healthcare, USA), the fusion proteins were separated from contaminants. The

procedure was similar to the one used to purify $BacA_{F130R}$-His_6 except for the buffer. To purify these proteins, B3 buffer (50 mM Tris/HCl pH8.0, 300 mM NaCl, 1 mM EDTA, 5% glycerol and 20 mM imidazole) was used. The purified proteins were dialyzed overnight against imidazole-free B3 buffer supplemented with 30 µl Ulp1-His_6 protease (approximately 7 mg/ml) and 1 mM DTT to cleave off the His_6-SUMO tag and remove the imidazole. Subsequently, the untagged BacA variants, the tag and the protease were separated by passage through the affinity column one more time. The flow-through fractions were collected and the presence of the desired protein was examined by SDS-PAGE gel. $BacA_{\Delta 2\text{-}8aa}$ was dialyzed against B4 buffer (50 mM Tris/HCl pH8.0, 200 mM NaCl, 1 mM EDTA, 5% glycerol), whereas the other variants were dialyzed in B5 buffer (50 mM MOPS/NaOH pH7.0, 200 mM NaCl, 1 mM EDTA, 5% glycerol). After dialysis, the protein sample was concentrated and stored in small aliquots at -80 °C for later use.

Purification of StrepII-tagged protein

Cells containing $BacA_{surfmut}$-StrepII were resuspended in B6 buffer (50 mM NaH_2PO_4 pH7.2, 300 mM NaCl, 1 mM EDTA and 10% glycerol) supplemented with 10 µg/mL DNase I and 100 µg/mL PMSF and lysed by three passages through a French press at 16,000 psi. The crude cell extract was centrifuged at 16,000 rpm, 4 °C for 30 min to remove the insoluble fraction. The cleared lysate was loaded onto an equilibrated 5 ml StrepTrap™ HP column (GE Healthcare, USA). The column was first washed with 10 CVs B6 buffer followed by an elution with 2.5 mM D-desthiobiotin over 6 CVs. After analysis on a 15% SDS-PAGE gel, fractions containing the protein of interest were combined and dialyzed against B6 buffer overnight. Subsequently, the purified proteins were concentrated using Amicon® Ultra Centrifugal Filters (Merke Millipore, Germany) and sent for TEM analysis.

Co-purification of His_6-BacA and CC1891

Cells were re-suspended in B1 buffer with 10 µg/mL DNase I and 100 µg/mL PMSF and lysed by three passages through a French press at 16,000 psi. The crude cell extract was centrifuged at 16,000 rpm, 4 °C for 30 min to remove the insoluble fraction. Ni-NTA agarose (Qiagen, Germany) was prepared according to the manufacturer's instruction. The cleared lysate was incubated with the Ni-NTA matrix at 4 °C for 1 h to facilitate the binding of proteins to the matrix. Afterwards, the mixture was loaded to gravity flow column and washed 2 times with 5 CVs B1 buffer, followed by 5 elution steps with 1 CV B1 buffer supplemented with 250 mM imidazole. All fractions were analyzed on 15% SDS-PAGE gel. Subsequently, the band corresponding to the size of CC1891 was sliced out and sent for mass spectrometric analysis.

4.5.3 Sodium dodecyl sulfate-polyacrylamide gel electrophoresis (SDS-PAGE)

Purified proteins were directly mixed with an equal volume of 2x SDS sample buffer (300 mM Tris Base, 50% (v/v) glycerol, 5% (w/v) SDS, 500 mM dithiothreitol, 0.05% bromophenol blue, pH6.8). Cells were first pelleted by centrifugation and resuspended in 2x SDS sample buffer according to their optical density (100 µl buffer per 1 ml of culture with an OD_{600} of 1). The protein samples were treated at 95 °C for 10 min. Subsequently, samples along with the PageRuler ™ Plus Prestained Protein Ladder, 10 to 250 kDa (Thermo Fisher Scientific, USA) were loaded on an SDS-PAGE gel consisting of a 5% stacking gel and an 11% or 15% resolving gel (*Table 10*). Electrophoresis was conducted in Tris/Glycine buffer (25 mM Tris Base, 192 mM glycine, 0.1 % (w/v) SDS) at 30 mA per gel using a PerfectBlue™ Twin S system (Peqlab, USA).

For the visualization of proteins, SDS-PAGE gels were stained after electrophoresis for 45 min in Coomassie solution (40 % methanol, 10 % acidic acid, 0.1 % (w/v) Brilliant Blue R 250) and excess dye was removed by incubation in destaining solution (20 % ethanol, 10 % acidic acid). Occasionally, InstantBlue® (Abcam, UK) was used to accelerate the detection process.

Table 10 Composition of stacking and resolving gel

Component	5% stacking gel (2.5 ml)	11% resolving gel (5 ml)	15% resolving gel (5 ml)
ddH_2O	1.43 ml	1.874 ml	1.2 ml
4x stacking buffer (0.5 M Tris Base, 0.4% (w/v) SDS, pH6.8)	625 µl	-	-
4x resolving buffer (1.5 M Tris Base, 0.4% (w/v) SDS, pH8.8)	-	1.25 ml	1.25 ml
30% Rotiphorese® Acrylamide/Bis (29:1)	417 µl	1.833 ml	2.5 ml
10% (w/v) APS (Ammoniumperoxodisulfate)	25 µl	40 µl	40 µl
TEMED (N,N,N',N'-Terramethyletheylendiamine)	1.9 µl	3 µl	3 µl

4.5.4 Immunoblot

To detect specific proteins using immunoblot, proteins separated by SDS-PAGE were transferred onto a polyvinylidene fluoride (PVDF) membrane (Merke Millipore, Germany) using a Trans-Blot Turbo Transfer System (Bio-Rad, USA). To this end, the membrane was first activated in methanol for 15 sec, followed by washing in H_2O for 2 min and equilibration in 1x Turbo transfer buffer (300 mM glysine, 300 mM Tris, 0.05% SDS) for 5 min. The transfer was performed according to the manufacturer's instruction using the preprogrammed Turbo protocol. Subsequently, the membrane was blocked with 5 % (w/v) skim milk in 1x TBST (10 mM Tris base, 150 mM NaCl, 0.1 % (w/w) Tween 20, pH 7.5) overnight at 4 °C with gentle agitation. On the following day, the membrane was first incubated with an anti-GFP (1:10,000;

Sigma-Aldrich, USA), anti-BacA (1:10,000) [136] or anti-mCherry (1:10,000; BioVision, USA) antibody diluted in blocking buffer at room temperature for 2 h. Before incubation of the membrane with a secondary antibody for 1 h, it was washed for 10 min in 1x TBST for three times. Goat anti-Rabbit IgG (H+L) secondary antibody conjugated to horsedish peroxidase (1:20,000, Invitrogen, USA) was the used to visualize the protein of interest. After the incubation, the membrane was rinsed three times and incubated with Western Lightning™ Chemiluminescence Reagent Plus (PerkinElmer, USA) according to the manual for 5 min. The signal was detected with a ChemiDoc™ MP Imaging System (Bio-Rad, USA).

4.5.5 *In vitro* crosslinking

Purified BacA was dialysed against a non-amine-containing buffer (20 mM HEPES pH7.8, 150 mM NaCl) and BS^3 (Thermo Fischer Scientific, USA) was dissolved in water according to the manufacturer's instructions. The freshly dissolved BS^3 was mixed with proteins at different molar ratios, specifically, 10:1, 20:1 and 40:1. The reaction was conducted at room temperature. Samples were taken from the mixture after 5 min, 15 min and 30 min incubation and quenching buffer (1 M Tris/HCl, pH7.5) was added to a final concentration of 50 mM Tris to stop the reaction. Afterwards, samples were separated in a 15% SDS-PAGE gel. Protein bands corresponding to crosslinked species were sliced out, decolored by 3 rounds of buffering (30% Isopropanol, 60 mM $(NH_4)_2CO_3$, 30 mM thioglycolic acid) and shrinking (isopropanol), and dried in a SpeedVac™ concentrator (Thermo Scientific, USA). In-gel digestion was performed by soaking the gels in protease solution (0.0025 g/L trypsin, 10% acetonitrile, 5 mM $NH_4H_2CO_3$, 8 mM DTT) overnight at 900 rpm, 30 °C. On the next day, 50 µl 5% formic acid and 200 µl 0.15% formic acid were added into the samples sequentially and the reaction were incubated for 1 h after each addition. C18-columns were conditioned twice with 150 µl acetonitrile and equilibrated three times with 150 µl buffer A (0.1% TFA). Subsequently, the supernatants were loaded to the columns, which were washed three times with 150 µl buffer C (5% acetonitrile, 95% water, 0.1 % TFA). To elute bond peptides, the columns were washed three times with 100 µl buffer B (50% acetonitrile, 50 % water, 0.1% TFA). The collected peptides were concentrated by vacuum drying and analyzed by liquid chromatography-mass spectrometry/mass spectrometry (LC-MS/MS), which was carried out by Dr. Timo Glatter (Max Plank Institute for Terrestrial Microbiology, Marburg, Germany).

4.5.6 Liposome preparation

1-palmitoyl-2-oleoyl-sn-glycero-3-phospho-(1'-rac-glycerol) (16:0-18:1 PG) (10 mg/mL in chloroform; Avanti® Polar Lipids, USA) was used to generate liposomes. Briefly, the chloroform was evaporated in a rotatory evaporator, and the resulting lipid film was further dried overnight. The lipids were subsequently resuspended in liposome buffer (50 mM MOPS/NaOH pH7.0, 200 mM NaCl). The mixture was incubated at RT for 1 h with occasional vigorous vortexing. The final concentration of the resuspended lipids was 20 mg/mL. To produce ~100 nm single unilamellar vesicles (SUV), the lipid was extruded using a mini-extruder (Avanti® Polar Lipids, USA) equipped with polycarbonate membranes of 0.1 µm pore size.

4.5.7 Co-sedimentation assay

A 100 µl mixture of 20 µM protein ± 1.0 mg/mL liposomes was assembled in the liposome buffer. The mixture was incubated at room temperature for 20 min before being centrifuged at 100,000 ×g, 20 °C for 20 min (TLA-55 rotor, Optima™ MAX-XP Ultracentrifuge). After centrifugation, the supernatant was transferred to a new 1.5-mL Eppendorf tube. The pellet was resuspended in 100 µl of liposome buffer. An equal volume of 2x SDS-PAGE sample buffer was then added and the samples were treated at 95 °C for 10 min before being loaded onto 15% SDS-PAGE gels. Subsequently, proteins were stained in Coomassie blue solution. Protein band intensity was quantified using Fiji software [204].

4.5.8 Co-flotation assay

A 100 µl mixture containing 20 µM protein ± 1.0 mg/mL liposomes was prepared in a liposome buffer. The mixture was incubated at room temperature for 20 min before being gently mixed with 100 µl of 60% (w/v) sucrose in liposome buffer. Afterwards, 250 µl of 25% (w/v) sucrose in liposome buffer and 150 µl liposome buffer were overlaid sequentially. The solution was centrifuged at 200,000 ×g, 20 °C for 20 min (TLA-120.2 rotor, Optima™ MAX-XP Ultracentrifuge). After centrifugation, three equal volumes (200 µl each) were drawn from the ultracentrifugation tube and mixed with 2x SDS-PAGE sample buffer. The samples were treated at 95 °C for 10 min before being loaded onto 15% SDS-PAGE gels. Subsequently, proteins were stained in Coomassie blue solution. Protein band intensity was quantified using Fiji software [204].

4.5.9 Bio-layer interferometry

Bio-layer interferometry experiments were conducted using a BLItz system equipped with Octet® High Precision Streptavidin 2.0 (SAX2) Biosensors (Satorius, Germany). First, biotinylated $PbpC_{1\text{-}13aa}$ peptide (GenScript, USA) was immobilized on the sensor. After the establishment of a stable baseline, association reactions were monitored at various BacA concentrations. At the end of each binding step, the sensor was transferred into an analyte-free buffer to measure the dissociation kinetics. The extent of non-specific binding was assessed by monitoring the interaction of the analyte with unmodified sensors. All analyses were performed in BLItz binding buffer (50 mM MOPS/NaOH pH 7.0, 100 mM NaCl, 1 mM EDTA, 5% glycerol, 10 µM BSA, 0.01 % Tween).

4.5.10 Hydrogen-deuterium exchange mass spectrometry

Samples were prepared using a two-arm robotic autosampler (LEAP technologies, Denmark). 7.5 µl of BacA (25 µM) or the mixture of BacA (25 µM) and $PbpC_{aa\ 1\text{-}13}$ (100 µM) were added into 67.5 µl of D_2O-containing buffer (20 mM HEPES/NaOH pH 8.0, 300 mM NaCl) to start the exchange reaction. After 10, 100, 1000 and 10,000 sec of incubation at 25 °C, 55 µl samples were taken from the reaction and mixed with an equal volume of quench buffer (400 mM KH_2PO_4/H_3PO_4, 2 M guanidine-HCl, pH 2.2) kept at 1 °C. 95 µl of the resulting mixture were immediately injected into an ACQUITY UPLC M-class system with HDX technology (Waters™, USA) [208]. Undeuterated samples of BacA and the mixture of BacA and $PbpC_{aa\ 1\text{-}13}$ were prepared similarly by 10-fold dilution into H_2O-containing buffer. Proteins were digested online on an Enzymate BEH Pepsin column (300 Å, 5 µm, 2.1 mm × 30 mm; Waters™, USA) at 12 °C with a constant flow (100 µl/min) of water + 0.1 % (v/v) formic acid, and the resulting peptic peptides were collected on a trap column (2 mm × 2 cm) that was filled with POROS 20 R2 material (Thermo Fisher Scientific, USA) and kept at 0.5 °C. After 3 min, the trap column was placed in line with an ACQUITY UPLC BEH C18 1.7 µm 1.0 × 100 mm column (Waters™, USA), and the peptides were eluted at 0.5 °C using a gradient of water + 0.1 % (v/v) formic acid (A) and acetonitrile + 0.1 % (v/v) formic acid (B) at a flow rate of 30 µl/min as follows: 0-7 min/95-65 % A, 7-8 min/65-15 % A, 8-10 min/15 % A, 10-11 min/5 % A, 11-16 min/95 % A. Peptides were ionized with an electrospray ionization source operated at 250 °C capillary temperature and a spray voltage of 3.0 kV. Mass spectra were acquired over a range of 50 to 2000 m/z on a G2-Si HDMS mass spectrometer with ion mobility separation (Waters™, USA) in $HDMS^E$ or HDMS mode for undeuterated and deuterated samples, respectively [209, 210]. [Glu1]-Fibrinopeptide B standard (Waters™, USA)

was employed for lock mass correction. After each run, the pepsin column was washed three times with 80 µl of 4 % (v/v) acetonitrile and 0.5 M guanidine hydrochloride, and blanks were performed between each sample. All measurements were carried out in triplicate.

Peptides from the non-deuterated samples (aquired with $HDMS^E$) were identified with ProteinLynx Global SERVER (PLGS, Waters™, USA), employing low energy, elevated energy and intensity thresholds of 300, 100 and 1000 counts, respectively. Peptides were matched using a database containing the amino acid sequences of the proteins of interest, pepsin and their reversed sequences. The search parameters were as follows: peptide tolerance = automatic; fragment tolerance = automatic; min fragment ion matches per peptide = 1; min fragment ion matches per protein = 7; min peptide matches per protein = 3; maximum hits to return = 20; maximum protein mass = 250,000; primary digest reagent = non-specific; missed cleavages = 0; false discovery rate = 100. Deuterium incorporation was quantified with DynamX 3.0 (Waters™, USA), using peptides that fulfilled the following criteria: minimum intensity = 10,000 counts; maximum length = 30 amino acids; minimum number of pro- ducts = 3; minimum number of products per amino acid = 0.05; maximum mass error = 25 ppm; retention time tolerance = 0.5 min. After automated data processing with DynamX, all spectra were manually inspected and, if necessary, peptides were omitted (e.g. in case of a low signal-to-noise ratio or the presence of overlapping peptides).

4.5.11 Co-immunoprecipitation and mass spectrometry

Exponentially growing cells (M2G medium, OD_{600} ~0.6) were incubated at 37 °C for 5 min in the presence of 0.6% formaldehyde. After quenching of the crosslinking reaction by addition of glycine (prepared as a 1.25 M stock solution in PBS) to a final concentration of 125 mM and a 5 min incubation at room temperature, cells were collected by centrifugation, washed twice with 200 ml C1 buffer (50 mM Na_3PO_4 pH 7.4, 5 mM $MgCl_2$), snap-frozen in liquid nitrogen, and stored at -80 °C until further use. Cells were thawed on ice and resuspended in 10 ml C2 buffer (20 mM HEPES/NaOH pH 7.4, 100 mM NaCl, 20% glycerol, 0.5% Triton X-100). The suspension was supplemented with 10 mM $MgCl_2$, 10 mg/ml lysozyme, 5 mg/ml DNase I and 100 mg/ml PMSF, and incubated on ice for 30 min. After disruption of the cells using a French press, cell debris was removed by centrifugation at 13,000 rpm, 4 °C for 5 min. 15 µl of anti-HA-tag mAb-magnetic beads (MBL, Japan) were added to the cleared lysate, which was then incubated at 4 °C for 1 h with gentle agitation. The beads were collected by centrifugation at 5000 ×g for 1 min and suspended in 700 µl of 100 mM ammoniumbicabonate (ABC). Using a magnetic separator, beads were washed 3 times in 100 mM ABC and then

incubated in 100 µl E1 buffer (1.6 M urea, 100 mM ABC, 5 µg/ml trypsin) at 1200 rpm, 27 °C for 30 min. The supernatant was collected in a new tube and beads were washed twice in 40 µl E2 buffer (1.6 M urea, 100 mM ABC, 1 mM tris(2-carboxyethyl)phosphine (TCEP)). The three elutions were combined and left for trypsin digestion overnight. On the following day, the peptides were first alkylated by addition of 40 µl lodoacetamid (5 mg/ml in 100 mM ABC) in the dark for 30 min. Subsequently, the samples were acidified with 150 µl trifluoroacetic acid (TFA), pH < 2. C18-columns were conditioned twice with 150 µl acetonitrile and equilibrated three times with 150 µl buffer A (0.1% TFA). Afterwards, the supernatants were loaded onto the columns, which then were washed three times with 150 µl buffer C (5% acetonitrile, 95% water, 0.1 % TFA). To elute bond peptides, the columns were washed three times with 100 µl buffer B (50% acetonitrile, 50 % water, 0.1% TFA). Collected peptides were concentrated by vacuum drying. The subsequent analyses by LC-MS/MS were carried out by Dr. Timo Glatter (Max Plank Institute for Terrestrial Microbiology, Marburg, Germany).

4.6 Bioinformatic analyses

4.6.1 Sequence analyses

C. crescentus CB15N nucleotide and protein sequences were obtained from the National Center for Biotechnology Information (NCBI) (https://www.ncbi.nlm.nih.gov) or UniProt (https://www.uniprot.org). Sequences were compared and analyzed with NCBI Blastn-, Blastp- or PSI-Blast algorithm. Multiple sequence alignments were conducted by Muscle (https://www.ebi.ac.uk/Tools/msa/muscle/) and the alignments were viewed and edited by Jalview [211]. The conservation score based on the sequence alignment was calculated using the Scorecons server (scoring method: entropic, 21 types) (https://www.ebi.ac.uk/thornton-srv/databases/cgi-bin/valdar/scorecons_server.pl). The phylogenetic tree of homologues sequences was annotated and viewed with iTOL (https://itol.embl.de). The Predictions for the transmembrane domains and signal peptides were carried out by TMHMM-2.0 and SignalP-6.0 (https://services.healthtech.dtu.dk), respectively. Information about conserved protein domains and the domain organization of proteins were obtained from the Pfam protein family database (http://pfam.xfam.org). The I-TASSER server (https://zhanggroup.org/I-TASSER/) with default setting was used to predict the structure of proteins, which was viewed and manipulated in PyMol (Schrödinger, USA).

4.6.2 *In silico* modelling of BacA

The structure of the bactofilin domain of BacA (PDB ID: 2N3D) were docked using the ClusPro 2.0 server [144]. To generate the head-head dimer and tail-tail dimer, identified hydrophobic residues were set to be attractive. As for the prediction of lateral interaction, the default settings with no restraints were used and models were selected for the presence of lateral interaction. Models generated by the ClusPro server were automatically grouped into four categories based upon the weighting of the interactions calculated: balanced, electrostatic-favored, hydrophobic-favored, and Van der Waals combined with electrostatics.

4.6.3 Data analysis

Data analyses were performed by using Excel (Microsoft Office) or RStudio (Version 1.4.1717). The visualization of data was mainly achieved using the ggplot2 and plotly packages in R. The further modification of the generated plots was performed with Adobe Illustrator CS6 (Adobe Systems).

5 References

1. Woese CR, Kandlert O, Wheelis ML. Towards a natural system of organisms: Proposal for the domains Archaea, Bacteria, and Eucarya (Euryarchaeota/Crenarchaeota/kingdom/evolution). 1990;87:4576–4579.

2. Stove Poindexter JL, Cohen-Bazire G. The fine structure of stalked bacteria belonging to the family caulobacteraceae. 1964; 23:587–607.

3. Wagner JK, Setayeshgar S, Sharon LA, Reilly JP, Brun YV. A nutrient uptake role for bacterial cell envelope extensions. Proc Natl Acad Sci. 2006;103:11772–11777.

4. Schlimpert S, Klein EA, Briegel A, Hughes V, Kahnt J, Bolte K, et al. General Protein Diffusion Barriers Create Compartments within Bacterial Cells. Cell. 2012;151:1270–1282.

5. Hershey DM, Porfírio S, Black I, Jaehrig B, Heiss C, Azadi P, et al. Composition of the Holdfast Polysaccharide from *Caulobacter crescentus*. J Bacteriol. 2019;201:1–19.

6. Schmidt JM, Stanier RY. The development of cellular stalks in bacteria. J Cell Biol. 1966;28:423–436.

7. Schmidt JM. Stalk Elongation in Mutants of *Caulobacter crescentus*. J Gen Microbiol. 1968;53:291–298.

8. Gonin M, Quardokus EM, O'Donnol D, Maddock J, Brun YV. Regulation of Stalk Elongation by Phosphate in *Caulobacter crescentus*. J Bacteriol. 2000;182:337–347.

9. Klein EA, Schlimpert S, Hughes V, Brun YV, Thanbichler M, Gitai Z. Physiological role of stalk lengthening in *Caulobacter crescentus*. Commun Integr Biol. 2013;6:e24561.

10. Evinger M, Agabian N. Envelope associated nucleoid from *Caulobacter crescentus* stalked and swarmer cells. J Bacteriol. 1977;132:294–301.

11. Skerker JM. Identification and cell cycle control of a novel pilus system in *Caulobacter crescentus*. EMBO J. 2000;19:3223–3234.

12. Mignolet J, Panis G, Viollier PH. More than a Tad: spatiotemporal control of *Caulobacter* pili. Curr Opin Microbiol. 2018;42:79–86.

13. Del Medico L, Cerletti D, Schächle P, Christen M, Christen B. The type IV pilin PilA couples surface attachment and cell-cycle initiation in *Caulobacter crescentus*. Proc Natl Acad Sci U S A. 2020;117:9546–9553.

14. Snyder RA, Ellison CK, Severin GB, Whitfield GB, Waters CM, Brun YV. Surface sensing stimulates cellular differentiation in *Caulobacter crescentus*. Proc Natl Acad Sci U S A. 2020;117:17984–17991.

15. Govers SK, Jacobs-Wagner C. *Caulobacter crescentus*: model system extraordinaire. Curr Biol. 2020;30:R1151–R1158.

16. Laub MT, McAdams HH, Feldblyum T, Fraser CM, Shapiro L. Global Analysis of the Genetic Network Controlling a Bacterial Cell Cycle. Science. 2000;290:2143–2148.

17. Hottes AK, Shapiro L, McAdams HH. DnaA coordinates replication initiation and cell cycle transcription in *Caulobacter crescentus*. Mol Microbiol. 2005;58:1340–1353.

18. Holtzendorff J, Hung D, Brende P, Reisenauer A, Viollier PH, McAdams HH, et al. Oscillating Global Regulators Control the Genetic Circuit Driving a Bacterial Cell Cycle. Science. 2004;304:983–987.

19. Quon KC, Marczynski GT, Shapiro L. Cell Cycle Control by an Essential Bacterial Two-Component Signal Transduction Protein. Cell. 1996;84:83–93.

20. Tan HM, Kozdon JB, Shen X, Shapiro L, McAdams HH. An essential transcription factor, SciP, enhances robustness of *Caulobacter* cell cycle regulation. Proc Natl Acad Sci U S A. 2010;107:18985–18990.

21. Collier J, McAdams HH, Shapiro L. A DNA methylation ratchet governs progression through a bacterial cell cycle. Proc Natl Acad Sci. 2007;104:17111–17116.

22. Quon KC, Yang B, Domian IJ, Shapiro L, Marczynski GT. Negative control of bacterial DNA replication by a cell cycle regulatory protein that binds at the chromosome origin. Proc Natl Acad Sci. 1998;95:120–125.

23. Iniesta AA, McGrath PT, Reisenauer A, McAdams HH, Shapiro L. A phospho-signaling pathway controls the localization and activity of a protease complex critical for bacterial cell cycle progression. Proc Natl Acad Sci U S A. 2006;103:10935–10940.

24. Smith SC, Joshi KK, Zik JJ, Trinh K, Kamajaya A, Chien P, et al. Cell cycle-dependent adaptor complex for ClpXP-mediated proteolysis directly integrates phosphorylation and second messenger signals. Proc Natl Acad Sci U S A. 2014;111:14129–14134.

25. Jacobs C, Domian IJ, Maddock JR, Shapiro L. Cell cycle-dependent polar localization of an essential bacterial histidine kinase that controls DNA replication and cell division. Cell. 1999;97:111-120.

26. Biondi EG, Reisinger SJ, Skerker JM, Arif M, Perchuk BS, Ryan KR, et al. Regulation of the bacterial cell cycle by an integrated genetic circuit. Nature. 2006;444:899–904.

27. Tsokos CG, Perchuk BS, Laub MT. A Dynamic Complex of Signaling Proteins Uses Polar Localization to Regulate Cell-Fate Asymmetry in *Caulobacter crescentus*. Dev Cell. 2011;20:329–341.

28. Wheeler RT, Shapiro L. Differential localization of two histidine kinases controlling bacterial cell differentiation. Mol Cell. 1999;4:683–694.

29. Lori C, Ozaki S, Steiner S, Böhm R, Abel S, Dubey BN, et al. Cyclic di-GMP acts as a cell cycle oscillator to drive chromosome replication. Nature. 2015;523:236–239.

30. Zhou B, Schrader JM, Kalogeraki VS, Abeliuk E, Dinh CB, Pham JQ, et al. The Global Regulatory Architecture of Transcription during the *Caulobacter* Cell Cycle. PLoS Genet. 2015;11:e1004831.

31. Bi E, Lutkenhaus J. FtsZ ring structure associated with division in *Escherichia coli*. Nature. 1991;354:161–164.

32. Jones LJ, Carballido-López R, Errington J. Control of cell shape in bacteria: helical, actin-like filaments in *Bacillus subtilis*. Cell. 2001;104:913–922.

33. Møller-Jensen J, Borch J, Dam M, Jensen RB, Roepstorff P, Gerdes K. Bacterial Mitosis: ParM of Plasmid R1 Moves Plasmid DNA by an Actin-like Insertional Polymerization Mechanism. Mol Cell. 2003;12:1477–1487.

34. Bulyha I, Lindow S, Lin L, Bolte K, Wuichet K, Kahnt J, et al. Two Small GTPases Act in Concert with the Bactofilin Cytoskeleton to Regulate Dynamic Bacterial Cell Polarity. Dev Cell. 2013;25:119–31.

35. Erickson HP, Taylor DW, Taylor KA, Bramhill D. Bacterial cell division protein FtsZ assembles into protofilament sheets and minirings, structural homologs of tubulin polymers. Proc Natl Acad Sci U S A. 1996;93:519–523.

36. Dyer N. Tubulin and its Prokaryotic Homologue FtsZ: A Structural and Functional Comparison. Sci Prog. 2009;92:113–137.

37. De Boer P, Crossley R, Rothfield L. The essential bacterial cell-division protein FtsZ is a GTPase. Nature. 1992;359:254–256.

38. Bramhill D, Thompson CM. GTP-dependent polymerization of *Escherichia coli* FtsZ protein to form tubules. Proc Natl Acad Sci U S A. 1994;91:5813–5817.

39. Nogales E, Downing KH, Amos LA, Löwe J. Tubulin and FtsZ form a distinct family of GTPases. Nat Struct Biol. 1998;5:451–458.

40. Biteen JS, Goley ED, Shapiro L, Moerner WE. Three-dimensional super-resolution imaging of the midplane protein FtsZ in live *Caulobacter crescentus* cells using astigmatism. ChemPhysChem. 2012;13:1007–1012.

41. Holden SJ, Pengo T, Meibom KL, Fernandez CF, Collier J, Manley S. High throughput 3D super-resolution microscopy reveals *Caulobacter crescentus* in vivo Z-ring organization. Proc Natl Acad Sci U S A. 2014;111:4566–4571.

42. Rowlett VW, Margolin W. 3D-SIM Super-resolution of FtsZ and its membrane tethers in *Escherichia coli* cells. Biophys J. 2014;107:L17–L20.

43. Fu G, Huang T, Buss J, Coltharp C, Hensel Z, Xiao J. *In Vivo* structure of the *E. coli* FtsZ-ring revealed by photoactivated localization microscopy (PALM). PLoS ONE. 2010;5:1–16.

44. Lyu Z, Coltharp C, Yang X, Xiao J. Influence of FtsZ GTPase activity and concentration on nanoscale Z-ring structure in vivo revealed by three-dimensional Superresolution imaging. Biopolymers. 2016;105:725–734.

45. Jennings PC, Cox GC, Monahan LG, Harry EJ. Super-resolution imaging of the bacterial cytokinetic protein FtsZ. Micron. 2011;42:336–341.

46. Strauss MP, Liew ATF, Turnbull L, Whitchurch CB, Monahan LG, Harry EJ. 3D-SIM Super Resolution Microscopy Reveals a Bead-Like Arrangement for FtsZ and the Division Machinery: Implications for Triggering Cytokinesis. PLoS Biol. 2012;10:e1001389.

47. Thanbichler M, Shapiro L. MipZ, a Spatial Regulator Coordinating Chromosome Segregation with Cell Division in *Caulobacter*. Cell. 2006;126:147–162.

48. de Boer PAJ, Crossley RE, Rothfield LI. A division inhibitor and a topological specificity factor coded for by the minicell locus determine proper placement of the division septum in *E. coli*. Cell. 1989;56:641–649.

49. Levin PA, Margolis PS, Setlow P, Losick R, Sun D. Identification of *Bacillus subtilis* genes for septum placement and shape determination. J Bacteriol. 1992;174:6717–6728.

50. Perez AJ, Cesbron Y, Shaw SL, Villicana JB, Tsui HCT, Boersma MJ, et al. Movement dynamics of divisome proteins and PBP2x: FtsW in cells of *Streptococcus pneumoniae*. Proc Natl Acad Sci U S A. 2019;116:3211–3220.

51. Bisson-Filho AW, Hsu YP, Squyres GR, Kuru E, Wu F, Jukes C, et al. Treadmilling by FtsZ filaments drives peptidoglycan synthesis and bacterial cell division. Science. 2017;355:739–743.

52. Loose M, Mitchison TJ. The bacterial cell division proteins ftsA and ftsZ self-organize into dynamic cytoskeletal patterns. Nat Cell Biol. 2014;16:38–46.

53. Yang X, Lyu Z, Miguel A, McQuillen R, Huang KC, Xiao J. GTPase activity-coupled treadmilling of the bacterial tubulin FtsZ organizes septal cell wall synthesis. Science. 2017;355:744–747.

54. Margolin W. FtsZ and the division of prokaryotic cells and organelles. Nat Rev Mol Cell Biol. 2005;6:862–871.

55. Goehring NW, Gonzalez MD, Beckwith J. Premature targeting of cell division proteins to midcell reveals hierarchies of protein interactions involved in divisome assembly. Mol Microbiol. 2006;61:33–45.

56. Goehring NW, Beckwith J. Diverse paths to midcell: Assembly of the bacterial cell division machinery. Curr Biol. 2005;15:514–526.

57. Goley ED, Yeh Y-C, Hong S-H, Fero MJ, Abeliuk E, McAdams HH, et al. Assembly of the *Caulobacter* cell division machine. Mol Microbiol. 2011;80:1680–1698.

58. Ozaki S, Jenal U, Katayama T. Novel divisome-associated protein spatially coupling the z-ring with the chromosomal replication terminus in *Caulobacter crescentus*. mBio. 2020;11: e00487–20.

59. Ozaki S, Wakasugi Y, Katayama T. Z-ring-associated proteins regulate clustering of the replication terminus-binding protein ZapT in *Caulobacter crescentus*. mBio. 2021;12: e02196–20.

60. Ebersbach G, Galli E, Møller-Jensen J, Löwe J, Gerdes K. Novel coiled-coil cell division factor ZapB stimulates Z ring assembly and cell division. Mol Microbiol. 2008;68:720–735.

61. Castillo DE, Yang D, Siopsis G, Männik J. The role of MatP, ZapA and ZapB in chromosomal organization and dynamics in *Escherichia coli*. Nucleic Acids Res. 2016;44:1216–1226.

62. Nguyen LT, Oikonomou CM, Ding HJ, Kaplan M, Yao Q, Chang YW, et al. Simulations suggest a constrictive force is required for Gram-negative bacterial cell division. Nat Commun. 2019;10:1–11.

63. Coltharp C, Buss J, Plumer TM, Xiao J. Defining the rate-limiting processes of bacterial cytokinesis. Proc Natl Acad Sci U S A. 2016;113:E1044–E1053.

64. Montabana EA, Agard DA. Bacterial tubulin TubZ-Bt transitions between a two-stranded intermediate and a four-stranded filament upon GTP hydrolysis. Proc Natl Acad Sci U S A. 2014;111:3407–3412.

65. Fink G, Löwe J. Reconstitution of a prokaryotic minus end-tracking system using TubRC centromeric complexes and tubulin-like protein TubZ filaments. Proc Natl Acad Sci U S A. 2015;112:E1845–E1850.

66. Deng X, Fink G, Bharat TAM, He S, Kureisaite-Ciziene D, Löwe J. Four-stranded mini microtubules formed by *Prosthecobacter* BtubAB show dynamic instability. Proc Natl Acad Sci U S A. 2017;114:E5950–E5958.

67. Jenkins C, Samudrala R, Andersont I, Hedlund BP, Petroni G, Michailova N, et al. Genes for the cytoskeletal protein tubulin in the bacterial genus *Prosthecobacter*. Proc Natl Acad Sci U S A. 2002;99:17049–17054.

68. Pilhofer M, Ladinsky MS, McDowall AW, Petroni G, Jensen GJ. Microtubules in Bacteria: Ancient tubulins build a five-protofilament homolog of the eukaryotic cytoskeleton. PLoS Biol. 2011;9: e1001213.

69. Kraemer JA, Erb ML, Waddling CA, Montabana EA, Zehr EA, Wang H, et al. A phage tubulin assembles dynamic filaments by an atypical mechanism to center viral DNA within the host cell. Cell. 2012;149:1488–1499.

70. Chaikeeratisak V, Nguyen K, Khanna K, Brilot AF, Erb ML, Coker JKC, et al. Assembly of a nucleus-like structure during viral replication in bacteria. Science. 2017;355:194–197.

71. Figge RM, Divakaruni AV, Gober JW. MreB, the cell shape-determining bacterial actin homologue, co-ordinates cell wall morphogenesis in *Caulobacter crescentus*. Mol Microbiol. 2004;51:1321–1332.

72. Bendezú FO, De Boer PAJ. Conditional lethality, division defects, membrane involution, and endocytosis in mre and mrd shape mutants of *Escherichia coli*. J Bacteriol. 2008;190:1792–1811.

73. Van den Ent F, Amos LA, Löwe J. Prokaryotic origin of the actin cytoskeleton. Nature. 2001;413:39–44.

74. Esue O, Wirtz D, Tseng Y. GTPase activity, structure, and mechanical properties of filaments assembled from bacterial cytoskeleton protein MreB. J Bacteriol. 2006;188:968–976.

75. Salje J, van den Ent F, de Boer P, Löwe J. Direct Membrane Binding by Bacterial Actin MreB. Mol Cell. 2011;43:478–487.

76. van den Ent F, Izoré T, Bharat TAM, Johnson CM, Löwe J. Bacterial actin MreB forms antiparallel double filaments. eLife. 2014;3:1–22.

77. Martins A, Contreras-Martel C, Janet-Maitre M, Miyachiro MM, Estrozi LF, Trindade DM, et al. Self-association of MreC as a regulatory signal in bacterial cell wall elongation. Nat Commun. 2021;12:2987.

78. Wachi M, Doi M, Okada Y, Matsuhashi M. New *mre* genes *mreC* and *mreD*, responsible for formation of the rod shape of *Escherichia coli* cells. J Bacteriol. 1989;171:6511–6516.

79. Van Den Ent F, Leaver M, Bendezu F, Errington J, De Boer P, Löwe J. Dimeric structure of the cell shape protein MreC and its functional implications. Mol Microbiol. 2006;62:1631–1642.

80. Shiomi D, Sakai M, Niki H. Determination of bacterial rod shape by a novel cytoskeletal membrane protein. EMBO J. 2008;27:3081–3091.

81. Alyahya SA, Alexander R, Costa T, Henriques AO, Emonet T, Jacobs-Wagner C. RodZ, a component of the bacterial core morphogenic apparatus. Proc Natl Acad Sci U S A. 2009;106:1239–1244.

82. Colavin A, Shi H, Huang KC. RodZ modulates geometric localization of the bacterial actin MreB to regulate cell shape. Nat Commun. 2018;9:1280.

83. Cho H, Wivagg CN, Kapoor M, Barry Z, Rohs PDA, Suh H, et al. Bacterial cell wall biogenesis is mediated by SEDS and PBP polymerase families functioning semi-Autonomously. Nat Microbiol. 2016;1:1–8.

84. Domínguez-Escobar J, Chastanet A, Crevenna AH, Fromion V, Wedlich-Söldner R, Carballido-López R. Processive movement of MreB-associated cell wall biosynthetic complexes in bacteria. Science. 2011;333:225–228.

85. Van Teeffelen S, Wang S, Furchtgott L, Huang KC, Wingreen NS, Shaevitz JW, et al. The bacterial actin MreB rotates, and rotation depends on cell-wall assembly. Proc Natl Acad Sci U S A. 2011;108:15822–15827.

86. Garner EC, Bernard R, Wang W, Zhuang X, Rudner DZ, Mitchison T. Coupled, circumferential motions of the cell wall synthesis machinery and MreB filaments in *B. subtilis*. Science. 2011;333:222–225.

87. Ouellette SP, Karimova G, Subtil A, Ladant D. *Chlamydia* co-opts the rod shape-determining proteins MreB and Pbp2 for cell division. Mol Microbiol. 2012;85:164–178.

88. Treuner-Lange A, Macia E, Guzzo M, Hot E, Faure LM, Jakobczak B, et al. The small G-protein MglA connects to the MreB actin cytoskeleton at bacterial focal adhesions. J Cell Biol. 2015;210:243–256.

89. Mauriello EMF, Mouhamar F, Nan B, Ducret A, Dai D, Zusman DR, et al. Bacterial motility complexes require the actin-like protein, MreB and the Ras homologue, MglA. EMBO J. 2010;29:315–326.

90. Van den Ent F, Møller-Jensen J, Amos LA, Gerdes K, Löwe J. F-actin-like filaments formed by plasmid segregation protein ParM. EMBO J. 2002;21:6935–6943.

91. Bharat TAM, Murshudov GN, Sachse C, Löwe J. Structures of actin-like ParM filaments show architecture of plasmid-segregating spindles. Nature. 2015;523:106–110.

92. Becker E, Herrera NC, Gunderson FQ, Derman AI, Dance AL, Sims J, et al. DNA segregation by the bacterial actin AlfA during *Bacillus subtilis* growth and development. EMBO J. 2006;25:5919–5931.

93. Polka JK, Kollman JM, Mullins RD. Accessory factors promote AlfA-dependent plasmid segregation by regulating filament nucleation, disassembly, and bundling. Proc Natl Acad Sci U S A. 2014;111:2176–2181.

94. Forde AJ, Albrecht N, Klingl A, Donovan C, Bramkamp M. Polymerization dynamics of the prophage-encoded actin-like protein AlpC is influenced by the DNA-binding adapter AlpA. Front Microbiol. 2017;8:2–11.

95. Ausmees N, Kuhn JR, Jacobs-Wagner C. The Bacterial Cytoskeleton: An Intermediate Filament-Like Function in Cell Shape. Cell. 2003;115:705–713.

96. Charbon G, Cabeen MT, Jacobs-Wagner C. Bacterial intermediate filaments: In vivo assembly, organization, and dynamics of crescentin. Genes Dev. 2009;23:1131–1143.

97. Esue O, Rupprecht L, Sun SX, Wirtz D. Dynamics of the bacterial intermediate filament crescentin in vitroand *in vivo*. PLoS ONE. 2010;5:e8855.

98. Cabeen MT, Herrmann H, Jacobs-Wagner C. The domain organization of the bacterial intermediate filament-like protein crescentin is important for assembly and function. Cytoskeleton. 2011;68:205–219.

99. Cabeen MT, Charbon G, Vollmer W, Born P, Ausmees N, Weibel DB, et al. Bacterial cell curvature through mechanical control of cell growth. EMBO J. 2009;28:1208–1219.

100. Holmes NA, Walshaw J, Leggett RM, Thibessard A, Dalton KA, Gillespie MD, et al. Coiled-coil protein Scy is a key component of a multiprotein assembly controlling polarized growth in *Streptomyces*. Proc Natl Acad Sci U S A. 2013;110:397–406.

101. Fröjd MJ, Flärdh K. Apical assemblies of intermediate filament-like protein FilP are highly dynamic and affect polar growth determinant DivIVA in *Streptomyces venezuelae*. Mol Microbiol. 2019;112:47–61.

102. Fuchino K, Bagchi S, Cantlay S, Sandblad L, Wu D, Bergman J, et al. Dynamic gradients of an intermediate filament-like cytoskeleton are recruited by a polarity landmark during apical growth. Proc Natl Acad Sci U S A. 2013;110:1889–1897.

103. Martin NR, Blackman E, Bratton BP, Chase KJ, Bartlett TM, Gitai Z. CrvA and CrvB form a curvature-inducing module sufficient to induce cell-shape complexity in Gram-negative bacteria. Nat Microbiol. 2021;6:910–920.

104. Specht M, Schätzle S, Graumann PL, Waidner B. *Helicobacter pylori* possesses four coiled-coil-rich proteins that form extended filamentous structures and control cell shape and motility. J Bacteriol. 2011;193:4523–4530.

105. Schätzle S, Specht M, Waidner B. Coiled coil rich proteins (Ccrp) influence molecular pathogenicity of *Helicobacter pylori*. PLoS ONE. 2015;10:1–21.

106. Bowman GR, Perez AM, Ptacin JL, Ighodaro E, Folta-Stogniew E, Comolli LR, et al. Oligomerization and higher-order assembly contribute to sub-cellular localization of a bacterial scaffold. Mol Microbiol. 2013;90:776–795.

107. Holmes JA, Follett SE, Wang H, Meadows CP, Varga K, Bowman GR. *Caulobacter* PopZ forms an intrinsically disordered hub in organizing bacterial cell poles. Proc Natl Acad Sci U S A. 2016;113:12490–12495.

108. Bowman GR, Comolli LR, Zhu J, Eckart M, Koenig M, Downing KH, et al. A Polymeric Protein Anchors the Chromosomal Origin/ParB Complex at a Bacterial Cell Pole. Cell. 2008;134:945–955.

109. Ptacin JL, Gahlmann A, Bowman GR, Perez AM, Von Diezmann ARS, Eckart MR, et al. Bacterial scaffold directs pole-specific centromere segregation. Proc Natl Acad Sci U S A. 2014;111: E2046-E2055.

110. Lasker K, von Diezmann L, Zhou X, Ahrens DG, Mann TH, Moerner WE, et al. Selective sequestration of signalling proteins in a membraneless organelle reinforces the spatial regulation of asymmetry in *Caulobacter crescentus*. Nat Microbiol. 2020:5:418–429.

111. Oliva MA, Halbedel S, Freund SM, Dutow P, Leonard TA, Veprintsev DB, et al. Features critical for membrane binding revealed by DivIVA crystal structure. EMBO J. 2010;29:1988–2001.

112. Hay NA, Tipper DJ, Gygi D, Hughes C. A novel membrane protein influencing cell shape and multicellular swarming of *Proteus mirabilis*. J Bacteriol. 1999;181:2008–2016.

113. Kühn J, Briegel A, Mörschel E, Kahnt J, Leser K, Wick S, et al. Bactofilins, a ubiquitous class of cytoskeletal proteins mediating polar localization of a cell wall synthase in *Caulobacter crescentus*. EMBO J. 2010;29:327–339.

114. Deng X, Gonzalez Llamazares A, Wagstaff JM, Hale VL, Cannone G, McLaughlin SH, et al. The structure of bactofilin filaments reveals their mode of membrane binding and lack of polarity. Nat Microbiol. 2019;4:2357–2368.

115. Lin L, Thanbichler M. Nucleotide-independent cytoskeletal scaffolds in bacteria. Cytoskeleton. 2013;70:409–423.

116. Vasa S, Lin L, Shi C, Habenstein B, Riedel D, Kühn J, et al. β-Helical architecture of cytoskeletal bactofilin filaments revealed by solid-state NMR. Proc Natl Acad Sci. 2015;112:E127–E136.

117. Kassem MM, Wang Y, Boomsma W, Lindorff-Larsen K. Structure of the Bacterial Cytoskeleton Protein Bactofilin by NMR Chemical Shifts and Sequence Variation. Biophys J. 2016;110:2342–2348.

118. Holtrup S, Heimerl T, Linne U, Altegoer F, Noll F, Waidner B. Biochemical characterization of the *Helicobacter pylori* bactofilin-homolog HP1542. Plos One. 2019;14:e0218474.

119. Zuckerman DM, Boucher LE, Xie K, Engelhardt H, Bosch J, Hoiczyk E. The bactofilin cytoskeleton protein BacM of *Myxococcus xanthus* forms an extended β-sheet structure likely mediated by hydrophobic interactions. PloS One. 2015;10:e0121074.

120. Taylor JA, Bratton BP, Sichel SR, Blair KM, Jacobs HM, DeMeester KE, et al. Distinct cytoskeletal proteins define zones of enhanced cell wall synthesis in *Helicobacter pylori*. eLife. 2020;9: e52482.

121. Pichoff S, Lutkenhaus J. Tethering the Z ring to the membrane through a conserved membrane targeting sequence in FtsA. Mol Microbiol. 2005;55:1722–1734.

122. Whited AM, Johs A. The interactions of peripheral membrane proteins with biological membranes. Chem Phys Lipids. 2015;192:51–59.

123. Contreras I, Shapiro L, Henry S. Membrane phospholipid composition of *Caulobacter crescentus*. J Bacteriol. 1978;135:1130–1136.

124. Caccamo PD, Jacq M, VanNieuwenhze MS, Brun YV. A Division of Labor in the Recruitment and Topological Organization of a Bacterial Morphogenic Complex. Curr Biol. 2020;30:3908-3922.e4.

125. Jackson KM, Schwartz C, Wachter J, Rosa PA, Stewart PE. A widely conserved bacterial cytoskeletal component influences unique helical shape and motility of the spirochete *Leptospira biflexa*. Mol Microbiol. 2018;108:77-89.

126. Koch MK, Mchugh CA, Hoiczyk E. BacM, an N-terminally processed bactofilin of *Myxococcus xanthus*, is crucial for proper cell shape. Mol Microbiol. 2011;80:1031–1051.

127. Lin L, Osorio Valeriano M, Harms A, Søgaard-Andersen L, Thanbichler M. Bactofilin-mediated organization of the ParABS chromosome segregation system in *Myxococcus xanthus*. Nat Commun. 2017;8:1817.

128. Anand D, Schumacher D, Søgaard-Andersen L. SMC and the bactofilin/PadC scaffold have distinct yet redundant functions in chromosome segregation and organization in *Myxococcus xanthus*. Mol Microbiol. 2020;114:839–856.

129. Den Blaauwen T, De Pedro MA, Nguyen-Distèche M, Ayala JA. Morphogenesis of rod-shaped sacculi. FEMS Microbiol Rev. 2008;32:321–344.

130. Vollmer W, Bertsche U. Murein (peptidoglycan) structure, architecture and biosynthesis in Escherichia coli. Biochim Biophys Acta. 2008;1778:1714–1734.

131. Typas A, Banzhaf M, Gross CA, Vollmer W. From the regulation of peptidoglycan synthesis to bacterial growth and morphology. Nat Rev Microbiol. 2012;10:123–136.

132. Egan AJF, Errington J, Vollmer W. Regulation of peptidoglycan synthesis and remodelling. Nat Rev Microbiol. 2020;18:446–460.

133. Vermassen A, Leroy S, Talon R, Provot C, Popowska M, Desvaux M. Cell wall hydrolases in bacteria: Insight on the diversity of cell wall amidases, glycosidases and peptidases toward peptidoglycan. Front Microbiol. 2019;10:331.

134. Strobel W, Mll A, Kiekebusch D, Klein KE, Thanbichler M. Function and localization dynamics of bifunctional penicillin-binding proteins in *Caulobacter crescentus*. J Bacteriol. 2014;196: 1627–1639.

135. Ghuysen J-M. Serine β-lactamases and penicillin-binding proteins. Annu Rev Microbiol. 1991;45:37–67.

136. Kühn J, Briegel A, Mörschel E, Kahnt J, Leser K, Wick S, et al. Bactofilins, a ubiquitous class of cytoskeletal proteins mediating polar localization of a cell wall synthase in *Caulobacter crescentus*. EMBO J. 2010;29:327–339.

137. Hughes HV, Lisher JP, Hardy GG, Kysela DT, Arnold RJ, Giedroc DP, et al. Co-ordinate synthesis and protein localization in a bacterial organelle by the action of a penicillin-binding-protein. Mol Microbiol. 2013;90:1162–1177.

138. Randich AM, Brun YV. Molecular mechanisms for the evolution of bacterial morphologies and growth modes. Front Microbiol. 2015;6:1–13.

139. Wagner JK, Brun YV. Out on a limb: How the *Caulobacter* stalk can boost the study of bacterial cell shape. Mol Microbiol. 2007;64:28–33.

140. Billini M, Biboy J, Kühn J, Vollmer W, Thanbichler M. A specialized MreB-dependent cell wall biosynthetic complex mediates the formation of stalk-specific peptidoglycan in *Caulobacter crescentus*. 2019;15: e1007897.

141. Vasa S, Lin L, Shi C, Habenstein B, Riedel D, Kühn J, et al. β-Helical architecture of cytoskeletal bactofilin filaments revealed by solid-state NMR. Proc Natl Acad Sci. 2015;112:E127–E136.

142. Mistry J, Chuguransky S, Williams L, Qureshi M, Salazar GA, Sonnhammer ELL, et al. Pfam: The protein families database in 2021. Nucleic Acids Res. 2021;49:D412–D419.

143. Valdar WSJ. Scoring residue conservation. Proteins Struct Funct Genet. 2002;48:227–241.

144. Kozakov D, Hall DR, Xia B, Porter KA, Padhorny D, Yueh C, et al. The ClusPro web server for protein–protein docking. Nat Protoc. 2017;12:255–728.

145. Brenke R, Hall DR, Chuang G-Y, Comeau SR, Bohnuud T, Beglov D, et al. Application of asymmetric statistical potentials to antibody-protein docking. Bioinformatics. 2012;28:2608–2614.

146. Harding SE. Chapter 7 Protein hydrodynamics. 1999. p. 271–305.

147. Hong P, Koza S, Bouvier ESP. A review size-exclusion chromatography for the analysis of protein biotherapeutics and their aggregates. J Liq Chromatogr Relat Technol. 2012;35:2923–2950.

148. Schmidt C, Robinson CV. A comparative cross-linking strategy to probe conformational changes in protein complexes. Nat Protoc. 2014;9:2224–2236.

149. Baker JA, Wong WC, Eisenhaber B, Warwicker J, Eisenhaber F. Charged residues next to transmembrane regions revisited: "Positive-inside rule" is complemented by the "negative inside depletion/outside enrichment rule." BMC Biol. 2017;15:1–29.

150. von Heljne G. Control of topology and mode of assembly of a polytopic membrane protein by positively charged residues. Nature. 1989; 341:456–458.

151. Williamson MP. The structure and function of proline-rich regions in proteins. Biochem J. 1994;297:249–60.

152. Masson GR, Burke JE, Ahn NG, Anand GS, Borchers C, Brier S, et al. Recommendations for performing, interpreting and reporting hydrogen deuterium exchange mass spectrometry (HDX-MS) experiments. Nat Methods. 2019;16:595–602.

153. Konermann L, Pan J, Liu YH. Hydrogen exchange mass spectrometry for studying protein structure and dynamics. Chem Soc Rev. 2011;40:1224–1234.

154. Yakushi T, Masuda K, Narita SI, Matsuyama SI, Tokuda H. A new ABC transporter mediating the detachment of lipid-modified proteins from membranes. Nat Cell Biol. 2000;2:212–218.

155. Okuda S, Tokuda H. Lipoprotein sorting in bacteria. Annu Rev Microbiol. 2011;65:239–259.

156. Szczepaniak J, Press C, Kleanthous C. The multifarious roles of Tol-Pal in Gram-negative bacteria. FEMS Microbiol Rev. 2020;44:490–506.

157. Bernadac A, Gavioli M, Lazzaroni JC, Raina S, Lloubès R. *Escherichia coli* tol-pal mutants form outer membrane vesicles. J Bacteriol. 1998;18:4872-4878.

158. Zückert WR. Secretion of Bacterial Lipoproteins: Through the Cytoplasmic Membrane, the Periplasm and Beyond. Biochim Biophys Acta BBA - Mol Cell Res. 2014;1843:1509–16.

159. Noinaj N, Guillier M, Barnard, TJ, Buchanan SK. TonB-Dependent Transporters: Regulation, Structure, and Function. Annu Rev Microbiol. 2010;64:43–60.

160. Teufel F, Almagro Armenteros JJ, Johansen AR, Gíslason MH, Pihl SI, Tsirigos KD, et al. SignalP 6.0 predicts all five types of signal peptides using protein language models. Nat Biotechnol. 2022;40:1023–1025.

161. Lasker K, Schrader JM, Men Y, Marshik T, Dill DL, McAdams HH, et al. CauloBrowser: A systems biology resource for *Caulobacter crescentus*. Nucleic Acids Res. 2016;44:D640–D645.

162. Green JB, Lower RPJ, Young JPW. The NfeD protein family and its conserved gene neighbours throughout prokaryotes: Functional implications for stomatin-like proteins. J Mol Evol. 2009;69:657–667.

163. Black K, Buikema WJ, Haselkorn R. The hglK gene is required for localization of heterocyst-specific glycolipids in the cyanobacterium *Anabaena* sp. strain PCC 7120. J Bacteriol. 1995;177:6440–6448.

164. Vetting MW, Hegde SS, Wang M, Jacoby GA, Hooper DC, Blanchard JS. Structure of QnrB1, a plasmid-mediated fluoroquinolone resistance factor. J Biol Chem. 2011;286:25265–25273.

165. Yang J, Yan R, Roy A, Xu D, Poisson J, Zhang Y. The I-TASSER Suite: protein structure and function prediction. Nat Methods. 2015;12:7–8.

166. García-Bayona L, Gozzi K, Laub MT. Mechanisms of Resistance to the Contact-Dependent Bacteriocin CdzC/D in *Caulobacter crescentus*. J Bacteriol. 2019;201:1–19.

167. Costa TRD, Felisberto-Rodrigues C, Meir A, Prevost MS, Redzej A, Trokter M, et al. Secretion systems in Gram-negative bacteria: Structural and mechanistic insights. Nat Rev Microbiol. 2015;13:343–359.

168. Awram P, Smit J. The *Caulobacter crescentus* Paracrystalline S-Layer Protein Is Secreted by an ABC Transporter (Type I) Secretion Apparatus. 1998;180: 3062-3069.

169. García-Bayona L, Guo MS, Laub MT. Contact-dependent killing by *Caulobacter crescentus* via cell surface-associated, glycine zipper proteins. eLife. 2017;6:1–26.

170. Gentschev I, Hess J, Goebel W. Change in the cellular localization of alkaline phosphatase by alteration of its carboxy-terminal sequence. Mol Gen Genet MGG. 1990;222:211–216.

171. Ghigo JM, Wandersman C. A carboxyl-terminal four-amino acid motif is required for secretion of the metalloprotease PrtG through the *Erwinia chrysanthemi* protease secretion pathway. J Biol Chem. 1994;269:8979–8985.

172. Duong F, Lazdunski A, Murgier M. Protein secretion by heterologous bacterial ABC-transporters: the C-terminus secretion signal of the secreted protein confers high recognition specificity. Mol Microbiol. 1996;21:459–470.

173. Létoffé S, Ghigo JM, Wandersman C. Secretion of the *Serratia marcescens* HasA protein by an ABC transporter. J Bacteriol. 1994;176:5372–5377.

174. Welch RA. Pore-forming cytolysins of Gram-negative bacteria. Mol Microbiol. 1991;5:521–528.

175. Holland IB, Peherstorfer S, Kanonenberg K, Lenders M, Reimann S, Schmitt L. Type I Protein Secretion—Deceptively Simple yet with a Wide Range of Mechanistic Variability across the Family. EcoSal Plus. 2016;7.

176. Ye H. Simultaneous determination of protein aggregation, degradation, and absolute molecular weight by size exclusion chromatography-multiangle laser light scattering. Anal Biochem. 2006;356:76–85.

177. Sahin E, Roberts CJ. Size-Exclusion Chromatography with Multi-angle Light Scattering for Elucidating Protein Aggregation Mechanisms. In: Voynov V, Caravella JA, editors. Totowa, NJ: Humana Press; 2012. p. 403–23.

178. Wyatt PJ. Light scattering and the absolute characterization of macromolecules. Anal Chim Acta. 1993;272:1–40.

179. Guan F, Yu J, Yu J, Liu Y, Li Y, Feng XH, et al. Lateral interactions between protofilaments of the bacterial tubulin homolog FtsZ are essential for cell division. eLife. 2018;7:1–22.

180. Hale CA, Rhee AC, De Boer PAJ. ZipA-induced bundling of FtsZ polymers mediated by an interaction between C-terminal domains. J Bacteriol. 2000;182:5153–5166.

181. Gueiros-Filho FJ, Losick R. A widely conserved bacterial cell division protein that promotes assembly of the tubulin-like protein FtsZ. Genes Dev. 2002;16:2544–2556.

182. Durand-Heredia JM, Yu HH, De Carlo S, Lesser CF, Janakiraman A. Identification and characterization of ZapC, a stabilizer of the FtsZ ring in *Escherichia coli*. J Bacteriol. 2011;193:1405–1413.

183. Chen Y, Milam SL, Erickson HP. SulA inhibits assembly of FtsZ by a simple sequestration mechanism. Biochemistry. 2012;51:3100–3109.

184. LaBreck CJ, Conti J, Viola MG, Camberg JL. MinC N- and C-Domain Interactions Modulate FtsZ Assembly, Division Site Selection, and MinD-Dependent Oscillation in *Escherichia coli*. J Bacteriol. 2019;201:1–19.

185. Niggli V. Structural properties of lipid-binding sites in cytoskeletal proteins. Trends Biochem Sci. 2001;26:604–611.

186. Zhang W, Sato T, Smith SO. NMR spectroscopy of basic/aromatic amino acid clusters in membrane proteins. Prog Nucl Magn Reson Spectrosc. 2006;48:183–199.

187. Wimley WC, White SH. Experimentally determined hydrophobicity scale for proteins at membrane interfaces. Nat Struct Mol Biol. 1996;3:842–848.

188. Dersch S, Reimold C, Stoll J, Breddermann H, Heimerl T, Defeu Soufo HJ, et al. Polymerization of *Bacillus subtilis* MreB on a lipid membrane reveals lateral co-polymerization of MreB paralogs and strong effects of cations on filament formation. BMC Mol Cell Biol. 2020;21:1–17.

189. Pande V, Mitra N, Bagde SR, Srinivasan R, Gayathri P. Filament organization of the bacterial actin MreB is dependent on the nucleotide state. J Cell Biol. 2022;221:e202106092.

190. Erickson HP, Anderson DE, Osawa M. FtsZ in Bacterial Cytokinesis: Cytoskeleton and Force Generator All in One. Microbiol Mol Biol Rev. 2010;74:504–528.

191. Melzer ES, Sein CE, Chambers JJ, Sloan Siegrist M. DivIVA concentrates mycobacterial cell envelope assembly for initiation and stabilization of polar growth. Cytoskeleton. 2018;75:498–507.

192. Altschul SF, Madden TL, Schäffer AA, Zhang J, Zhang Z, Miller W, et al. Gapped BLAST and PSI-BLAST: A new generation of protein database search programs. Nucleic Acids Res. 1997;25:3389–3402.

193. Chiba S, Ito K, Akiyama Y. The *Escherichia coli* plasma membrane contains two PHB (prohibitin homology) domain protein complexes of opposite orientations. Mol Microbiol. 2006;60:448–457.

194. Vetting MW, Hegde SS, Fajardo JE, Fiser A, Roderick SL, Takiff HE, *et al.* Pentapeptide Repeat Proteins †. Biochemistry. 2006;45:1–10.

195. Zhang R, Ni S, Kennedy MA. Type I beta turns make a new twist in pentapeptide repeat proteins: Crystal structure of Alr5209 from Nostoc sp. PCC 7120 determined at 1.7 angström resolution. J Struct Biol X. 2019;3:100010.

196. Tao J, Han J, Wu H, Hu X, Deng J, Fleming J, et al. Mycobacterium fluoroquinolone resistance protein B, a novel small GTPase, is involved in the regulation of DNA gyrase and drug resistance. Nucleic Acids Res. 2013;41:2370–2381.

197. Ni S, Sheldrick GM, Benning MM, Kennedy MA. The 2 Å resolution crystal structure of HetL, a pentapeptide repeat protein involved in regulation of heterocyst differentiation in the cyanobacterium Nostoc sp. strain PCC 7120. J Struct Biol. 2009;165:47–52.

198. Ni S, McGookey ME, Tinch SL, Jones AN, Jayaraman S, Tong L, *et al.* The 1.7 Å resolution structure of At2g44920, a pentapeptide-repeat protein in the thylakoid lumen of *Arabidopsis thaliana*. Acta Crystallograph Sect F Struct Biol Cryst Commun. 2011;67:1480–1484.

199. Vetting MW, Hegde SS, Zhang Y, Blanchard JS. Pentapeptide-repeat proteins that act as topoisomerase poison resistance factors have a common dimer interface. Acta Crystallograph Sect F Struct Biol Cryst Commun. 2011;67:296–302.

200. Hegde SS, Vetting MW, Roderick SL, Mitchenall LA, Maxwell A, Takiff HE, et al. Biochemistry: A fluoroquinolone resistance protein from *Mycobacterium tuberculosis* that mimics DNA. Science. 2005;308:1480–1483.

201. Green MR, Sambrook J, editors. Molecular Cloning: A Laboratory Manual. In: Molecular Cloning: A Laboratory Manual. Cold Spring Harbir Laboratory Press; 2012.

202. Ausubel FM, Brent R, Kingston RE, Moore DD, Seidman JG, Smith JA, et al., editors. Current Protocols in Molecular Biology. John Wiley & Sons, Inc.; 2003.

203. Ely B. Genetics of *Caulobacter crescentus*. In: Methods. 1991. p. 372–384.

204. Schindelin J, Arganda-Carreras I, Frise E, Kaynig V, Longair M, Pietzsch T, et al. Fiji: an open-source platform for biological-image analysis. Nat Methods. 2012;9:676–682.

205. Hartmann R, van Teeseling MCF, Thanbichler M, Drescher K. BacStalk: a comprehensive and interactive image analysis software tool for bacterial cell biology. Mol Microbiol. 2020; November 2019:1–11.

206. Plank M, Wadhams GH, Leake MC. Millisecond timescale slimfield imaging and automated quantification of single fluorescent protein molecules for use in probing complex biological processes. Integr Biol. 2009;1:602–612.

207. Jaqaman K, Loerke D, Mettlen M, Kuwata H, Grinstein S, Schmid SL, et al. Robust single-particle tracking in live-cell time-lapse sequences. Nat Methods. 2008;5:695–702.

208. Wales TE, Fadgen KE, Gerhardt GC, Engen JR. High-speed and high-resolution UPLC separation at zero degrees celsius. Anal Chem. 2008;80:6815–6820.

209. Geromanos SJ, Vissers JPC, Silva JC, Dorschel CA, Li GZ, Gorenstein MV, *et al.* The detection, correlation, and comparison of peptide precursor and product ions from data independent LC-MS with data dependant LC-MS/MS. Proteomics. 2009;9:1683–1695.

210. Li GZ, Vissers JPC, Silva JC, Golick D, Gorenstein MV, Geromanos SJ. Database searching and accounting of multiplexed precursor and product ion spectra from the data independent analysis of simple and complex peptide mixtures. Proteomics. 2009;9:1696–1719.

211. Waterhouse AM, Procter JB, Martin DMA, Clamp M, Barton GJ. Jalview Version 2-A multiple sequence alignment editor and analysis workbench. Bioinformatics. 2009;25:1189–1891.

212. West L, Yang D, Stephens C. Use of the *Caulobacter crescentus* genome sequence to develop a method for systematic genetic mapping. J Bacteriol. 2002;184:2155–2166.

213. Thanbichler M, Iniesta AA, Shapiro L. A comprehensive set of plasmids for vanillate- and xylose-inducible gene expression in *Caulobacter crescentus*. Nucleic Acids Res. 2007;35:e137–e137.

214. Bendezú FO, Hale CA, Bernhardt TG, De Boer PAJ. RodZ (YfgA) is required for proper assembly of the MreB actin cytoskeleton and cell shape in *E. coli*. EMBO J. 2009;28:193–204.

215. Jurrus E, Engel D, Star K, Monson K, Brandi J, Felberg LE, et al. Improvements to the APBS biomolecular solvation software suite. Protein Sci. 2018;27:112–128.

6 Appendix

Table S1 Strains used in this study

Strain	Genotype	Source
C. crescentus		
LY1	Δ*bacAB xylX*::P*xyl-bacA*$_{L46R}$-*venus*	Transformation of JK5 with pLY001
LY2	Δ*bacAB xylX*::P*xyl-bacA*$_{L42E}$-*venus*	Transformation of JK5 with pLY004
LY3	Δ*bacAB xylX*::P*xyl-bacA*$_{V52R}$-*venus*	Transformation of JK5 with pLY002
LY4	Δ*bacAB xylX*::P*xyl*-bacA$_{F130R}$-*venus*	Transformation of JK5 with pLY003
LY5	Δ*bacAB xylX*::P*xyl-bacA*$_{L46R}$-*venus*	Transformation of JK5 with pLY005
LY6	Δ*bacAB xylX*::P*xyl-bacA*$_{L46R}$-*venus*	Transformation of JK5 with pLY006
LY7	Δ*bacAB xylX*::P*xyl-bacA*$_{L46R}$-*venus*	Transformation of JK5 with pLY014
LY25	*xylX*::P*xyl-mCherry-CC1891*	Transformation of CB15N with pLY041
LY34	*xylX*::P*xyl-CC1891-mCherry*	Transformation of CB15N with pLY039
LY42	Δ*CC3376 bacA*::*bacA-ecfp*	Transformation of MT260 with pLY050
LY49	Δ*CC2139 xylX*::P*xyl-CC1891-bla*	Transformation of CS606 with pLY058
LY61	Δ*CC3376 bacB*::*bacB-venus*	Transformation of MT262 with pLY050
LY70	Δ*bacA* Δ*pbpC*	Transformation of MT304 with pMT813
LY71	Δ*bacB* Δ*pbpC*	Transformation of MT304 with pMT815
LY72	Δ*bacA* Δ*pbpC xylX*::P*xyl-mvenus-pbpC*	Transformation of LY70 with pLY073
LY75	Δ*bacB* Δ*pbpC xylX*::P*xyl-mvenus-pbpC*	Transformation of LY71 with pLY073
LY76	Δ*bacB* Δ*pbpC xylX*::P*xyl-mvnus-pbpC*$_{Δ4-39nt}$	Transformation of LY71 with pLY074
LY77	Δ*bacB* Δ*pbpC xylX*::P*xyl-mvenus- pbpC*$_{1-39nt}$-*dipM*$_{670-888nt}$-*pbpC*$_{249-2199nt}$	Transformation of LY71 with pLY075
LY83	Δ*bacAB xylX*::P*xyl-bacA*$_{surfmut}$-*mvenus*	Transformation of JK5 with pLY072
LY84	Δ*bacAB xylX*::P*xyl-bacA*$_{Δ4-32nt}$-*mvenus*	Transformation of JK5 with pLY076
LY88	Δ*bacAB xylX*::P*xyl-bacA*$_{K4S}$-*mvenus*	Transformation of JK5 with pLY087
LY89	Δ*bacAB xylX*::P*xyl-bacA*$_{K4SK7S}$-*mvenus*	Transformation of JK5 with pLY088
LY90	Δ*bacAB xylX*::P*xyl-bacA-mvenus*	Transformation of JK5 with pLY086
LY91	Δ*bacAB xylX*::P*xyl-bacA*$_{A6S}$-*mvenus*	Transformation of JK5 with pLY101
LY92	Δ*bacAB xylX*::P*xyl-bacA*$_{K7S}$-*mvenus*	Transformation of JK5 with pLY102
LY95	Δ*bacAB xylX*::P*xyl-bacA*$_{S3A}$-*mvenus*	Transformation of JK5 with pLY99
LY96	Δ*bacAB xylX*::P*xyl-bacA*$_{Q5A}$-*mvenus*	Transformation of JK5 with pLY100
LY97	Δ*bacAB xylX*::P*xyl-bacA*$_{F2Y}$-*mvenus*	Transformation of JK5 with pLY104
LY103	Δ*bacAB xylX*::P*xyl*-2x *mreB*$_{EC\ 1-33nt}$-*bacA*$_{Δ4-32nt}$-mvenus	Transformation of JK5 with pLY115
CB15N	Synchronizable variant of wild-type strain CB15 lacking holdfasts	[10]
CS606	Δ*bla*$_{175-837nt}$	[212]
KL7	*bacA*::*bacA-HA*	[136]
KL8	*bacB*::*bacB-HA*	[136]
JK5	Δ*bacA* Δ*bacB*	[136]
MT260	*bacA*::*bacA-ecfp*	[136]
MT262	*bacB*::*bacB-venus*	[136]
MT304	Δ*pbpC*	[136]
SS165	Δ*bla*$_{175-837nt}$ *xylX*::P*xyl-stpB-bla*	[4]
SS172	Δ*bla*$_{175-837nt}$ *xylX*::P*xyl-stpA-bla*	[4]

Table S1 Strains used in this study (continued)

Strain	Genotype	Source
E. coli		
TOP10	F-*mcrA* Δ(*mrr-hsd*RMS-*mcr*BC) Φ80*LacZ*ΔM15 Δ *Lac*X74 *rec*A1 *ara*D139 Δ(*araleu*) 7697 *gal*U *gal*K *rps*L (StrR) *end*A1 *nup*G	Invitrogen
Rosetta(DE3) pLysS	F- *ompT* $hsdS_B(r_B^- m_B^-)$ *gal dcm* (DE3) pRARE (Cam^R)	Merck Millipore

Table S2 Plasmids used in this study

Name	Description	Construction/reference
pLY001	pXVENC-2 harboring *bacA*$_{L46R}$	Mutagenesis PCR of *bacA* in pMT812 using oLY006 and oLY007.
pLY002	pXVENC-2 harboring *bacA*$_{V52R}$	Mutagenesis PCR of *bacA* in pMT812 using oLY008 and oLY009.
pLY003	pXVENC-2 harboring *bacA*$_{F130R}$	Mutagenesis PCR of *bacA* in pMT812 using oLY004 and oLY005.
pLY004	pXVENC-2 harboring *bacA*$_{L42E}$	Mutagenesis PCR of *bacA* in pMT812 using oLY010 and oLY011.
pLY005	pXVENC-2 harboring *bacA*$_{L122SM124S}$	Mutagenesis PCR of *bacA* in pMT812 using oLY014 and oLY015.
pLY006	pXVENC-2 harboring *bacA*$_{L42EV52S}$	Mutagenesis PCR of *bacA* in pMT812 using oLY012 and oLY013.
pLY007	pTB146 harboring *bacA*$_{112\text{-}483nt}$	PCR of *bacA* (112-483) from pMT812 using oLY002 and oLY003. Cloned into pTB146 between *Sap*I and *BamH*I sites.
pLY009	pTB146 harboring *bacA*$_{F130R}$	PCR of *bacA*$_{F130R}$ from pLY003 using oLY001 and oLY002. Cloned into pTB146 between *Sap*I and *BamH*I sites.
pLY014	pXVENC-2 harboring *bacA*$_{I48E}$	Mutagenesis PCR of *bacA* in pMT812 using oLY016 and oLY017.
pLY020	pET21a(+) harboring *bacA*$_{F130R}$	PCR of *bacA*$_{F130R}$ from pLY009 using oLY018 and oLY019. Cloned into pET21(+) between *Nde*I and *Hind*III sites.
pLY039	pXCHYC-2 harboring *CC1891*	PCR of *CC1891* from the genomic DNA of CB15N using oLY066 and oLY067. Cloned into pXCHYC-2 between *Nde*I and *Bgl*II sites.
pLY041	pXCHYN-2 harboring *CC1891*	PCR of *CC1891* from the genomic DNA of CB15N using oLY070 and oLY071. Cloned into pXCHYN-2 between *Kpn*I and *Eco*RI sites.
pLY050	pNPTS138 derivative for in-frame deletion of *CC3376*	PCR of *CC3376* upstream using oLY092 and oLY093 and downstream region using oLY094 and oLY095 from the genomic DNA of CB15N. Cloned into pNPTS138 between *Hind*III and *Eco*RI sites.
pLY058	pXBlaMC-2 harboring *CC1891*	Digestion of pLY039 by *Nde*I and *Hind*III. Cloned the gel extracted *CC1891* into pXBlaMC-2 between corresponding sites.
pLY070	pXCHYC-2 harboring *pbpC*$_{1\text{-}39nt}$-*dipM*$_{670\text{-}888nt}$-*pbpC*$_{250\text{-}2202nt}$	PCR of fragment containing *pbpC*$_{1\text{-}39nt}$ from pMT993 using oCS008 and oLY158, *dipM*$_{670\text{-}888nt}$ from pAI038 using oLY159 and oLY160, and *pbpC*$_{250\text{-}2202nt}$-*mCherry* from pMT993 using oLY161 and oLY162. Cloned into pXCHYC-2 between *Asc*I and *Nhe*I sites.
pLY071	pET21a(+) harboring *bacA*$_{surfmut}$ (D61, E88, D116 and E120 to T)	PCR of the synthesized gene block of *bacA*$_{surfmut}$ using oLY018 and oLY019. Cloned into pET21(+) between *Nde*I and *Hind*III sites.
pLY072	pXmVENC-2 harboring *bacA*$_{surfmut}$	PCR of the synthesized gene block of *bacA*$_{surfmut}$ using oLY165 and oLY166. Cloned into pXmVENC-2 between *Nde*I and *Mlu*I sites.
pLY073	pXmVENN-1 harboring *pbpC*	Digestion of pMT906 by *Nhe*I and *Kpn*I. Cloned the gel extracted *pbpC* into pXmVENN-1 between corresponding sites.
pLY074	pXmVENN-1 harboring *pbpC*$_{\Delta4\text{-}39nt}$	PCR of pbpC$_{40\text{-}2202nt}$ from pMT906 using oLY169 and CC3277-rev2. Cloned into pXmVENN-1 between *Nhe*I and *Kpn*I sites.
pLY075	pXmVENN-1 harboring *pbpC*$_{1\text{-}39nt}$-*dipM*$_{670\text{-}888nt}$-*pbpC*$_{250\text{-}2202nt}$	PCR of *pbpC*$_{1\text{-}39nt}$-*dipM*$_{670\text{-}888nt}$ from pLY070 using CC3277-for and oLY170 and *pbpC*$_{250\text{-}2202nt}$ from pMT906 using oLY171 and CC3277-rev2. Cloned into pXmVENN-1 between *Nhe*I and *Kpn*I sites.
pLY076	pXmVENC-2 harboring *bacA*$_{\Delta4\text{-}32nt}$	PCR of *bacA*$_{33\text{-}483nt}$ from pMT812 using oLY172 and CC1873-rev. Cloned into pXmVENC-2 between *Nde*I and *Sac*I sites.
pLY086	pXmVENC-2 harboring *bacA*	Digestion of pMT812 by *Nde*I and *Sac*I. Cloned the gel extracted *bacA* into pXmVENC-2 between *Nde*I and *Sac*I sites.
pLY087	pXmVENC-2 harboring *bacA*$_{K4S}$	Mutagenesis PCR of *bacA* in pLY086 using oLY192 and oLY193.
pLY088	pXmVENC-2 harboring *bacA*$_{K4S\ K7S}$	Mutagenesis PCR of *bacA*$_{K4S}$ in pLY087 using oLY194 and oLY195.
pLY094	pET42a(+) harboring *bacA*$_{surfmut}$-*StrepII*	Digestion of pLY071 by *Nde*I and *Xho*I. Cloned the gel extracted *bacA*$_{surfmut}$ and Strep-II tag from oLY201 and oLY202 hybridization into pET42a(+) between *Nde*I and *Avr*II sites.

Table S2 Plasmids used in this study (continued)

Name	Description	Construction/reference
pLY094	pET42a(+) harboring *bacA*$_{surfmut}$-*StrepII*	Digestion of pLY071 by *Nde*I and *Xho*I. Cloned the gel extracted *bacA*$_{surfmut}$ and Strep-II tag from oLY201 and oLY202 hybridization into pET42a(+) between *Nde*I and *Avr*II sites.
pLY099	pXmVENC-2 harboring *bacA*$_{S3A}$	PCR of the synthesized gene block of *bacA*$_{S3A}$ using oLY217 and oLY218 and *bacA*$_{106-483nt}$ from pLY086 using oLY213 and CC1873-rev. Cloned into pXmVENC-2 between *Nde*I and *Sac*I sites.
pLY100	pXmVENC-2 harboring *bacA*$_{Q5A}$	PCR of the synthesized gene block of *bacA*$_{Q5A}$ using oLY217 and oLY218 and *bacA*$_{106-483nt}$ from pLY086 using oLY213 and CC1873-rev. Cloned into pXmVENC-2 between *Nde*I and *Sac*I sites.
pLY101	pXmVENC-2 harboring *bacA*$_{A6S}$	PCR of the synthesized gene block of *bacA*$_{A6S}$ using oLY217 and oLY218 and *bacA*$_{106-483nt}$ from pLY086 using oLY213 and CC1873-rev. Cloned into pXmVENC-2 between *Nde*I and *Sac*I sites.
pLY102	pXmVENC-2 harboring *bacA*$_{K7S}$	PCR of the synthesized gene block of *bacA*$_{K7S}$ using oLY217 and oLY218 and *bacA*$_{106-483nt}$ from pLY086 using oLY213 and CC1873-rev. Cloned into pXmVENC-2 between *Nde*I and *Sac*I sites.
pLY117	pTB146 harboring *bacA*$_{F2Y}$	PCR of *bacA*$_{F2Y}$ from pLY104 using oLY252 and oLY002. Cloned into pTB146 between *Sap*I and *BamH*I sites.
pLY118	pTB146 harboring *bacA*$_{K4S\ K7S}$	PCR of *bacA*$_{K4S\ K7S}$ from pLY088 using oLY253 and oLY002. Cloned into pTB146 between *Sap*I and *BamH*I sites.
pLY119	pTB146 harboring *bacA*	PCR of *bacA* from pMT812 using oLY001 and oLY002. Cloned into pTB146 between *Sap*I and *BamH*I sites.
pXmVENN-1	Plasmid for integrating genes encoding N-terminal fusion to the yellow fluorescent protein mVenus at the *xylX* locus, Strep^R/Spec^R	Digestion of pXmVENC-2 by NdeI and BsrGI. Cloned the gel extracted *mvenus* into pXVENN-2 between the corresponding sites.
pMT812	pXVENC-2 harboring *bacA*	[136]
pMT813	pNPTS138 derivative for in-frame deletion of *bacA*	[136]
pMT815	pNPTS138 derivative for in-frame deletion of *bacB*	[136]
pXmVENC-2	Plasmid for integrating genes encoding C-terminal fusion to the yellow fluorescent protein mVenus at the *xylX* locus, Kan^R	Laboratory stock
pXVENC-2	Plasmid for integrating genes encoding C-terminal fusion to the yellow fluorescent protein Venus at the *xylX* locus, Kan^R	[213]
pXVENN-1	Plasmid for integrating genes encoding N-terminal fusion to the yellow fluorescent protein Venus at the *xylX* locus, Strep^R/Spec^R	[213]
pXCHYC-2	Plasmid for integrating genes encoding C-terminal fusion to the red fluorescent protein mCherry at the *xylX* locus, Kan^R	[213]
pXCHYN-2	Plasmid for integrating genes encoding N-terminal fusion to the red fluorescent protein mCherry at the *xylX* locus, Kan^R	[213]
pTB146	Plasmid for overexpression of protein with N-terminal His-SUMO fusion	[214]
pET21a(+)	Plasmid for the overexpression of His-tagged protein	Novagen
pET42a(+)	Plasmid for overexpressing GST fusion proteins with a Factor Xa site.	Novagen
pET51b(+)	Plasmid for overexpressing proteins with a cleavable N-terminal Strep-II tag and a C-terminal 10xHis tag	Novagen

Table S3 Oligonucleotides used in this study

Name	Sequence (5' -> 3')
oLY001	ctcacagagaacagattggtggtatgttcagcaagcaagctaaatcg
oLY002	gctttgttagcagccggatccttagccggcgctcttggcgatc
oLY003	ctcacagagaacagattggtggtaaggtcgcctcgctgctgtca
oLY004	aaccggcgccttccgccagggccgcagc
oLY005	gctgcggccctggcggaaggcgccggtt
oLY006	ctgtcagccgaccggaccatcgagggc
oLY007	gccctcgatggtccggtcggctgacag
oLY008	catcgagggcggccgtaccggcgaaggc
oLY009	gccttcgccggtacggccgccctcgatg
oLY010	ggtcgcctcgctggagtcagccgacctg
oLY011	caggtcggctgactccagcgaggcgacc
oLY012	catcgagggcggcagtaccggcgaaggc
oLY013	gccttcgccggtactgccgccctcgatg
oLY014	atcacccacgagcagtcggccagcgaaaccggcgccttc
oLY015	gaaggcgccggtttcgctggccgactgctcgtgggtgat
oLY016	tgtcagccgacctgaccgaggagggcggcgttaccgg
oLY017	ccggtaacgccgccctcctcggtcaggtcggctgaca
oLY018	ctttaagaaggagatatacatatgttcagcaagcaagctaaatcgaac
oLY019	ggtgctcgagtgcggccgcaagcttgccggcgctcttggcgatcg
oLY066	tttggggagacgaccatatgtgcgccaattgcgacctgg
oLY067	attctccggagctcgagatctcttggggcctttgggggcc
oLY070	gccttaattaatatgcatggtaccatgtgcgccaattgcgacct
oLY071	tacgcgtaacgttcgaattcttacttggggcctttgggggcctt
oLY092	aagccggctggcgccaagcttttctggccctcggcgcgg
oLY093	ttggcgataaccagcctcctccatccaacttcaagttggggagc
oLY094	caacttgaagttggatggaggaggctggttatcgccaactcc
oLY095	tcacggccgaagctagcgaattcaagtcgctgatcacggccct
oLY101	gggcctcagcgtcgcggaa
oLY102	cgatcgccctggctttgct
oLY158	ggtggtcttgatcgggtcgtcgaacttgtagggcggc
oLY159	cctacaagttcgacgacccgatcaagaccacccaggtgattcc
oLY160	Agtgccccacacccagacctgacgcggccccgcca
oLY161	gggccgcgtcaggtctgggtgtggggcactctgctg
oLY162	tatagctagcttacttgtacagctcgtccatgcc
oLY165	ttacatatgttcagcaagcaagctaaatcgaac
oLY166	ttaacgcgtgccggcgctcttggcgatc
oLY169	ttggtaccatggggaagagtcccggagagc
oLY170	gtcctcgaagcgaatgcccggcgcccggttcac
oLY171	aaccgggcgccgggcattc
oLY172	tatcatatgaacaacaaggccccggccc
oLY192	agccaagctaaatcgaacaacaaggccccgg
oLY193	gctgaacatatggtcgtctcccccaaaactcg

Table S3 Oligonucleotides used in this study (continued)

Name	Sequence (5' -> 3')
oLY194	agctcgaacaacaaggccccggcc
oLY195	agcttggctgctgaacatatggtcgtct
oLY201	tcgagtggagccacccgcagttcgaaaagtaac
oLY202	ctaggttacttttcgaactgcgggtggctccac
oLY213	acggccgaagctagcgaattctgaaaaacaggactcgactcgcgc
oLY217	acgctcgagttttggggagacgacc
oLY218	cgaggcgaccttgggcggtgcgcgacgcgcgggct
oLY227	gtttaactttaagaaggagatataccatatgcctgcaggcgccttaattaatatgc
oLY228	tcagcggtggcagcagcctaggttacttgtacagctcgtccatgccgagag
oLY240	tatgttgaaaaaatttcgtggcatgttttccaatggtac
oLY241	cattggaaaacatgccacgaaatttttttcaaca
oLY242	tcgagacatgttgaaaaaatttcgtggcatgttttccaattcg
oLY243	aattcgaattggaaaacatgccacgaaatttttttcaacatgtc
oLY249	ttggggagacgaccatatgatgttgaaaaaatttcgtggcatgttttccaatggtac
oLY250	gggccttgttgttcatatgggtggccgaccggtgacgc
oLY251	ctcacagagaacagattggtggtatgaacaacaaggccccggcc
oLY252	ctcacagagaacagattggtggtatgtacagcaagcaagctaaatcgaacaacaagg
oLY253	ctcacagagaacagattggtggtatgttcagcagccaagctagctcgaac
CC1873-rev	tagagctccgccggcgctcttggcgatcgccaga
CC3277-for	ttggtaccatgaacgactggacgctgccgcccta
CC3277-rev2	tatagctagcctagtagggcaggttgtccgggggcgg
MT693	ctatttcggcgcgggcacctatgg
oCS008	ttcggcgcgccgcccgctt
IntSpec-1	atgccgtttgtgatggcttccatgtcg
IntXyl-2	tcttccggcaggaattcactcacgcc
M13for	gccagggttttcccagtcacga
M13rev	gagcggataacaatttcacacagg
Pxyl-1	cccacatgttagcgctaccaagtgc
Pxyl-for	tgtcggcggcttctagcatggaccg
pET-for	cctttcagcaaaaaaccccctcaagacccg
pET-rev	cctttcagcaaaaaaccccctcaagacccg
mCherry-up	ctcgccctcgccctcgatctcgaac
mCherry-down	ggcgcctacaacgtcaacatcaagttgg
eGYC-up	cttgccgtaggtggcatcgccctcg
eGYC-down	gctgctgcccgacaaccactacctgag
TEM-1_rev	gctcatcattggaaaacgttcttcg

Table S4 Significantly enriched proteins in the Co-IP analysis of BacA-HA

Identified proteins	Accession number	BacA-HA	BacA-HA	BacA-HA	BacA	BacA	BacA
Bactofilin A BacA OS=*Caulobacter crescentus* (strain NA1000 / CB15N) GN=bacA PE=4 SV=1	A0A0H3C8L7_CAUCN	45	34	62	0	0	0
Bactofilin B BacB OS=*Caulobacter crescentus* (strain NA1000 / CB15N) GN=bacB PE=4 SV=1	A0A0H3CDZ6_CAUCN	29	20	52	1	1	1
Multimodular transpeptidase-transglycosylase PbpC OS=*Caulobacter crescentus* (strain NA1000 / CB15N) GN=pbpC PE=4 SV=1	A0A0H3CES2_CAUCN	27	23	38	0	0	0
Pentapeptide repeats containing protein OS=*Caulobacter crescentus* (strain NA1000 / CB15N) GN=CCNA_01968 PE=4 SV=1	A0A0H3CAS8_CAUCN	20	14	26	0	0	0
Uncharacterized protein OS=*Caulobacter crescentus* (strain NA1000 / CB15N) GN=CCNA_03486 PE=4 SV=1	A0A0H3CF25_CAUCN	11	6	14	0	0	0

Table S5 Significantly enriched proteins in the Co-IP analysis of BacB-HA.

Identified proteins	Accession number	BacB-HA	BacB-HA	BacB-HA	BacB	BacB	BacB
Bactofilin B BacB OS=*Caulobacter crescentus* (strain NA1000 / CB15N) GN=bacB PE=4 SV=1	A0A0H3CDZ6_CAUCN	297	277	249	1	1	2
Bactofilin A BacA OS=*Caulobacter crescentus* (strain NA1000 / CB15N) GN=bacA PE=4 SV=1	A0A0H3C8L7_CAUCN	221	222	225	2	2	2
Multimodular transpeptidase-transglycosylase PbpC OS=*Caulobacter crescentus* (strain NA1000 / CB15N) GN=pbpC PE=4 SV=1	A0A0H3CES2_CAUCN	95	85	101	0	0	0
Pentapeptide repeats containing protein OS=*Caulobacter crescentus* (strain NA1000 / CB15N) GN=CCNA_01968 PE=4 SV=1	A0A0H3CAS8_CAUCN	46	46	49	0	0	0
Uncharacterized protein OS=*Caulobacter crescentus* (strain NA1000 / CB15N) GN=CCNA_03486 PE=4 SV=1	A0A0H3CF25_CAUCN	24	22	26	0	0	0
Uroporphyrin-III C-methyltransferase/Precorrin-2 dehydrogenase/Sirohydrochlorin ferrochelatase OS=*Caulobacter crescentus* (strain NA1000 / CB15N) GN=CCNA_00024 PE=4 SV=1	A0A0H3C2J6_CAUCN	20	17	18	0	0	0
Lipoprotein-releasing system ATP-binding protein LolD OS=*Caulobacter crescentus* (strain NA1000 / CB15N) GN=lolD PE=3 SV=1	A0A0H3C8R0_CAUCN	26	22	26	0	0	0

Table S5 Significantly enriched proteins in the Co-IP analysis of BacB-HA (continued).

Identified proteins	Accession number	BacB-HA	BacB-HA	BacB-HA	BacB	BacB	BacB
Lipoprotein releasing system transmembrane protein lolE OS=*Caulobacter crescentus* (strain NA1000 / CB15N) GN=CCNA_02007 PE=3 SV=1	A0A0H3C9A2_CAUCN	25	18	26	0	1	1
Pole-organizing protein popZ OS=*Caulobacter crescentus* (strain NA1000 / CB15N) GN=popZ PE=4 SV=1	A0A0H3C7Y4_CAUCN	5	9	7	0	0	0
Stalk-specific protein X OS=*Caulobacter crescentus* (strain NA1000 / CB15N) GN=stpX PE=4 SV=1	A0A0H3C927_CAUCN	5	9	7	0	0	0
Ring hydroxylating dioxygenase, alpha-subunit OS=*Caulobacter crescentus* (strain NA1000 / CB15N) GN=CCNA_03222 PE=4 SV=1	A0A0H3CB50_CAUCN	3	5	4	0	0	0
Uncharacterized protein OS=*Caulobacter crescentus* (strain NA1000 / CB15N) GN=CCNA_01226 PE=4 SV=1	A0A0H3C7M2_CAUCN	3	4	5	0	0	0

Table S6 Significantly reduced proteins in the Co-IP analysis of BacA-HA in Δ*pbpC* background.

Identified proteins	Accession number	Δ*pbpC*	Δ*pbpC*	Δ*pbpC*	WT	WT	WT
Multimodular transpeptidase-transglycosylase PbpC OS=*Caulobacter crescentus* (strain NA1000 / CB15N) GN=pbpC PE=4 SV=1	A0A0H3CES2_CAUCN	0	0	0	42	35	31
Uncharacterized protein OS=*Caulobacter crescentus* (strain NA1000 / CB15N) GN=CCNA_03486 PE=4 SV=1	A0A0H3CF25_CAUCN	0	0	0	18	15	13
Acylamino-acid-releasing enzyme OS=*Caulobacter crescentus* (strain NA1000 / CB15N) GN=CCNA_03355 PE=4 SV=1	A0A0H3CC42_CAUCN	1	1	1	4	10	16
RNA polymerase-binding transcription factor DksA OS=*Caulobacter crescentus* (strain NA1000 / CB15N) GN=dksA PE=3 SV=1	DKSA_CAUCN	0	1	0	3	6	5
Myo-inositol-hexaphosphate 3-phosphohydrolase OS=*Caulobacter crescentus* (strain NA1000 / CB15N) GN=CCNA_01353 PE=4 SV=1	A0A0H3C7P7_CAUCN	0	0	0	1	4	6
M28-family zinc peptidase OS=*Caulobacter crescentus* (strain NA1000 / CB15N) GN=CCNA_03205 PE=4 SV=1	A0A0H3CE84_CAUCN	0	2	0	3	7	5

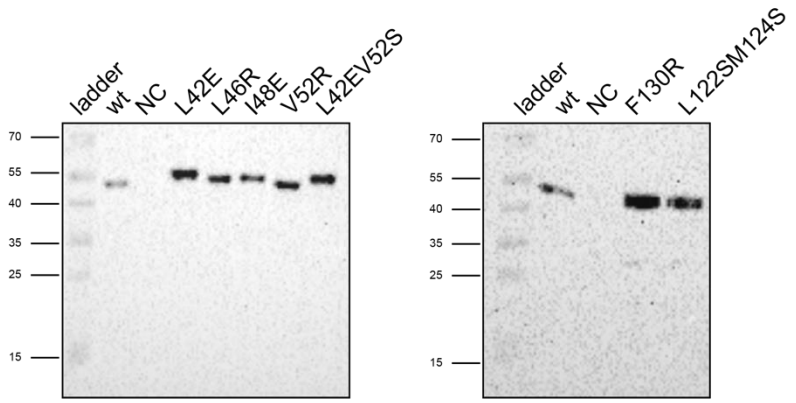

Figure S1 The fusion proteins of BacA variants are stable. Derivatives of strain JK5 (Δ*bacAB*) carrying the indicated alleles of *bacA-venus* under the control of the xylose-inducible P*xyl* promoter were grown to late exponential phase, diluted to an OD600 of ~ 0.1, and incubated for another hour. Cells were then induced with 0.005% xylose for 1 h and subjected to immunoblot analysis with an anti-BacA antibody. Cells of strain JK 150 (Δ*bacAB xylX*::P*xyl-bacA-venus*) and JK5 (Δ*bacAB*) served as positive and negative control, respectively. The positions of standard proteins (in kDa) are indicated on the left of image.

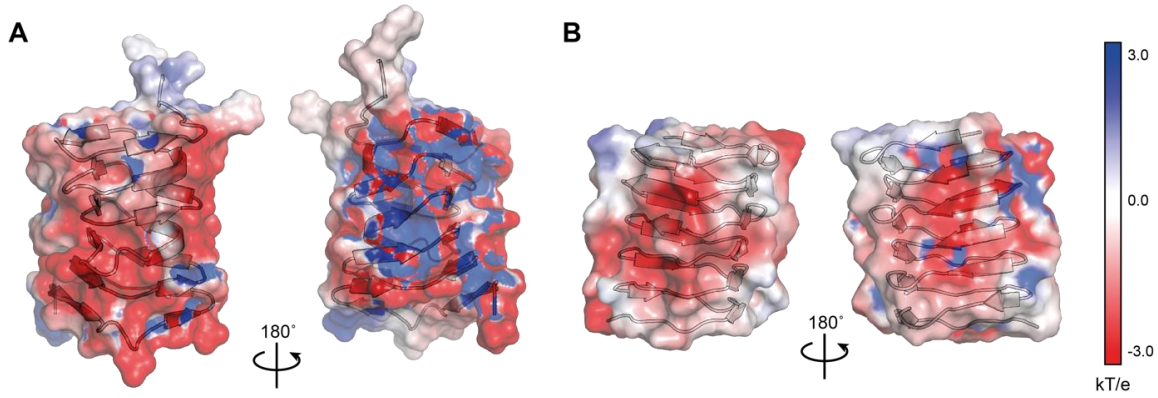

Figure S2 The electrostatic potential on the surface of BacA and TtBac. The electrostatics was solved by Adaptive Poisson-Boltzmann Solver (APBS) [215]. The potentials are on a [-3.0, 3.0] red-white-blue colormap in units of kT/e, where red and blue correspond to negative and positive electrostatic potential, respectively.

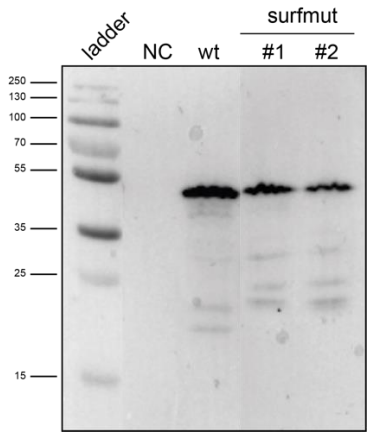

Figure S3 The BacA$_{surfmut}$-mVenus fusion is stable. Equal amounts of cells were loaded and the fusion protein was detected using anti-GFP antibody. Cells of strain LY90 (Δ*bacAB xylX*::P*xyl-bacA-mvenus*) and CB15N served as positive and negative control, respectively. The positions of standard proteins (in kDa) are indicated on the left of image.

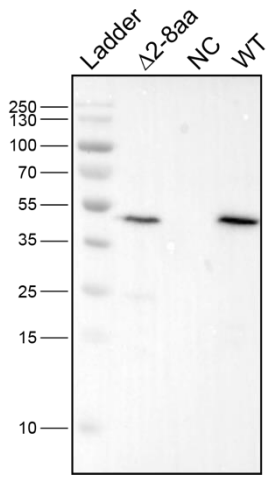

Figure S4 The BacA$_{\Delta 2\text{-}8aa}$-mVenus fusion is stable. Strain JK5 (Δ*bacAB*) carrying *bacA*$_{\Delta 2\text{-}8aa}$-*mvenus* under the control of the xylose-inducible P*xyl* promoter were grown to late exponential phase, diluted to an OD600 of ~ 0.1, and incubated for another hour. Cells were then induced for 3 h with 0.3 % xylose and subjected to immunoblot analysis with an anti-GFP antibody. Cells of strain LY90 (Δ*bacAB xylX*::P*xyl-bacA-mvenus*) and CB15N served as positive and negative control, respectively. The positions of standard proteins (in kDa) are indicated on the left of image.

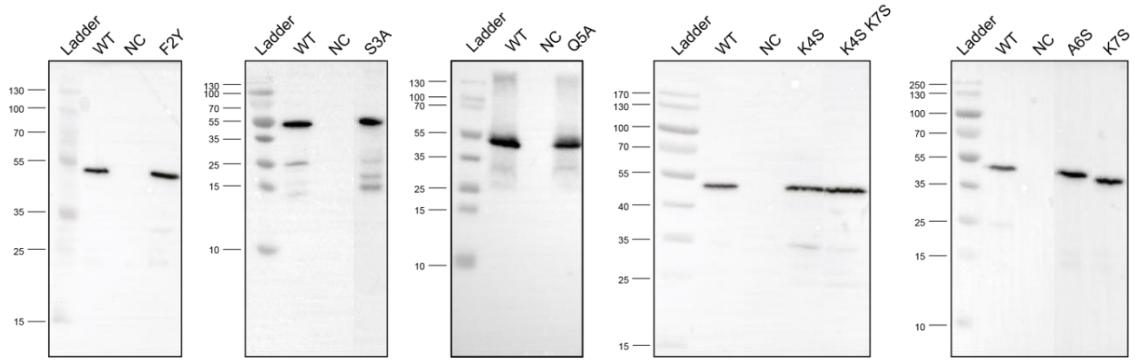

Figure S5 The fusion proteins of BacA variants with mutations in the membrane targeting sequence are stable. Strain JK5 (Δ*bacAB*) carrying indicated alleles of *bacA-mvenus* under the control of the xylose-inducible P*xyl* promoter were grown to late exponential phase, diluted to an OD600 of ~ 0.1, and incubated for another hour. Cells were then induced for 1.5 h with 0.3 % xylose and subjected to immunoblot analysis with an anti-GFP antibody. Cells of strain LY90 (Δ*bacAB xylX*::P*xyl-bacA-mvenus*) and CB15N served as positive and negative control, respectively. The positions of standard proteins (in kDa) are indicated on the left of image.

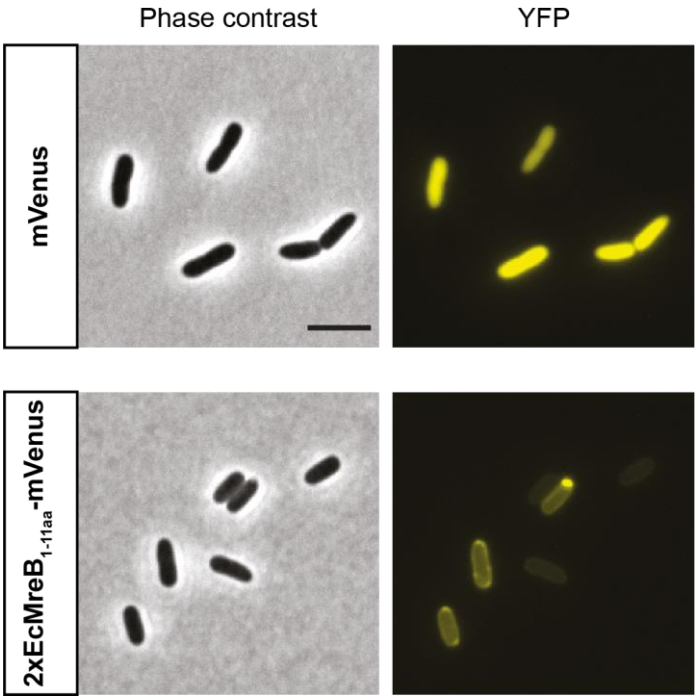

Figure S6 The amphipathic helix of EcMreB binds to the cell membrane. *E. coli* TOP10 cells harbouring pLY124 (pBAD24::*mvenus*) and pLY125 (pBAD24::2x *mreB*$_{1\text{-}33nt}$-*mvenus*) were induced with 0.001% arabinose for 1.5 h and imaged by phase contrast (Ph3) and fluorescence microscopy. Scale bar: 3 µm.

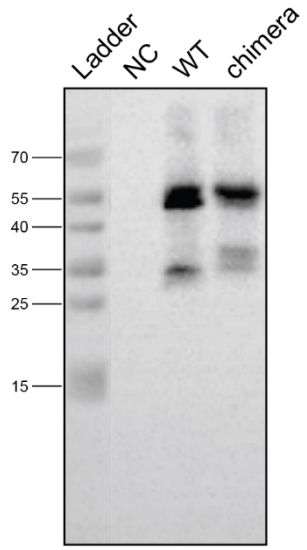

Figure S7 The 2x EcMreB$_{aa1\text{-}11}$-BacA$_{\Delta\ aa2\text{-}8}$-mVenus fusion is stable. Strain JK5 (Δ*bacAB*) carrying indicated alleles of *bacA-mvenus* under the control of the xylose-inducible P*xyl* promoter were grown to late exponential phase, diluted to an OD600 of ~0.1, and incubated for another hour. Cells were then induced for 2 h with 0.3 % xylose and subjected to immunoblot analysis with an anti-GFP antibody. Cells of strain LY90 (Δ*bacAB xylX*::P*xyl-bacA-mvenus*) and CB15N served as positive and negative control, respectively. The positions of standard proteins (in kDa) are indicated on the left of image.

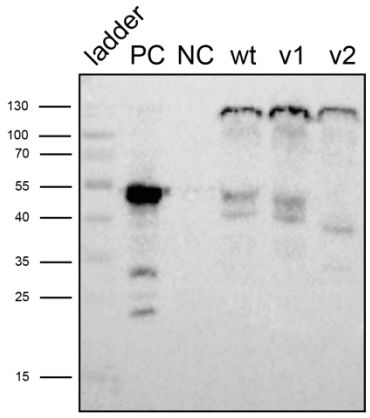

Figure S8 The fusion proteins of PbpC variants are stable. Strain LY70 (Δ*bacB* Δ*pbpC*) carrying *mvenus-pbpC* (wt), *mvenus-pbpC*$_{\perp 4\text{-}39nt}$ (v1) and *mvenus-pbpC*$_{1\text{-}39nt}$-*dipM*$_{670\text{-}888nt}$-*pbpC*$_{249\text{-}2199nt}$ (v2) under the control of the xylose-inducible P*xyl* promoter were grown to late exponential phase, diluted to an OD600 of ~0.1, and incubated for another hour. Cells were then induced for 1.5 h with 0.3 % xylose and subjected to immunoblot analysis with an anti-GFP antibody. Cells of strain LY90 (Δ*bacAB xylX*::P*xyl-bacA-mvenus*) and CB15N served as positive and negative control, respectively. The positions of standard proteins (in kDa) are indicated on the left of image.

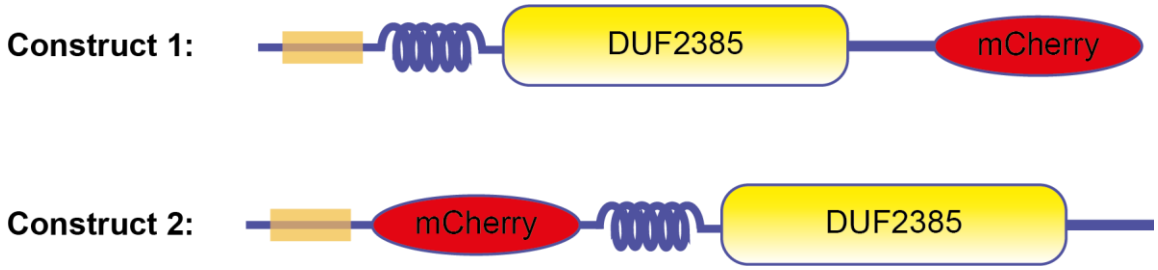

Figure S9 The fluorescent fusions used to localize CC3376. Construct 1 has a mCherry fluorescent protein fused to the C-terminus of CC3376, whereas the second construct has mCherry sandwiched by the signal peptide and transmembrane helix.

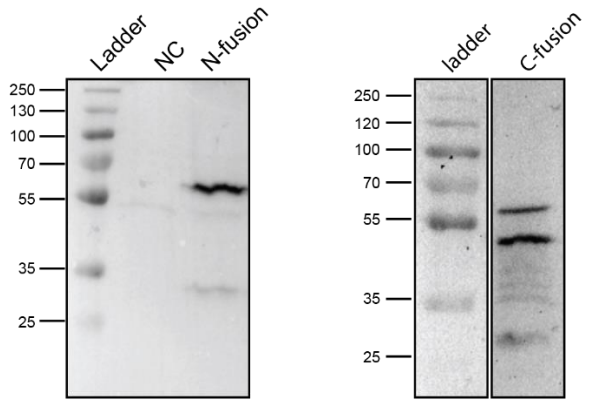

Figure S10 The mCherry-CC1891 fusion is relatively stable, whereas the C-terminal fusion protein, CC1891-mCherry, show signs of degradation in addition to the protein of expected size. Strain CB15N carrying *mCherry-CC1891* (N-fusion) and *CC1891-mCherry* (C-fusion) under the control of the xylose-inducible P*xyl* promoter were grown to late exponential phase, diluted to an OD600 of ~0.1, and incubated for another hour. Cells were then induced for 1 h with 0.03 % xylose and subjected to immunoblot analysis with an anti-mCherry antibody. The positions of standard proteins (in kDa) are indicated on the left of image.

7 Acknowledgement

It is hard to express my gratitude in a few paragraphs, as there are so many people who have helped, supported and encouraged me during my doctoral time. Without them, it is impossible for me to reach this point of my life. Despite the limited space, I would like to thank them with the deepest sincerity.

First, I would like to acknowledge the support and guidance from Prof. Dr. Martin Thanbichler, who is the best supervisor I can imagine. When I was applying for the PhD position, you were highly recommended by a friend. I appreciate that suggestion all the time, because you are such a wonderful scientist and mentor. Thank you for always being available for discussions whenever I felt lost and continuously providing great scientific advice that leads to the completion of this work.

I also would like to thank members of my thesis committee: Dr. Andreas Diepold, Prof. Dr. Peter Graumann and Prof. Dr. Lennart Randau, especially, Dr. Andreas Diepold, who kindly agreed to be my second reviewer.

Furthermore, I am indebted to our collaborators, Dr. Timo Glatter and Jörg Kahnt (MPI Marburg) for the mass spectrometry analyses, Dr. Wieland Steinchen (Philipps-Universität Marburg) for the HDX and Dr. Thomas Heirmel (Philipps-Universität Marburg) for the transmission electron microscopy. I greatly appreciate your contributions to this work.

I am also thankful for the former and present members of Thanbichler lab. Thank you for creating a pleasant and inspiring working environment, which makes my PhD an unforgettable experience.

Einverstandniserklärung

Ich versichere, dass ich meine Dissertation:

"Comprehensive Analysis of the Cytoskeletal Protein Bactofilin in *Caulobacter crescentus*"

selbstständig, ohne unerlaubte Hilfe angefertigt und mich dabei keiner anderen als der von mir ausdrücklich bezeichneten Quellen und Hilfen bedient habe. Die Dissertation wurde in der jetzigen oder einer ähnlichen Form noch bei keiner anderen Hochschule eingereicht und hat noch keinen sonstigen Prüfungszwecken gedient.

Marburg, ...

Ying Liu